NUI MAYNOOTH

Ollscoil na hÉireann Má Nuad

Mathematical modelling of autophagy pathway

by

Magdalena Zebrowska, MSc

Master Thesis

Hamilton Institute

National University of Ireland Maynooth

Maynooth

Co. Kildare

August 2010

Research Supervisor: Dr. Dimitris Kalamatianos

Collaborator: Dr. Markus Rehm

Head of Department: Prof. Douglas Leith

Abstract

A system modelling autophagy is a new area of research. Current understanding of each step in this biochemical pathway is limited. The study of this mechanism is interesting in several aspects: autophagy plays an important role in physiological cellular processes, is a survival mechanism under external stress and is also connected with cancer and neurodegenerative diseases [*Cuervo, 2004; Kondo et al., 2005; Levine, 2007; Pan et al., 2008*].

Autophagy is the pathway for degradation of redundant or faulty cell components. This important mechanism occurs in all eukaryotic cells as a part of cell's everyday activities and plays an important role in cell growth and development (cellular differentiation, immunity, cellular homeostasis).

This work proposes a simple mathematical model of autophagy pathway as a system with feedback, which controls the level of the total amino acid pool. Feedback comes from the amino acids which are produced during the autophagy mechanism which is induced as a result of starvation or rapamycin treatment.

Acknowledgements

I would like to thank everyone who contributed to this thesis.

First, I thank Prof. Peter Wellstead for giving me the opportunity to work at Hamilton Institute. I gratefully acknowledge the support of my supervisor Dr. Dimitrios Kalamatianos. My co-supervisors, Dr. Markus Rehm, deserve my sincere gratitude for his incredible patience and helpful suggestions. I would like to thank Dr. Mark Readman and Bartek Tomiczek for the constructive suggestions and help.

I would also like to thank my group mate, Fernando Lopez Caamal, for the helpful discussions; Prof. Rick Middleton, Dr. Oliver Mason and Ian Dangerfield for the final corrections. I also thank Rosemary Hunt and Kate Moriarty for their willingness to help in all administrative matters.

A number of people have made my stay in Hamilton Institute an enjoyable experience, especially Lukasz Budzisz, Buket Benek, Fernando Lopez Caamal, Shravan Sajja, Sabine Pilari, Ian Dangerfield, Arieh Schlote, Esteban Hernandez and Alessandro Checco. I would also like to mention lab mates from RCSI, Maximilian Wuerstle, Jasmin Schmid, Eugenia Delgado and Birgit Weyhenmeyer. Thank you all for your friendship!

Most of all, I would like to thank my parents, my sister and my grandparents for all their understanding and constant support.

Przede wszystkim chciałam podziękować moim rodzicom, siostrze oraz dziadkom za ich zrozumienie i nieustające wsparcie.

1. Introduction

Autophagy is derived from Greek roots: *auto*, meaning "self" and *phagy* – "to eat“. It is the pathway for degradation of redundant or faulty cell components. This important "housekeeping" complex dynamical system occurs in all eukaryotic cells as a part of cell’s everyday activities and plays an important role in cell growth and development (cellular differentiation, immunity, cellular homeostasis).

Autophagy activity is increased in some environmental cases such as a starvation, oxygen limitation, and hormonal stimulations or in intracellular stress such as microbial invasion, accumulation of mutant proteins and damaged organelles [*Levine, 2007*]. This survival promotion occurs by displacing nutrients from non–essential to more important processes. This lysosomal degradation system leads to the turnover of proteins and organelles. It includes the sequestration of cytoplasm and damaged or excess organelles into double–membrane vesicle called autophagosome and finally delivery to the lysosome for bulk degradation. Proteins and macromolecules destined for degradation during autophagy degrade into amino acids, peptide and fatty acids which are reused by the cell for biosynthesis and to fuel energy production. Autophagy adapts to stress by escaping from cell death but on the other hand can be an alternative path to cellular degradation (type II of PCD, programmed cell death). Autophagy is highly regulated by many factors such as amino acids, hormones and growth factors [*Klionsky, 1999*].

Paradoxically autophagy plays a dual role in cancer. It depends on the particular situation and phase in the pathological process. This system may lead to survival of cancer cells and may protect against some of the cancer treatments (ionizing radiation).

On the other hand, at early stages of carcinogenesis, autophagy plays a role of a tumor suppressor by removing damaged organelles that may generate mutations. Autophagy is also involved in the degradation of misfolded and aggregated proteins and therefore plays a role in neurodegenerative diseases, such as Huntington's and Parkinson's diseases.

1.1 Motivation

Systems biology leads to a better understanding of cellular dynamics by investigation the elements of cellular networks and interactions between them. Approaches which can be used to achieve these objectives integrate experiments and computational modelling.

Our intension is to develop a mathematical model for the autophagy pathway. An attempt to formulate the network of biochemical reactions in a mathematical framework can help with better understanding of the lysosomal degradation mechanism. In turn, better knowledge of the autophagy pathway could help improve future therapy (for example against cancer) and might contribute to recognition of alternative cell death mechanisms when some apoptotic pathways are inhibited. Also our work is motivated by current uncertainty of the role of autophagy; that is whether autophagy is a cell survival mechanism or rather another kind of cell death. Furthermore, the modelling might help in the future research to test the hypothesis for connection between autophagy and apoptosis, which has been already reported by experimental observations.

1.2 Aims and objectives

The objective of our work is to identify the molecular control systems regulating autophagy in cell death and survival. This is achieved by building mathematical model calibrated using published experimental data. This involves:

• developing a network of biochemical reactions involved in autophagy pathway,

• extracting rate expressions and state equations for analysis,

• simulations, which will be used to predict system behaviour in response to various stimuli.

1.3 Contributions

The main contributions in the thesis:

• A set of biochemical reactions involved in autophagy induction was extracted based on scientific literature reviews.

• Based on the network of biochemical reactions the set of rate expressions and ODE's was developed for computer simulations.

• Parameters for the simulation were proposed based on experimental literature about autophagy and mTOR signalling pathway.

• First test of an autophagy model was presented and tested. Mathematical model of autophagy pathway was detailed as a system with the feedback.

• The value of the feedback strength was obtained, as well as the autophagy contribution on the total amino acid pool during starvation.

1.4 Outline

This thesis is focused on the study of the dynamics of the autophagy pathway, which is involved in controlling of amino acid pool in cells during the starvations conditions. Special attention is paid on autophagy induction and reaction which are involved in that process.

Chapter 1 is focused on the introduction to autophagy pathway in general meaning. Chapter 2 describes in some details lysosomal degradation mechanisms. It explains the role of autophagy in health and diseases and gives an introduction to the steps of the autophagy pathway and autophagy related proteins. Also it presents an overview of our model from the biological point of view: explains set of reactions which are important for mTOR dependent autophagy induction and shows amino acids in the feedback loop. Chapter 3 gives an overview of biochemical pathway modelling. It presents a few approaches which are used in systems biology, such as the law of mass action and Michaelis-Menten kinetics. In the next chapter the dynamical model which reproduces the reactions in autophagy induction are presented. It hypothesises a novel model structure with references for the individual components of the pathway. It includes a diagrammatic representation of the proposed autophagy model, with the reactions involved and the ordinary differential equations that represent the system. This chapter also presents results of initial simulations. Chapter 5 explains how we extracted parameters essential for the model calibration from the experimental literature. The last chapter summaries the main results of our work, discuss the potential implications and gives some suggestions for future research.

2. The autophagy pathway

The balance between cellular biosynthesis and intracellular degradation is regulated by two powerful but independent mechanisms: the ubiquitin-proteasome system and the lysosome pathway [*Korolchuk et al., 2009*]. Some cross-talk between these pathways has been suggested even though there are many differences in the individual mechanisms. These differences include substrate differences (in autophagy bulkier and longer half-lives) and time scales (where autophagy is significantly slower than the proteasome system) [*Korolchuk et al., 2009*]. In the other words, autophagy degrades long-lived proteins and some cytoplasmic organelles [*Onodera and Ohsumi, 2005*], whereas the ubiquitin-proteasome system is involved in the degradation of specific short-lived proteins [*Yorimitsu and Klionsky, 2005*].

The lysosomal pathway has at least three variants: Cvt (cytosol to vacuole targeting) pathway, Vid (vacuolar import and degradation) pathway and autophagy. There are three types of autophagy: microautophagy, macroautophagy and chaperone-mediated autophagy. The most prevalent is macroautophagy. In general autophagy is a non-selective process; however in some cases it may select a target. Both types follow general steps including autophagosome formation and fusion with the lysosome. During non-selective autophagy, autophagic vacuoles enclose bulk cytoplasm. In general, this type of autophagy is induced by starvation and leads to increases in the size of the vesicle compared with the Cvt pathway. During selective autophagy only particular contents are sequestered into a vesicle.

One classic example of selective autophagy is the cytoplasm-to-vacuole targeting (Cvt) pathway, which is a preferential type of transport under normal nutrient

conditions. The cytoplasm to vacuole targeting pathway is a biosynthesis transport mechanism which delivers Ape1 (aminopeptidase 1) and Ams1 (alpha-mannosidase) enzymes to the vacuole. When cells are moved to a poor nutrient medium, the Cvt complex (Ape1, Ams1 and Atg19) is wrapped into the autophagosome together with other components. Formation of a Cvt vesicle is topologically the same as induced autophagy [*Baba et al., 1997*]. Delivery of organelles or proteins via the Cvt pathway is selective and occurs in basal growth conditions while transport by autophagosomes is non-selective and is induced by stress [*Scott et all, 2000*]. Some physiological level of autophagy is essential for cellular homeostasis. Excessive levels of autophagy promote cell death by digesting vital amounts of cell components while insufficient autophagy leads to the accumulation of damaged proteins and organelles.

The study of the autophagy pathway is interesting in many respects: it plays an important role in standard cellular processes, is a survival mechanism under external stress and also is connected with cancer and neurodegenerative diseases. In human diseases autophagy appears to play the role of a "double-edged sword", where in some cases it can mitigate pathogenesis whilst in others, it may aggravate pathologies.

2.1 Timeline

Identification of the autophagy pathway started with the discovery of the lysosome in 1955 by Christian de Duve [*Klionsky, 2007*], who subsequently coined the name "autophagy", which was introduced in 1963. It was morphologically identified first in mammalian cells [*Yorimitsu and Klionsky, 2005*], however studies with yeast have improved knowledge of the molecular mechanism involved in the autophagy pathway. In 1992 Ohsumi and colleagues showed that the morphology of this process in

yeast was similar to that in mammalian [*Takeshige, et al., 1992*]. This discovery proved very valuable for further studies in autophagy related genes and their orthologs.

Mortimore and his colleagues demonstrated that amino acids inhibit autophagy and at the same time he made a hypothesis that "autophagy could have a physiological role in the maintenance of body amino acid pools, although there is no direct experimental evidence for this" [*Mortimore, 1977; page 174*].

In 1993 the target of rapamycin (TOR) gene was isolated from yeast [*Kunz et al., 1993*], and from mammalians one year later. Shortly after this, the TOR gene was connected with protein synthesis, cell growth and cell-cycle progression. In 1995 Meijer and colleagues showed the stimulatory role of rapamycin for autophagy induction [*Blommaart, 1995*]. The same laboratory provided a link between amino acid-dependent and TOR-dependent regulation of autophagy pathway by demonstrating stimulation of TOR by amino acids.

In 1966 de Duve suggested that autophagy might be selective process (autophagy still is considered to be primarily nonspecific [*Kopitz, 1990*]). The first evidence for specific autophagy of an organelle was showed by Bolender and Weibel in 1973 [*Bolender & Weibel, 1973*]; four years later specific sequestration was demonstrated for mitochondria [*Beaulaton, 1977*], and afterwards for peroxisomes [*Veenhuis, 1983*]. The next example of degradation in a selective manner was the cytoplasm-to-vacuole targeting (Cvt) pathway [*Harding, 1995*]. Its morphology overlaps with non selective autophagy, as well as with proteins required [*Scott, 1996; Baba, 1997*].

In 1999 B. Levine's laboratory pointed out the essential connection between autophagy and diseases [*Liang, 1999*] and current research demonstrated that defects in autophagy

is associated with tumorgenesis [*Mathew, 2007*] and neurodegenerative diseases [*Rubinsztein 2005*].

Recent studies have confirmed the hypothesis of Beaulaton and Lockshin, who suggested that autophagy is involved in cell death [*Beaulaton and Lockshin, 1977*]. In particular, this shows a connection between programmed cell death (PCD) type I, apoptosis, and autophagy (sometimes called type II PCD). Mostly autophagy acts as a cytoprotective mechanism [*Boya et al., 2005*]. However, if apoptosis is disabled or if cellular damage is too large, autophagy may lead to cell death [*Boya et al., 2005*]. Better knowledge of this dual role of the autophagy pathway in cell death and survival is crucial for studies in regulation of those mechanisms. A more detailed description of the discovery and subsequent identification of the autophagosome process and pathway can be found in [*Klionsky, 2007*].

2.2 Autophagy functions

Autophagy plays a significant role in adaptation to starvation, development (birth, sporulation, fruiting body formation – for more details see Mizushima, 2005), programmed cell death, intracellular protein and organelle removal, elimination of microorganisms (degradation of bacteria), anti-aging, tumor suppression and prevention of neuron degradation [*Xie and Klionsky, 2007; Mizushima, 2007*]. This mechanism is an effective degradation process which can turn over proteins and remove redundant organelles.

In some cases is very difficult to determine the role of autophagy, for example in cancer (see section 2.6) and cell survival and cell death (see section 2.5). Subclassifying

autophagy into "basal" (Cvt pathway) and "induced" might be helpful to better understand the various roles of autophagy. However, the normal (or basal) level of autophagy is low; however, it can be upregulated by starvation (birth and fasting). The basal level of autophagy is essential for intracellular quality control while the induced autophagy – for intracellular production of amino acids during nutrient deprivation [*Mizushima, 2005*].

2.3 Steps of the autophagy pathway

The key steps in the autophagy process are:

1) Induction of autophagy,
2) Nucleation of phagophore,
3) Vesicle expansion and completion,
4) Retrieval of Atg9 from the PAS,
5) Targeting, docking and fusion with the lysosome,
6) Breakdown of the autolysosome,
7) Recycling of the macromolecular constituents.

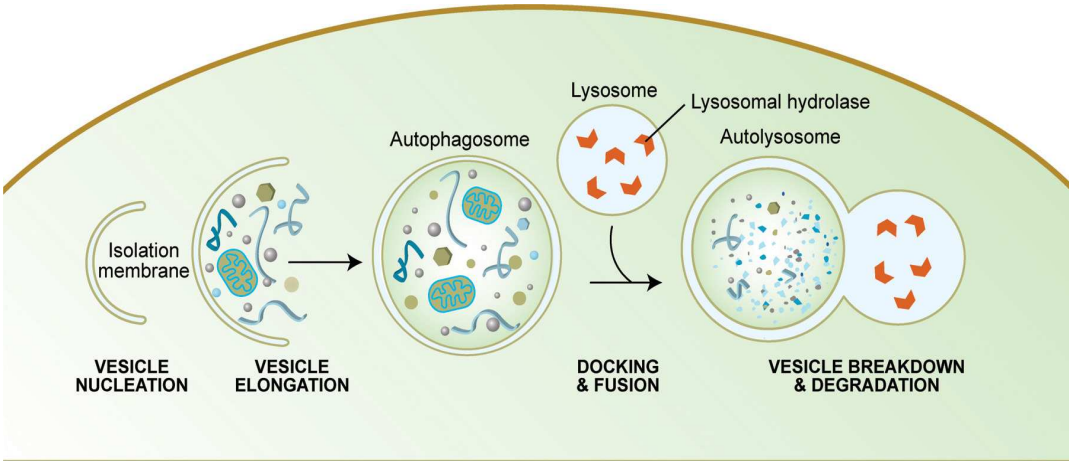

Figure 2.3 Steps of autophagy. *At the beginning of the autophagy pathway creation of the phagophore/isolation membrane is observed (vesicle nucleation). In the next step Atg proteins are involved which are responsible for vesicle expansion. The autophagosome sequesters a bulk cytoplasm with organelles. The outer membrane fuses with a lysosome and creates an autophagolysosome. Finally, wrapped material undergoes breakdown and recycling [Taken from Melendez and Levine, 2009].*

Each step requires many of the autophagy related proteins Atg. For further information about autophagy related proteins which are essential for lysosomal degradation pathway, see sub-chapter 2.4.

2.3.1 Induction of autophagy

During the normal vegetative nutrient conditions autophagy occurs at a basal level in yeast and mammalians. mTOR (mammalian target of rapamycin) is a master controller of nutrient and growth factors signalling, which suppress autophagy induction under nutrient-rich conditions.

mTOR signalling strongly regulates the binding between Atg1 and Atg13. The active form of TOR, in nutrient – rich conditions, affects hyperphosphorylation of Atg13,

which inhibits its association with Atg1 [*Kamada et al., 2000*]. After rapamycin treatment or during starvation (which is a classical inductor of the autophagy pathway) TOR activity is repressed and this causes rapid dephosphorylation of Atg13. This form of Atg13 has a high affinity for Atg1. This binding activates Atg1 kinase and leads to induction of autophagy.

Atg1 creates a complex with Atg13, Atg17 and Cvt9. All of the proteins are found to play a role in either the Cvt pathway or autophagy, but not both as Atg1. For example the Atg1-Atg13 association is essential for autophagy but not for a Cvt pathway. This suggests that the Atg1 complex acts as a switching point between two distinct pathways for targeting proteins in response to nutrient conditions.

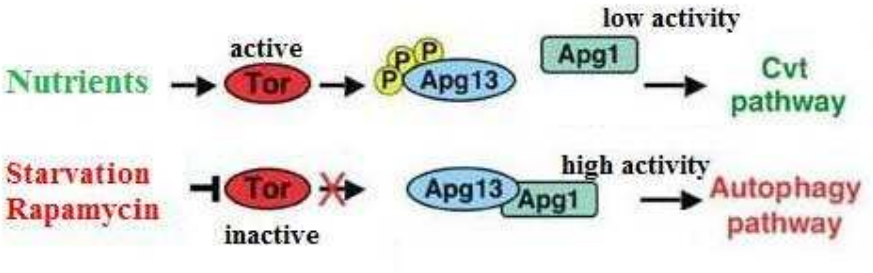

Figure 2.3.1 Autophagy induction by TOR inhibition. *In rich nutrients conditions that support transport via the Cvt pathway, Atg13 is hyperphosphorylated. In starvation autophagy pathway is induced by switching complex Atg1-Atg13. [Taken from Gozuacik and Kimchi, 2004].*

In mammalian cells, in response to ligand binding to the receptor (for example InR insulin receptor), a class I PI 3-K (class I phosphoinositide 3-kinase) is stimulated. Creation of the PtdIns(3)P (phosphatidylinositol 3-phosphate) at the membrane allows the attaching and activation of PDK1 (3-phosphoinositide-dependent protein kinase 1) and Akt/PKB (protein kinase B). Afterwards inhibition of TSC complex, which is a

GTP-ase activating protein for the Rheb (see chapter 2.7.2), by Akt resulting in the stabilization of the GTP-bounded form of Rheb. This form activates TOR and as a result – inhibits induction of autophagy [*Klionsky, 2005*]. For more detailed discussion of mTOR activation see chapter 2.7.

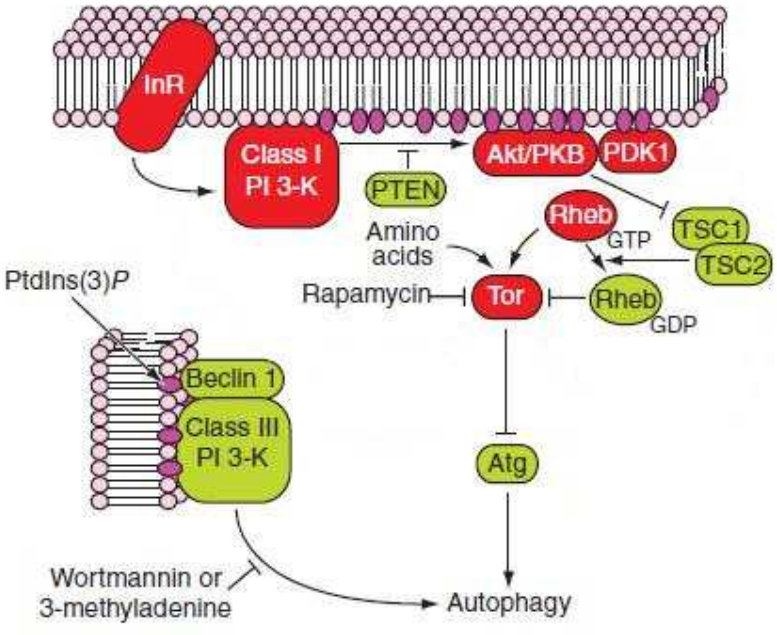

Figure 2.3.2 Regulation of autophagy induction in mammalian cells*. In higher eukaryotes, regulation of TOR is mediated via the action of a PI 3-K. Description of the roles of particular elements from the diagram see text above [Taken from Klionsky, 2005].*

2.3.2 Vesicle nucleation and autophagosome formation

In yeast the location for autophagosome formation is called the pre-autophagosomal structure or the phagophore assembly site (PAS) [*Xie and Klionsky, 2007; Mizushima, 2008*]. The PAS is a composite of the forming vesicle and the core

machinery proteins which lead to the process of expansion and transformation of the phagophore into an autophagosome.

The mechanism involved in vesicle formation and the genesis of the autophagosome membrane are not well known. In one of the model a vesicle is produced from pre-existing organelle (for example ER) by budding. The new-created vesicle has the same cellular topology as the membrane donor. Another model assumes that the vesicle is formed de novo [*Klionsky, 2005*].

2.3.3 Vesicle expansion and complexion

Most of the proteins which are involved in autophagy pathway appear during vesicle formation. Vesicle expansion and completion are parts of this process.

The proteins that perform in the vesicle expansion and completion create two sets of ubiquitin-like (Ubl) proteins: Atg8-PE (phosphatidylethanolamine) and Atg12-Atg5 [*Yorimitsu and Klionsky, 2005*]. Both of these proteins localize at the PAS.

At the beginning of the conjugation, Atg8 undergoes cleavage by Atg4 protease. This process results in removing arginine residue (R) from Atg8 to expose a glycine residue and converts a soluble Atg8 to a membrane-associated protein. The conjugation system requires an ubiquitin-activating E1-like enzyme, Atg7. Atg8, even as Atg 12 from the second conjugation system, is activated by Atg7. Afterwards, Atg8 and Atg12, via the action of an E2-like conjugating enzyme (Atg3 for Atg8 and Atg10 for Atg12), are attached to the PE (phosphatidylethanolamine) and Atg5, respectively. Next Atg12-Atg5 complex attaches Atg16 and all form a tetrameric complex, while Atg8-PE docks

to the PAS. In the complete vesicle Atg8 is released from membrane by Atg4 cleaving [*Klionsky, 2005*].

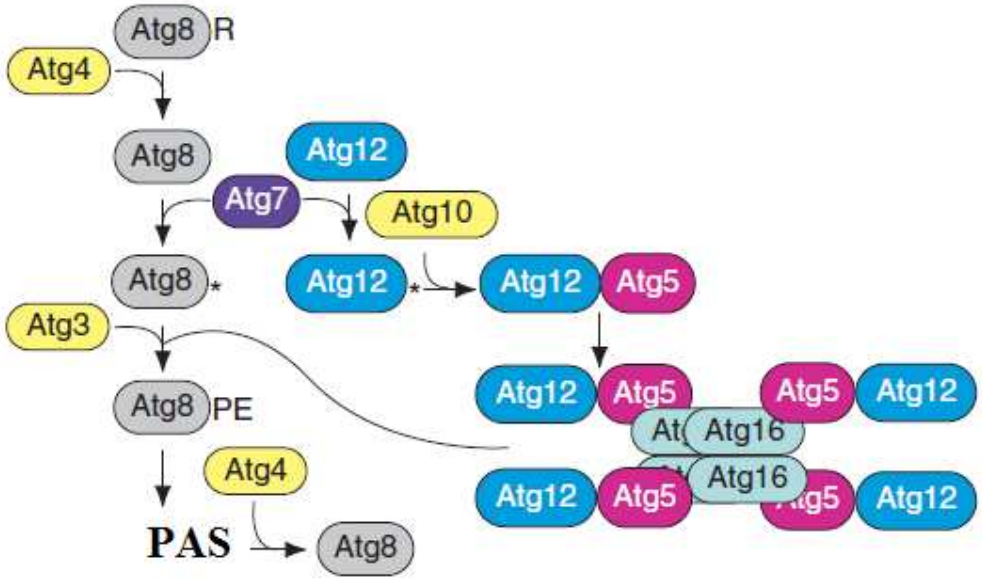

Figure 2.3.3 Atg proteins involved in vesicle expansion and completion*. Two ubiquitin-like proteins act in the process. For detailed description see text above [Klionsky, 2005].*

2.3.4 Retrieval of Atg9

In most cases Atg proteins present a single localization at the PAS but Atg9 and Atg23 are also delivered to the many another structures. The movement of the Atg9 between PAS and non-PAS structures is crucial for autophagosome formation [*Xie and Klionsky, 2007*]. The Atg9 transport factors (Atg23 and Atg27) are responsible for effective transfer of Atg9 to the PAS. The retrieval of Atg9 from the PAS involves Atg1 complex, Atg2 and Atg18.

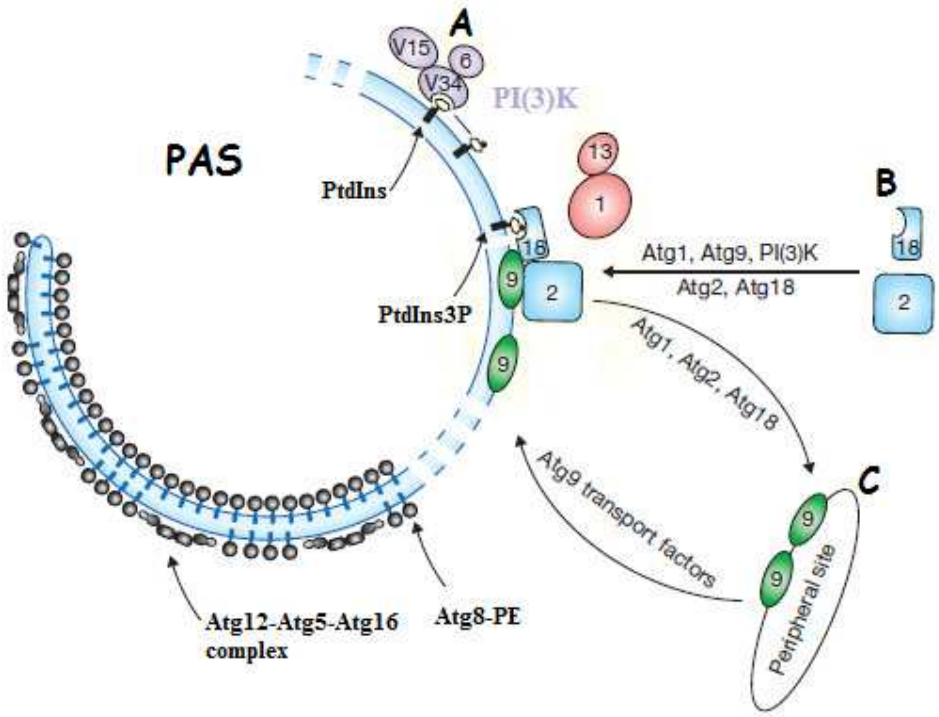

Figure 2.3.4 PAS. *Different proteins are localized in the PAS, depending on the phase of the vesicle formation. a) The PI(3)K complex: the lipid kinase Vps34, the enzyme Vps15 and Atg6. b) The position of Atg2 and Atg18 at the PAS depends on Atg9, Atg1, the PI(3)K complex and on each other. c) The cycling of Atg9 between PAS and the peripheral site. Effective delivery to the PAS requires Atg9 transport factors (Atg23 and Atg 27) while away from the PAS Atg18, Atg1 complex andAtg2 are involved [Taken from Xie and Klionsky, 2007].*

Based on figure 2.3 the retrieval Atg9 from the PAS has three stages:

a) Atg9 and Atg1 complex are gathered to the PAS

b) Atg18 and atg2 are recruited to the PAS where they interact with Atg9

c) Atg9 moves out from the PAS.

The probable function of Atg9 cycling is to provide lipids for autophagosome formation [*He et al., 2006*].

2.3.5 Fusion with a lysosome

The vesicle fusion with the lysosome must be controlled to prevent premature fusion. The complex of Atg12-Atg5-Atg16 and Atg8-PE, placed on the outer membrane of autophagosome, regulate the fusion process [*Klionsky, 2005*].

The proteins system required for fusion process include: the SNARE proteins (Vam3, Vam7, Vti1 and Ykt6), the NSF, SNAP and GDI homologs (Sec17, Sec18 and Sec19), the Rab protein Ypt7, members of the class C Vps/HOPS complex, proteins Ccz1 and Mon1 [*Klionsky, 2005*].

2.3.6 Breakdown of the autolysosome and recycling

After fusion autophagosome with the lysosome (or vacuole in yeast), the inner membrane of the autophagosome and its contents (cytoplasmic material) are degraded by lysosomal/vacuolar hydrolases [*Mizushima, 2008*]. This step of autophagy pathway depends on the acidic pH of the vacuole. Also Atg15 and Atg22 may be involved in the breakdown step.

Thereafter proteins and macromolecules are degraded in the lysosome/vacuole into simple elements (amino acids, peptide and fatty acids) which are exported to the cytosol for reuse by cell for biosynthesis of essential components and to fuel energy production. Amino acids produced via autophagy can be oxidized to produce energy in some tissues (such as muscles) or used for synthesis of proteins that are essential for adaptation to starvation [*Mizushima, 2005*].

2.4 Autophagy related proteins

The ATG genes encode proteins essential for all steps involved in autophagy pathway. There are four functional groups of Atg proteins [*Levine and Junying, 2005; Xie and Klionsky, 2007*]:

A) protein **serine/threonine kinase complex** which responds to TOR kinase (Atg1, Atg13, Atg17);

B) lipid kinase **signalling complex PI(3)K** which induces vesicle nucleation (the PI(3)K complex is formed by Atg6/Vps30, Atg14, Vps34/class III PI(3)K and Vps15 and is localized to the PAS);

C) **two ubiquitin-like Ubl protein conjugation system, Atg12 and Atg8**, which are essential for vesicle expansion and completion (includes an E1-like activating enzyme Atg7, two E2-like conjugating enzymes Atg10 (for Atg12) and Atg3 (for Atg8), an Atg8 modifying protease Atg4 (cause releasing PE from Atg8-PE), Atg5 and Atg16);

D) a retrieval pathway, **Atg9 and its cycling system**, involved in disassembly of Atg proteins from matured autophagosome (Atg9, Atg1-Atg13 complex, Atg2, Atg18).

For more detailed description of the core proteins required for autophagy and PAS see Xie and Klionsky, 2007.

2.5 Autophagy, cell survival and cell death

Apart from classical apoptosis, there are several types of programmed cell death (PCD). Nomenclatures "autophagic cell death" or "type II cell death" are used for a mechanism characterized by the presence of autophagolysosomes. A term "autophagy" is preferred when describing a degradation process rather than cell death. However, for this type of death the most adequate terminology is "cell death with autophagy" [*Mizushima, 2005*]. The role of autophagy is quite controversial and creates question whether autophagy is a cell death or a survival mechanism. Recent studies suggest that autophagy can mediate cell death [*Yu et al., 2004; Shimizu et al., 2004*] and conversely it can also act as a cytoprotective mechanism during starvation [*Lum et al., 2005*]. Furthermore, inhibition of autophagy triggers starvation-induced apoptosis [*Boya et al., 2005*]. For that reason, the role of autophagy as a cell death executor or cell protector might be connected with cellular nutrient conditions [*Mizushima, 2005*].

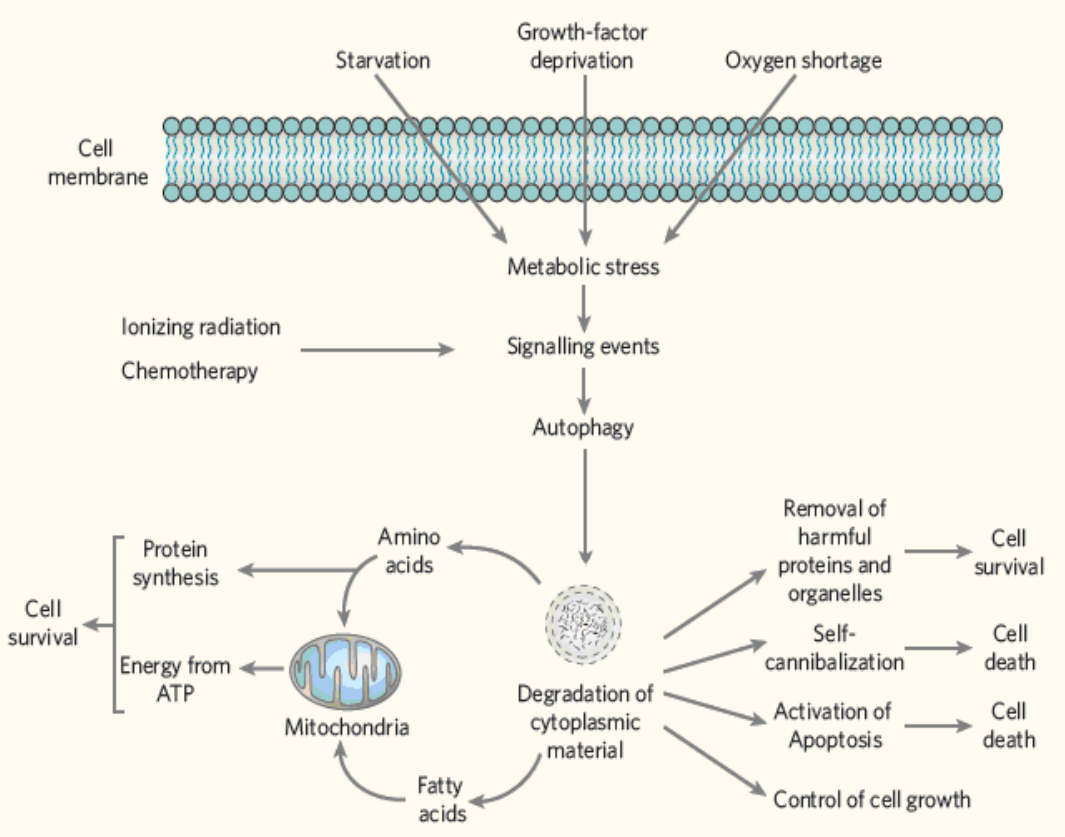

Figure 2.5. A motif function of autophagy. *Activation of signalling pathways that induce utophagy by metabolic stress and anti-cancer treatment. Dual role of autolysosomal degradation of cytoplasmic material: cell survival (generating fatty acids and amino acids for reuse and by removing harmful organelles and proteins) and cell death (self-cannibalisation). Also the turnover of proteins and organelles by autophagy can contribute to the control of cell growth [Levine, 2007].*

2.6 Autophagy and diseases

Autophagy is linked to several human pathologies, such as different kinds of cancer, Parkinson's disease and Alzheimer's disease [*Cuervo, 2004; Kondo et al., 2005; Levine, 2007; Pan et al., 2008*]. A better understanding of the role of autophagy in diseases is a great recent research interest; therefore the topic of lysosomal degradation

is developing very fast nowadays. Autophagy has been reported as a survival mechanism but also as a cell death, depending on the progression of the disease, the cellular surroundings and therapeutic treatment [*Cuervo, 2004*].

2.6.1 Neurodegenerative diseases

A hallmark of several neurodegenerative diseases, such as Parkinson's disease, Alzheimer's disease and Huntington's disease, is intracellular protein aggregates which contain mutant proteins. Induction of autophagy may be beneficial for removing those aggregates, while inhibition causes formation of them [*Mizushima, 2005*]. The main challenging question in the topic of neurodegeneration diseases is how to prevent or at least slow down the formation of aggregates by promoting the turnover of misfolded proteins. For more information about protein aggregations and neurodegenerative diseases see *Cuervo, 2005*.

2.6.2 Cancer

The evidence which linked cancer and autophagy results in greater interest in the topic of autophagy pathway. Better understanding the role of autophagy in individual stages of tumor development may lead to improvement of anticancer treatment.

Induction as well as inhibition of autophagy may enhance and inhibit progression and development of tumor. The relationship between autophagy regulation and tumor progression depends on the particular situation and phase in the pathological process. In typical cancer cells, due to autophagy suppression, protein synthesis prevails over degradation and cellular growth remains. Down-regulation of autophagy may

cause accumulation of toxic biochemical species that might stimulate mutation and support tumorgenesis [*Cuervo, 2004*]. Therefore, at early stages of carcinogenesis, autophagy plays a role of a tumor suppressor.

On the other hand, tumor cells in late states of development are often low in nutrient factors and oxygen, and therefore may require autophagy for continued growth. For this reason autophagy can be induced to assure survival of tumor cells under adverse circumstances, for example, the inner area of tumor, with low vascularisation. To compensate for the low supply of nutrients and oxygen, activation of autophagy helps to gain the materials for the synthesis of the essential components by degradation of unnecessary intracellular elements. Furthermore induction of autophagy is beneficial in some type of cancers as a response to radiation and chemotherapy – it helps eliminate damaged structures before they accumulate, thereby reducing the desired death rate of tumor cells.

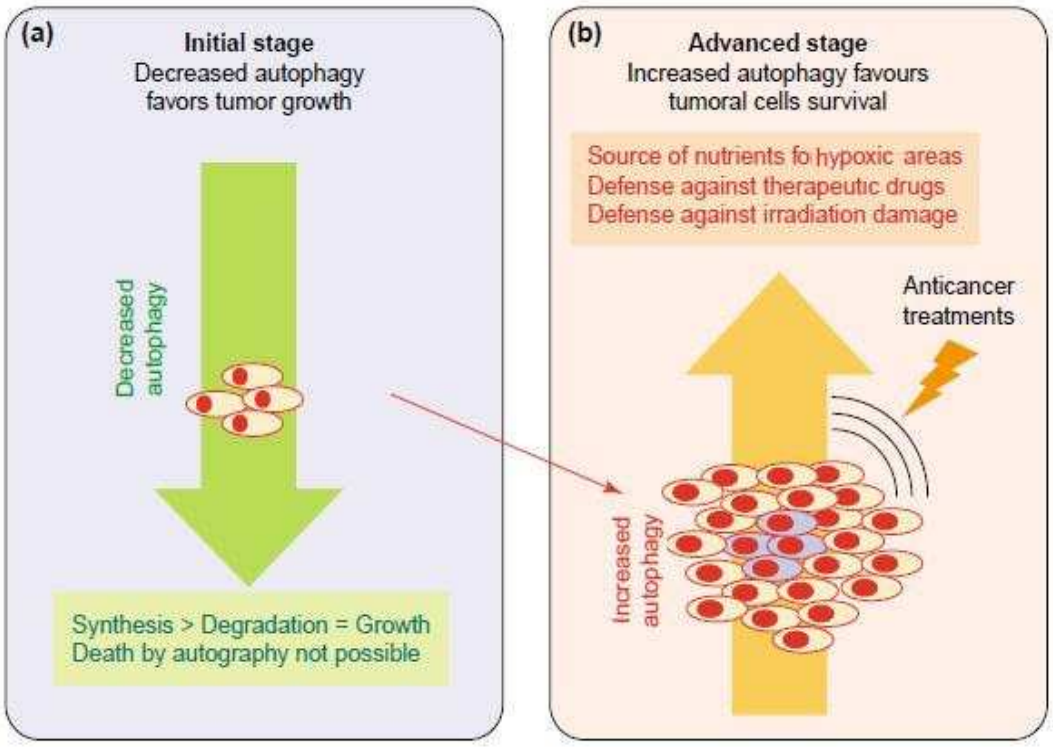

Figure 2.6 Double role of autophagy in cancer. *Depending on the stage of tumor development, both inhibition and activation of autophagy may be beneficial for cancer cells. a) In the early stages, decreased autophagy leads to increasing protein synthesis and cellular growth. b) In the late stages, increased autophagy may help to survival of the cells located in centre of the tumor, which have restricted access to nutrients and oxygen. Furthermore, induced autophagy may be a defensive system as a response to different anticancer treatment. [Taken from Cuervo, 2004].*

The conflicting pro-survival and pro-death autophagy performing makes the cancer treatment more complex. Efficacy of anticancer therapeutic may be improved by manipulation of autophagy [*Kondo et al., 2005*].

2.7 The mTOR kinase

The mammalian target of rapamycin (mTOR) is a serine/threonine kinase which is highly conserved in all eukaryotes. During the nutrient rich conditions mTOR occurs in a active form and controls many processes that are involved in cellular growth and metabolism in response to growth factors stimulations (insulin – via the PI3K-Akt/PKB pathway – figure 2.7.1), changes in cellular energy levels (ATP) and nutrients sufficiency (amino acids) – and in turn plays a role of a nutrient status sensor [*Zempleni, 2005; Meijer, 2008*]. mTOR also acts as a gatekeeper for autophagy induction. Inactivation of mTOR by starvation or rapamycin treatment causes dephosphorylation of Atg13. This in turn raises the affinity Atg13 to Atg1 and this association results in increasing Atg1 protein kinase activity [*Meijer, 2008*]. For more detailed discussion about autophagy induction see chapter 2.3.1 and references Kamada et al., 2000 and Klionsky, 2005.

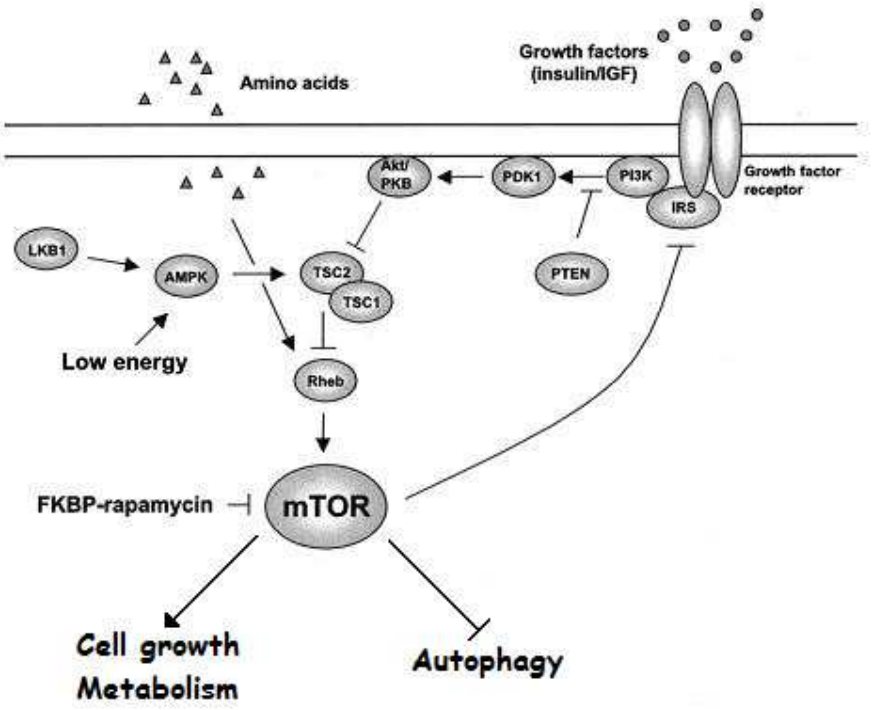

Figure 2.7.1 The mTOR signalling network *[taken from Hall, 2008].*

A lack of growth factors and energy can be repaid by high level of amino acids, but not vice versa [*Hall, 2008*]. This means that amino acids are a strong signal which positively regulates mTORC1 [*Laplante and Sabatini, 2009*]. An essential amino acid necessary for mTORC1 activation, as it was recently shown, is leucine. mTOR controls cell growth by both positively (protein synthesis, mitochondrial metabolism) and negatively (autophagy, apoptosis) regulating processes.

2.7.1 Complexes of mTOR: mTORC1/mTORC2

mTOR remains in two signalling muliprotein complexes: mTOR complex 1 (mTORC1) and mTOR complex 2 (mTORC2). mTORC1 is composed of mTOR, raptor

(regulatory associated protein of mTOR), mLST8/GβL protein, PRAS40 [*Vinod and Venkatesh, 2009; Kim, 2009*] and FKBP38 [*Kim, 2009; Bai et al., 2007*]. This complex controls protein synthesis and functions as a nutrient/energy sensor. The activity of mTORC1 is stimulated by insulin, growth factors, amino acids and oxidative stress, while inhibition is caused by nutrient deprivation, low growth factor levels and rapamycin. Complex 1 is called a rapamycin-sensitive complex. mTORC2 is composed of mTOR, Rictor (rapamycin-insensitive companion of mTOR), mLST8/GβL and mSIN1. mTORC2 is regulated by insulin and growth factors. Complex 2 is called a rapamycin-insensitive complex. For more information recommended further reading: Bai and Jiang, 2009; Laplante and Sabatini, 2009.

2.7.2 mTOR activation

The mechanism by which amino acids activate mTORC1 is not well known yet. Some of the research results suggested that upstream of mTOR are TSC1-TSC2 and small GTPase Rheb. Recently, Rheb was confirmed as an effector of the TSC1/TSC2 complex. TSC complex directly interacts with Rheb [*Bai and Jiang, 2009*] and modulates its GTP hydrolysis activity. Some evidence shows that Rheb is regulated by amino acids conditions [*Roccio et al., 2005*] when depletion of amino acids reduces the levels of GTP-bounded Rheb.

FKBP38, by directly binding to mTOR [*Bai and Jiang, 2009*], inhibits activity of mTORC1 [*Bai et al., 2007*]. The level of cytosolic FKBP38 is negatively correlated with the mTOR activity [*Bai and Jiang, 2009*]. The interaction FKBP38 with mTOR is controlled by Rheb, which inhibits its association by directly binding to FKBP38 [*Bai et*

al., 2007] – see figure 2.7.2. Rheb-FKBP38 binding is GTP-dependent [*Bai and Jiang, 2009*].

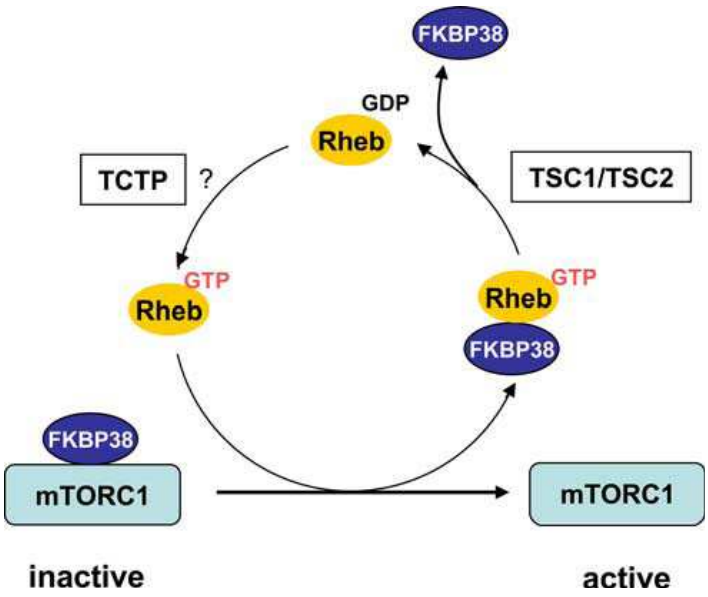

Figure 2.7.2 A model for the role of FKBP38 in mTORC1 regulation. *FKBP38 by direct binding to mTOR inhibits its activity. Rheb, in GTP-bounded form, interacts with FKBP38 and allow activation of mTORC1. TSC1/TSC2 complex promotes the hydrolysis of GTP to GDP. [Taken from Bai and Jiang, 2009].*

The association of Rheb with FKBP38 in cells is controlled by amino acids and growth factors and in starvation conditions it seems to be a weak binding [*Bai and Jiang, 2009*].

2.7.2.1 Rheb

Rheb (Ras-homology enriched in bran) is a small GTPase which is structurally close to Ras. The regions involved in GTP binding in Rheb are similar to those in Ras

and it is believed that the core action mechanism of Rheb is similar to Ras [*Bai and Jiang, 2009*]. There is one difference (Rheb contains an arginine, not a glycine like Rheb at the homologue position) which results in a high level of GTP-bound Rheb in cell.

The activity of the small GTPases depends on their nucleotide-binding states, which are controlled by their related GAPs (GTPase-activating protein) and GEFs (guanine nucleotide exchange factor). The GAP for Rheb is TSC1/TSC2 complex, which stimulates GTP hydrolysis. Recently TCTP (the translationally controlled tumor protein) has been suggested to be the GEF for Rheb [*Bai and Jiang, 2009*].

2.7.2.2 FKBP38

FKBP38 belongs to the PPIase (peptidyl prolyl cis/trans isomerase) family of FK506-binding protein. It has been suggested to be an inhibitor of mTOR [*Bai et al., 2007*] and its level was found in reverse relation with mTOR1 activity. It is a part of mTORC1 complex [*Kim, 2009; Bai et al., 2007*]. FKBP38 is structurally related to FKBP12 and it inhibits mTOR activity by binding to it, in a similar manner to the FKBP12-rapamycin complex [*Bai et al., 2007*].

2.7.2.3 GTPase switch proteins

In signal transduction pathways we can observe a group of intracellular switch proteins, which belong to the GTPase superfamily. The GTPase switch proteins occur in two forms: in active "on" GTP-bounded form and inactive "off" GDP-bounded form. GTP-bounded form modulates the activity of specific proteins [*Lodish, 2001*].

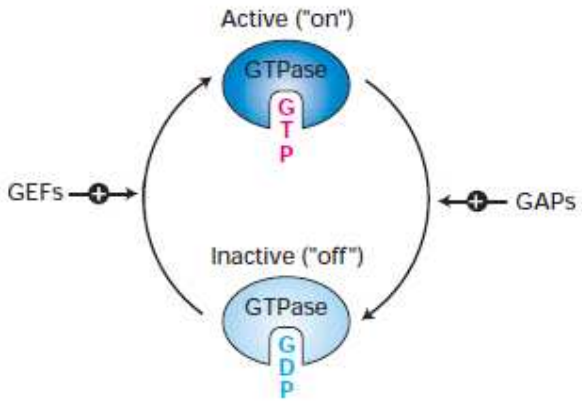

Figure 2.7.3 Cycling of GTPase switch proteins between the active and inactive forms *[Lodish, 2001].*

GAP (GTPase-activating protein) – promotes hydrolysis of bounded GTP to GDP; TSC1/TSC2 is a GAP for Rheb [*Laplante and Sabatini, 2009*]. Opposite reaction is catalyzed by GEF (guanine nucleotide exchange factor) and TCTP has been suggested to be the GEF for Rheb.

During the signal deficiency, the protein is bound to GDP, whereas signals activate the release of GDP and binding to GTP. For more detailed discussion see "Molecular cell biology" [*Lodish et al., 2001*].

2.8 Amino acid regulation of autophagy pathway

Amino acids are essential to life and have a variety of roles in metabolism. One particularly significant function is to building blocks of proteins. Also they are prominent as precursors for the biosynthesis of molecules and in many other metabolic pathways [*Murray, 2003*]. Due to their central role in biochemistry, amino acids are

very important in nutrition. Nutrients must be taken in from an environment in the shape of food (for human and animals) or nutriment (for cell culture).

Beside those functions, amino acids also play a role of signalling molecules that control signal transduction pathways [*Meijer, 2008*]. mTOR-dependent signalling pathway is activated by amino acids (especial leucine) in synergy with insulin. Induction of this pathways results in suppression of lysosomal degradation pathway and amino acids are known as inhibitors of autophagy.

All organisms use many metabolic changes to survive during nutrient shortage periods. One of them is the autophagy pathway, where cells degrade their intracellular contents to support essential functions. Onodera and Ohsumi have shown that protein synthesis under nitrogen starvation requires autophagy and the products of degradation via autophagy are essential for this biosynthesis [*Onodera and Ohsumi, 2005*]. This suggestion of the amino acids in a feedback loop from protein degradation and back to building processes is used in our initial model, in chapter 4. During cellular starvation without autophagy the free amino acid pool decrease dramatically and could be limited as a substrate for protein synthesis. Next they showed that autophagy is fundamental for the maintenance of a free amino acid pool under starvation. Without autophagy, many of the amino acids fall below critical levels.

Autophagy may be inhibited by the insulin-amino acid-mTOR signalling pathway (figure 2.8.1) and can be activated by amino acids depletion or rapamycin [*Meijer and Codogno, 2008*]. Insulin, in synergy with amino acids, inhibits autophagy by activating mTOR, which results in the phosphorylation of the protein kinase Atg13 and inhibition of its association with Atg1. Complex of Atg1 and Atg13 is essential for induction of autophagy.

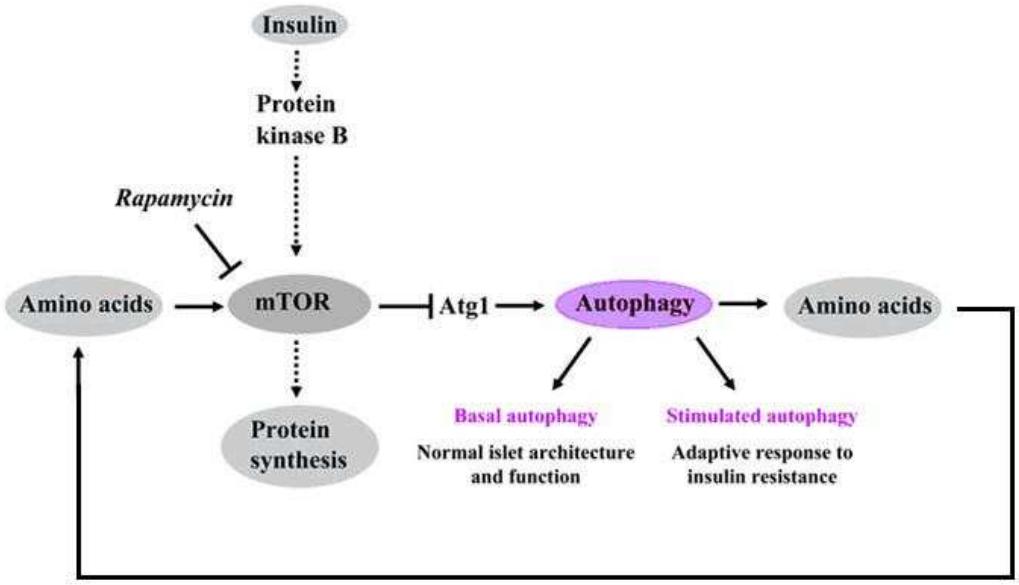

Figure 2.8.1 Regulation of autophagy by insulin and amino acids. Amino acids in a feedback loop*. Activation of mTOR requires input from amino acids and insulin, which next stimulates protein synthesis and phosphorylates Atg13, which results in inactive form of Atg1. Amino acids, which are the products of autophagy pathway, play a role of feedback regulator for the process [Yang et al., 2005; figure taken from Meijer and Codogno, 2008].*

2.8.1 Mechanism of amino acids sensing in mTOR-mediated signalling

Amino acids can regulate autophagy via modifications in the signalling pathways activity. The main question is how the level of amino acids is sensed and signals to mTOR (figure 2.8.2). Amino acids are provided into the cell via amino acid transporters. Currently few mechanisms of amino acid sensing are proposed, but recent studies suggest that intracellular amino acid concentration is responsible for the control of mTOR signalling pathway (intracellular amino acid receptor), rather than a membrane amino acid transporter [*Kim, 2009*].

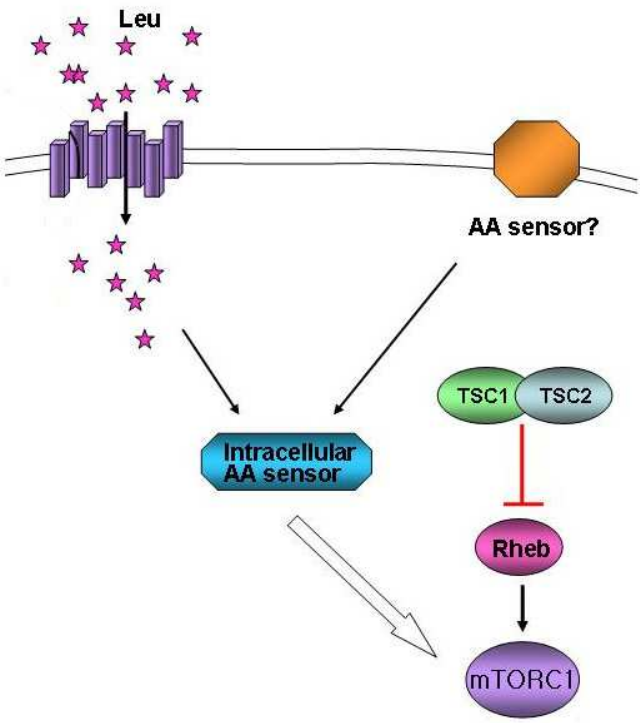

Figure 2.8.2 Mechanisms of amino acid sensing by mTOR. *Amino acids may activate mTORC1 by membrane sensor or intracellular amino acid sensor [Kim, 2009].*

Nutrients conditions regulate mTORC1 activity, despite the mechanism is not well known. Amino acids inhibit TSC1/2 complex and that could be one of the mechanisms for intracellular amino acid sensing. Another study suggests that amino acids stimulate the binding of Rheb with mTOR. Rheb activates mTORC1 by binding to mTOR via FKBP38 and this association is reduced when amino acids are depleted. It could be proposed that mTOR itself is the amino acid sensor – then the effect of nutrients is indirect and amino acids could lower the concentration of an inhibitor which is involved in with the Rheb-mTOR association [*Meijer, 2008*]. For more detailed information of the mTOR activation see chapter 2.7.2.

3. Biochemical Pathway Modelling

This section describes some simple ideas of biochemical pathway modelling and approaches which are used in systems biology. A main target of systems biology is to turn a biochemical reactions networks maps into dynamic models. Using mathematical analysis or computer simulations, these models can enhance the knowledge of biochemical mechanisms, help to understand of dynamical interactions between components and also can predict behaviour of the system in response to different kinds of stimuli.

Several modelling approaches for biochemical reactions or networks have been used to study metabolic networks and signalling cascades [*Klipp, 2005*]. Models of signalling cascades are often based on ordinary differential equations (ODE). According to Huber, they are "so far probably the most successful mathematical approaches to describe the molecular dynamics during cell death signalling" [*Huber et al., 2009*]. ODE models describe the fluctuation of states and assume a spatial homogeneity of distribution of the components within the modelled cell. They contain all biochemical reactions that can take a part in the modelled network and the relevant reaction rates and kinetic constants that characterize relations between reactants and products.

In this section we describe kinetic modelling of individual biochemical reactions. The elementary quantity expressions are:

a) the concentration S of a substance S (number of the molecules per volume)

b) the reaction rate υ (change of concentration S per time).

In biochemical kinetics we take advantage of assumption that "the reaction rate υ at a certain point in time and space can be expressed as a unique function of the concentrations of all substances at this point in time and space" [*Klipp, 2005*].

3.1 The law of mass action

Kinetics of the biochemical reactions is based on the mass action law, proposed in 1864 by Guldberg and Waage. It says that "the reaction rate is proportional to the probability of a collision of the reactants. This probability is in turn proportional to the concentration of reactants to the power of the molecularity, i. e., the number in which they enter the specific reaction" [*Klipp, 2005*].

In signalling networks most reactions are modelled using the law of mass action. Other approach used in systems biology is a Michaelis – Menten kinetic.

Based on some elementary biochemical reactions and on mass action kinetic, here are basic examples for ODE generation:

a) Binding/Dissociation:

This reaction is reversible and in biochemical sense it means protein synthesis (for example inhibitor – target interaction).

Consider the following reaction where A and B react to form a complex AB:

$$A + B \underset{k_{-1}}{\overset{k_1}{\leftrightarrow}} AB \tag{3.1.1}$$

According to the law of mass action the reaction rate v is proportional to the product of the reactant concentrations:

$$\upsilon = \upsilon_{+} - \upsilon_{-} = k_1 \cdot A \cdot B - k_{-1} \cdot AB \tag{3.1.2}$$

where:

υ_{+} forward reaction

υ_{-} backward reaction

k_1, k_{-1} kinetic/rate constants.

We can describe the temporal change in concentration of the proteins and the complex using the ordinary differential equations:

$$\frac{dA}{dt} = \frac{dB}{dt} = -\upsilon = -k_1 \cdot A \cdot B + k_{-1} \cdot AB \tag{3.1.3}$$

$$\frac{dAB}{dt} = \upsilon = k_1 \cdot A \cdot B - k_{-1} \cdot AB \tag{3.1.4}$$

b) Irreversible cleaving:

$$A + C \xrightarrow{k_2} A + C' + C'' \tag{3.1.5}$$

This reaction is irreversible and in a biochemical sense it can be analysed as an enzyme A, without being changed itself, cleaving protein C into two fragments C' and C'' and returning the enzyme.

From the law of mass action, reaction rate is:

$$\upsilon = k_2 \cdot A \cdot C \tag{3.1.6}$$

Based on this reaction we can illustrate the dynamic of the concentrations of reactants using ODEs:

$$\frac{dC}{dt} = -k_2 \cdot A \cdot C \tag{3.1.7}$$

$$A = const \Rightarrow \frac{dA}{dt} = 0 \tag{3.1.8}$$

$$\frac{dC^{'}}{dt} = \frac{dC^{''}}{dt} = k_2 \cdot A \cdot C \tag{3.1.9}$$

c) Degradation:

$$A \xrightarrow{k} 0 \tag{3.1.10}$$

The kinetics of this simple decay can be described by reaction rate:

$$\upsilon = k \cdot A \tag{3.1.11}$$

The dynamic of the concentration of substrate A can be illustrated by ODE:

$$\frac{dA}{dt} = -k \cdot A \tag{3.1.12}$$

The ODE's integration from time $t=0$ and initial concentration A_0, to time t with concentration $A(t)$ leads to the expression:

$$A(t) = A_0 \cdot e^{-k \cdot t} \tag{3.1.13}$$

The equation 3.1.13 formulates that the quantity decreases at a rate proportional to its value.

3.2 Michaelis – Menten Kinetics

In 1902 Brown introduced the first enzymatic mechanism which was for all one-substrate reactions [*Klipp, 2005*]:

$$E + S \underset{k_{-1}}{\overset{k_1}{\leftrightarrow}} ES \xrightarrow{k_2} E + P \tag{3.2.1}$$

The reaction illustrates a reversible formation of the enzyme-substrate complex ES from the enzyme E and substrate S and irreversible deliver of the product P. The systems of ODEs for this reaction are:

$$\frac{dS}{dt} = -k_1 \cdot E \cdot S + k_{-1} \cdot ES \tag{3.2.2}$$

$$\frac{dE}{dt} = -k_1 \cdot E \cdot S + (k_{-1} + k_2) \cdot ES \tag{3.2.3}$$

$$\frac{dES}{dt} = k_1 \cdot E \cdot S - (k_{-1} + k_2) \cdot ES \tag{3.2.4}$$

$$\frac{dP}{dt} = k_2 \cdot ES \tag{3.2.5}$$

The reaction rate is equivalent to the rate of decay of the substrate and of product formation:

$$v = -\frac{dS}{dt} = \frac{dP}{dt} \tag{3.2.6}$$

To simplify the ODE system some assumptions can be made:

a) the transformation of the enzyme E and substrate S to ES complex and the opposite reaction is much faster than the decay of ES complex into enzyme E and product P (*quasi-equilibrium* between the free enzyme and the ES complex). In terms of the kinetic constants this assumption can be expressed as:

$$k_1, k_{-1} >> k_2 \tag{3.2.7}$$

b) to reached a steady state the ES complex has to remain constant and this condition is accomplished only if the initial concentration of the substrate S is much larger than the concentration of enzyme E: $S(t=0) >> E$; the more general postulate of *quasi-steady state* of the ES complex:

$$\frac{dES}{dt} = 0 \tag{3.2.8}$$

The reaction rate can be extract by using above ODEs (3.2.2-3.2.5) and the assumption (3.2.8) for ES. Adding (3.2.3) and (3.2.4):

$$\frac{dE}{dt} + \frac{dES}{dt} = 0 \tag{3.2.9}$$

results in:

$$E_{total} = E + ES \tag{3.2.10}$$

what means that total concentration of enzyme, free form or in complex, remains constant – enzyme is not produced and not consumed.

Adding equation (3.2.10) to (3.2.4) under the steady-state assumption (3.3.8):

$$ES = \frac{E_{total} \cdot S}{S + \frac{k_{-1} + k_2}{k_1}} \tag{3.2.11}$$

and the reaction rate from (3.2.6) and (3.2.5):

$$\upsilon = k_2 \cdot ES = \frac{k_2 \cdot E_{total} \cdot S}{S + \frac{k_{-1} + k_2}{k_1}}. \tag{3.2.12}$$

Above equation we can write in shorter way, using:

$$V_{\max} = k_2 \cdot E_{total} \tag{3.2.13}$$

$$K_m = \frac{k_{-1} + k_2}{k_1} \tag{3.2.14}$$

where:

$V_{\max}$ is the maximal velocity – maximal ratio that can be obtained when the enzyme is completely saturated with substrate;

K_m is the Michaelis constant – is equivalent to the substrate concentration that produces the half-maximal reaction rate.

Now we can present equation (3.2.12) as an expression of Michaelis-Menten kinetics:

$$v = \frac{V_{\max} \cdot S}{S + K_m} \tag{3.2.15}$$

The figure below shows the dependence of reaction rate on substrate concentration, and helps illustrate the meaning of the parameters:

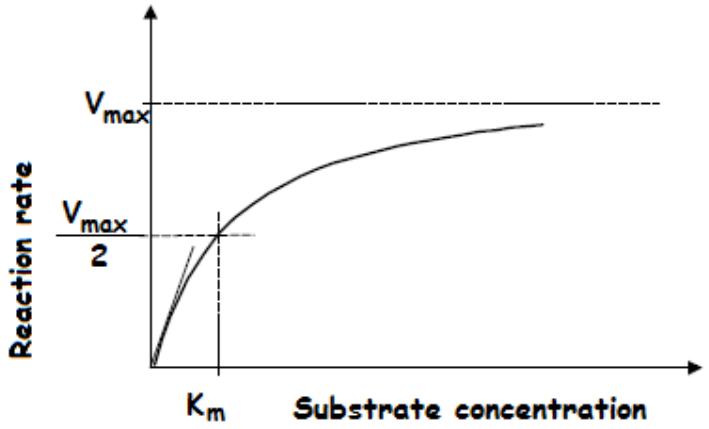

Figure 3.2.1 Plot of reaction rate versus substrate concentration in Michaelis-Menten kinetics *[taken from Klipp et al., 2005].*

3.3 Negative feedback loop

Feedback loops are the principal elements for all kind of regulation and control. In general, when a variable of a system inhibits its own level of activity, we say that this variable is subject to negative feedback. Negative feedback plays an important role in metabolic pathways, for example in amino acids synthesis, where a negative signal from the product at the end to the precursor at the beginning of the system can avoid an overproduction of this amino acid [*Klipp, 2005*]. Another example is a product of a gene which inhibits its own gene.

To illustrate some possible effects of negative feedback let's analyze a chain of six reactions with a substrate, five metabolites and final product:

$$P_0 \xleftrightarrow{v_1} S_1 \xleftrightarrow{v_2} S_2 ... S_5 \xleftrightarrow{v_6} P_6 \tag{3.3.1}$$

for which kinetics rate expressions is $v_i = S_{i-1} \cdot k_i$ for $i = 1,...,6$, where k_i corresponds to kinetics constant of i-th metabolite.

Feedback inhibition of the first reaction by the j-th metabolite is:

$$v_1 = \frac{S_1 \cdot k_1}{1 + S_j \cdot K_I} \tag{3.3.2}$$

where K_I corresponds to inhibition constant.

In the case of no feedback, all substrates concentrations reach a steady state in short time (see figure 3.4.1).

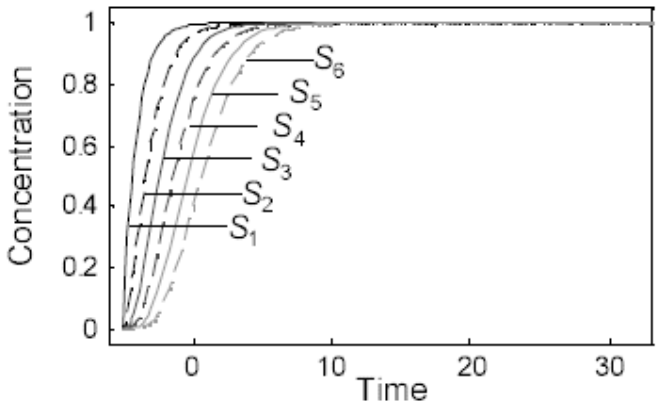

Figure 3.4.1 The dynamics of a simple reactions chain. *In the absence of feedback, all metabolite concentrations reach asymptotically a high constant level [Klipp, 2005].*

In the case when the feedback is from the second metabolite, the substrate concentrations reach a steady state but in significant lower level.

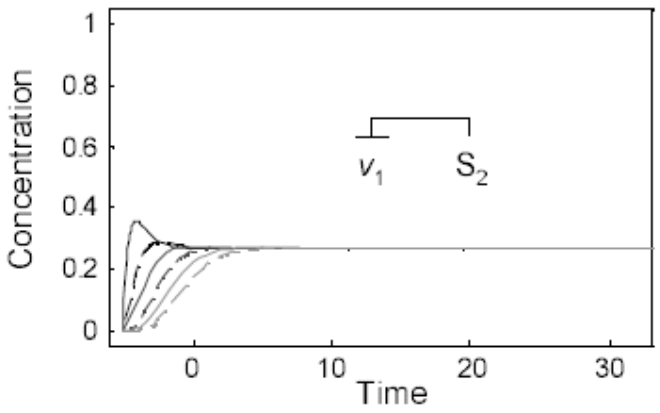

Figure 3.4.2 The dynamics of a simple reactions chain. *The second metabolite inhibits the first reaction [Klipp, 2005].*

In final example, when feedback is from the last metabolite resulting on inhibition of the first reaction, concentrations of substrates reach lower level than without feedback. A long acting feedback results in damped oscillations.

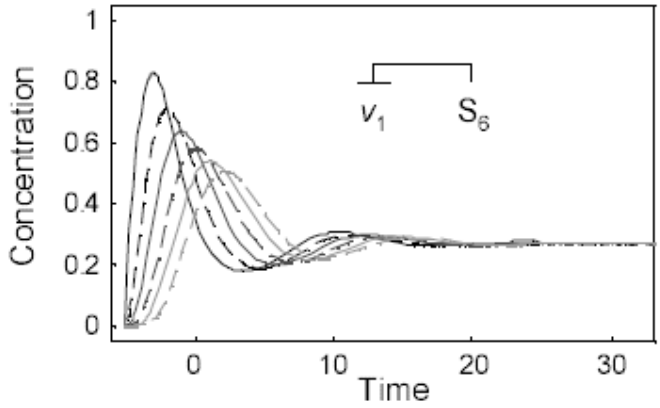

Figure 3.4.3 The dynamics of a simple reactions chain. *The long acting feedback creates damped oscillations and the level of substrate concentrations reach lower than without feedback steady state [Klipp, 2005].*

4. Mathematical modelling of amino acid control via autophagy as a feedback system

We propose a simple model of amino acid control in the cell via autophagy as the feedback system. The idea behind our model is based on literature which show amino acids in the feedback loop from degradation of proteins and back to building proteins. According to Yang, "Amino acids, which are the final products of autophagic protein degradation, act as negative feedback regulators for the process" [Yang et al., 2005]. In other words, the products of degradation via autophagy are essential for protein biosynthesis in nutrient limitation [Onodera and Ohsumi, 2005].

A brief description of the model is provided in this chapter, with biochemical reactions, mass balances, and kinetic equations and models parameters.

Chapter 4 describes mathematical modelling based on ODEs. In this part of the thesis we focus on the mTOR dependent induction of autophagy which occurs as a response of cells to amino acid depletion. A simplified version of autophagy induction is described by four reactions (R_1, R_3, R_5 and R_6). This model also trades on idea of amino acids from autophagy in a negative feedback to control level of total amino acid pool. We use here idea of time delay for the part of the pathway from autophagosome nucleation to degradation in lysosome and recycling.

Reactions involved in the induction of autophagy are complex. Autophagy can be initiated by many different interacting pathways (see figure 2.7.1, chapter 2): changes in cellular energy levels, nutrients availability and in response to growth factors stimulations. One of the main regulators of autophagy is the level of extracellular and

intracellular amino acids, which are sensed via mTOR. mTOR in an activated form promotes protein synthesis. Active mTOR keeps in hyperphosphorylated state Atg13, thus inhibits the induction of autophagy. Stressor signals, like starvation, inhibit mTOR activity and in turn induce autophagy. Autophagy also can be activated by intracellular debris (unfolded proteins and damaged organelles) and pathogens.

To simplify our work with autophagy model we start by modelling the mTOR – dependent pathway which is controlled via amino acid signalling and it involves: signal from amino acid external supply and from autophagy, Rheb, FKBP38, mTOR, Atg13 and Atg1. The diagram below displays connections between those elements.

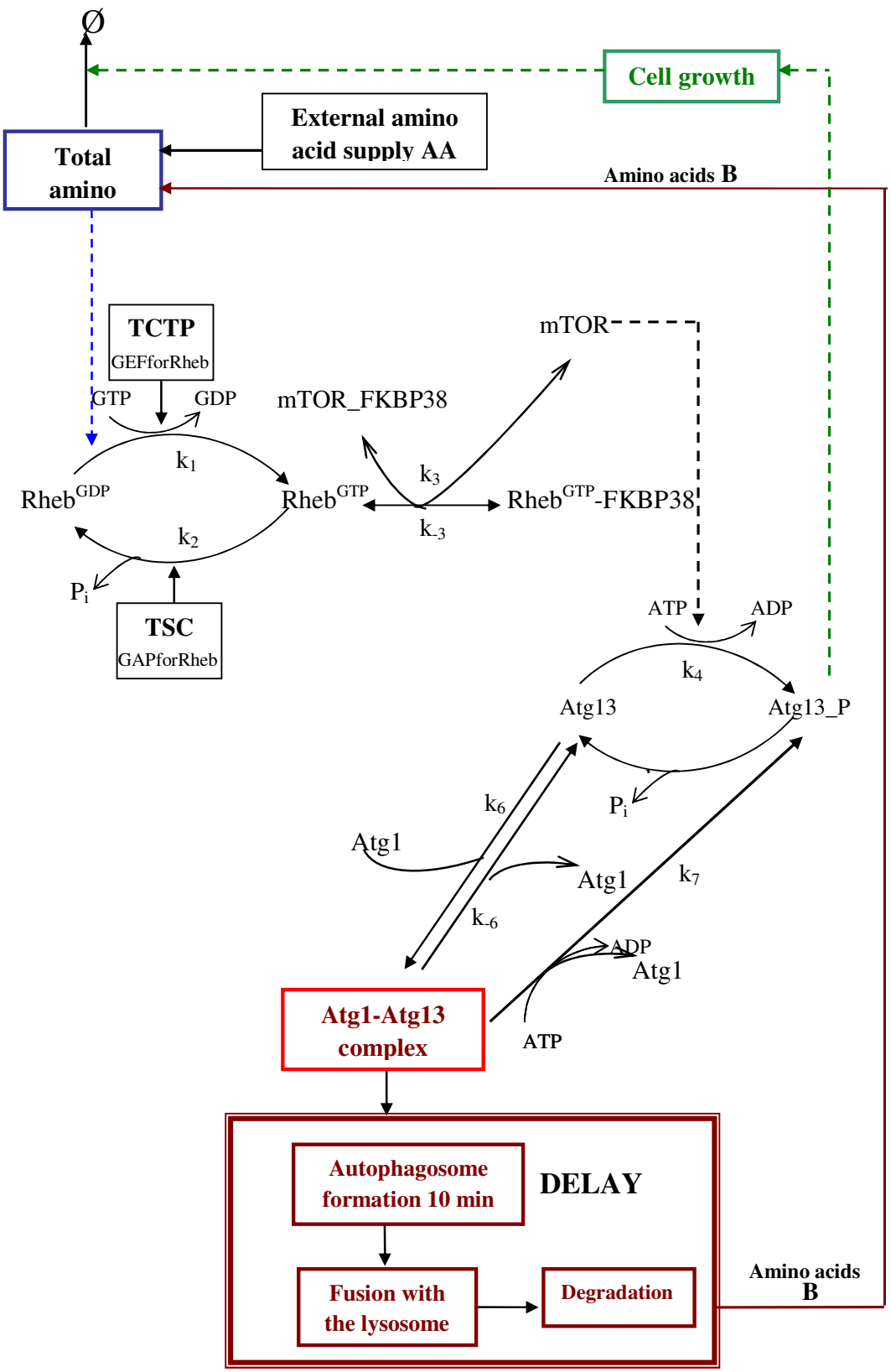
Ø
Cell growth
External amino acid supply AA
Total amino
Amino acids B
TCTP
GEFforRheb
GTP
GDP
mTOR
mTOR_FKBP38
k1
k3
Rheb^GDP
Rheb^GTP
Rheb^GTP-FKBP38
k2
k-3
Pi
TSC
GAPforRheb
ATP
ADP
k4
Atg13
Atg13_P
k6
Pi
Atg1
Atg1
k7
k-6
ADP
Atg1
Atg1-Atg13 complex
ATP
Autophagosome formation 10 min
DELAY
Fusion with the lysosome
Degradation
Amino acids B

Figure 4.1 Diagram of the autophagy induction. *Diagram was made based on scientific literature about autophagy pathway. It shows mTOR-dependent autophagy induction, which includes amino acid external supply, Rheb, FKBP38, mTOR, Atg13 and Atg1.*

The mTOR is a fundamental cell growth controller and its activity is regulated by Rheb in response to nutrient availability and growth factors [*Bai et al., 2007*]. Rheb regulates mTOR through FKBP38, which by binding to mTOR inhibits its activity. To prevent this association, Rheb interacts directly with FKBP38. In different words, FKBP38 is an inhibitor of mTOR, which in response to growth factor and nutrients conditions is antagonized by Rheb [*Bai et al., 2007*].

mTOR controls the level of phosphorylation of Atg13, one of the proteins involved in induction of autophagy pathway. Under nutrient – rich conditions, during the normal cell life, Atg13 occurs in highly phosphorylated form, which has low affinity for Atg1 kinase – another autophagy related protein, essential for induction of autophagy. In this case autophagy is suppressed [*T. Yorimitsu, 2005*]. Inhibition of mTOR results on dephosphorylation of Atg13, which in this form has higher affinity for Atg1. New created Atg1-Atg13 complex allows to switch from basal Cvt pathway (basal autophagy) to induced autophagy.

Reactions, which visualise mTOR activation/deactivation and autophagy induction, are based on diagram above:

Table 4.1 Reactions involved in autophagy induction.

Reaction	Reference
$R_1 : Rheb^{GDP} + GTP \xrightarrow[k_1 \downarrow]{\substack{TCTP \\ AA+B}} Rheb^{GTP} + GDP$	Bai & Jiang, 2009; Bai et al., 2007; Roccio et al., 2006; Avruch et al., 2006; Kim, 2009;
$R_2 : Rheb^{GTP} \xrightarrow[k_2 \downarrow]{TSC} Rheb^{GDP} + P_i$	Bai & Jiang, 2009; Bai et al., 2007; Kim, 2009; Zhang et al., 2003
$R_3 : Rheb^{GTP} + (mTOR\_FKBP38) \xleftrightarrow{k_3} \xleftrightarrow{k_3} (Rheb^{GTP}\_FKBP38) + mTOR$	Bai & Jiang, 2009; Bai et al., 2007; Kim, 2009; Sato et al., 2009; Wang et al., 2008
$R_4 : Atg13 + ATP \xrightarrow[k_4 \downarrow]{mTOR} (Atg13\_P) + ADP$	Kamada et al., 2000; Kamada et al., 2010; Klionsky and Emr, 2000;
$R_5 : (Atg13\_P) \xrightarrow[k_5 \downarrow]{?} Atg13 + P_i$	Kamada et al., 2000; Kamada et al., 2010; Hosokawa et al., 2009; Klionsky and Emr, 2000;
$R_6 : Atg13 + Atg1 \xleftrightarrow{k_6} (Atg1\_Atg13)$	Kamada et al., 2000; Hosokawa et al., 2009; Klionsky and Emr, 2000;
$R_7 : (Atg1\_Atg13) \xrightarrow[k_7 \downarrow]{mTOR} Atg1 + Atg13$	Kamada et al., 2000;

The rate expressions for reactions above are:

$$\upsilon_1 = k_1 \cdot Rheb^{GDP} \cdot (AA + B)$$
$$\upsilon_2 = k_2 \cdot Rheb^{GDP}$$
$$\upsilon_3 = k_3 \cdot Rheb^{GTP} \cdot (mTOR\_FKBP38)$$
$$\upsilon_{-3} = k_{-3} \cdot (Rheb^{GTP}\_FKBP38) \cdot mTOR$$
$$\upsilon_4 = k_4 \cdot Atg13 \cdot mTOR$$
$$\upsilon_5 = k_5 \cdot (Atg13\_P\_)$$
$$\upsilon_6 = k_6 \cdot Atg13 \cdot Atg1$$
$$\upsilon_{1-6} = k_{-6} \cdot (Atg1\_Atg13)$$
$$\upsilon_7 = k_7 \cdot (Atg1\_Atg13) \cdot mTOR$$

In the rate expressions some substrates are missing on purpose. If we assume that values of TSC and TSTP are constant, we do not have to take them into calculations (reaction R_1 and R_2). It is sufficient if the speed of the reaction R_1 is driven only by amino acids. Also to simplify our model initially we assume that energy equivalents such as GTP are not limited, therefore we can leave GTP, Pi and ATP out of the calculations (reaction R_1 and R_4). An unknown phosphatase takes part in reactionR_5, Atg13 dephosphorylation [*Klionsky and Emr, 2000; Kamada et al., 2000*]. With assumption that the amount of phosphatase does not change we do not include it into equations.

Based on reaction above we can describe the temporal change in concentration of the proteins and the complex by using an ordinary differential equation:

$$\frac{d(Rheb^{GDP})}{dt} = -k_1 \cdot Rheb^{GDP} \cdot [AA + B] + k_2 \cdot Rheb^{GTP}$$

$$\frac{d(Rheb^{GTP})}{dt} = k_1 \cdot Rheb^{GDP} \cdot [AA + B] - k_2 \cdot Rheb^{GTP} -$$
$$-k_3 \cdot Rheb^{GTP} \cdot (mTOR\_FKBP38) + k_{-3} \cdot mTOR \cdot (Rheb^{GTP}\_FKBP38)$$

$$\frac{d(Rheb^{GTP}\_FKBP38)}{dt} = k_3 \cdot Rheb^{GTP} \cdot (mTOR\_FKBP38) - k_{-3} \cdot mTOR \cdot (Rheb^{GTP}\_FKBP38)$$
$$\frac{d(mTOR\_FKBP38)}{dt} = -k_3 \cdot Rheb^{GTP} \cdot (mTOR\_FKBP38) + k_{-3} \cdot mTOR \cdot (Rheb^{GTP}\_FKBP38)$$
$$\frac{d(mTOR)}{dt} = k_3 \cdot Rheb^{GTP} \cdot (mTOR\_FKBP38) - k_{-3} \cdot mTOR \cdot (Rheb^{GTP}\_FKBP38)$$
$$\frac{d(Atg13)}{dt} = -k_4 \cdot Atg13 \cdot mTOR + k_5 \cdot (Atg13\_P) - k_6 \cdot Atg13 \cdot Atg1 + k_{-6} \cdot (Atg1\_Atg13)$$
$$\frac{d(Atg13\_P)}{dt} = k_4 \cdot Atg13 \cdot mTOR - k_5 \cdot (Atg13\_P) + k_7 \cdot (Atg1\_Atg13) \cdot mTOR$$
$$\frac{d(Atg1\_Atg13)}{dt} = k_6 \cdot Atg13 \cdot Atg1 - k_{-6} \cdot (Atg1\_Atg13)$$
$$\frac{d(Atg1)}{dt} = -k_6 \cdot Atg13 \cdot Atg1 + k_{-6} \cdot (Atg1\_Atg13) + k_7 \cdot (Atg1\_Atg13) \cdot mTOR$$

4.1 Model parameterization

This section with details describes model parameterization and implementation, and gives an explanation of methods which were used to obtain set of parameters. Our mathematical model is calibrated using published experimental data on the autophagy pathway in mammalian cells.

4.1.1 Parameterization of kinetic constants k_1 and k_2

Parameters k_1 and k_2 for the first pair of reactions (figure 4.1.1) were derived from the two publications by Inoki et al and Marshall et al [*Inoki et al., 2003 and Marshall et al., 2009*].

Figure 4.1.1 represents the first reactions which are implemented in our model. The activity of Rheb, which is a small GTPase, depends on its nucleotide-binding state, which is controlled by a GTPase-activating protein (GAP) and a guanine nucleotide exchange factor (GEF). The GAP for Rheb is the TSC1/TSC2 complex, which stimulates GTP hydrolysis. Recently, TCTP has been suggested to be the GEF for Rheb [*Bai and Jiang, 2009*].

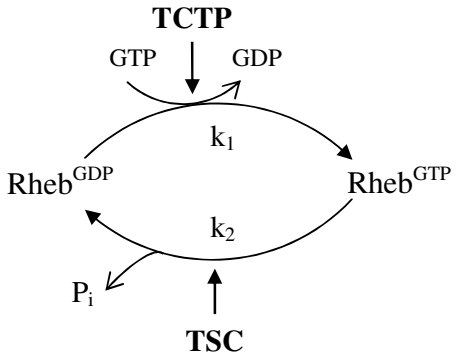

Figure 4.1.1 Cycling of Rheb GTPase protein between the active and inactive forms. *Conversion of the active $Rheb^{GTP}$ into the inactive $Rheb^{GDP}$ form by hydrolysis of GTP is catalyzed by TSC (GAP for Rheb). The reverse reaction is promoted by TCTP (GEF for Rheb) [references: Bai & Jiang, 2009; Bai et al., 2007; Roccio et al., 2006; Avruch et al., 2006; Kim, 2009; Zhang et al., 2003].*

As was mentioned in the previous chapter, we can assume that the amounts of TSC and TSTP are constant, so here we do not need to consider them in the calculations. Also to simplify our model, initially we assume that energy equivalents

such as GTP are not limited. Therefore we can leave GTP, GDP and P_i out of the calculations.

Simplified rate expressions extracted from the figure 4.1.1:

$$v_1 = k_1 \cdot Rheb^{GDP}$$
$$v_2 = k_2 \cdot Rheb^{GTP}$$

4.1.1.1 Parameter k_2

Inoki et al. showed that the TSC1/TSC2 complex stimulates the GTP hydrolysis of Rheb. In figure 1C from that publication the authors displayed the time-dependent GTP hydrolysis of Rheb stimulated by TSC, as measured by radioactive counting of free ^{32}P-phosphate, which is released during hydrolysis. From the experimental data shown we quantified that after 30 minutes the relative activity of free ^{32}P-phosphate slowly approached saturation. Based on that partial set of data we extrapolated that in the presence of TSC almost all (95%) $Rheb^{GTP}$ is converted into $Rheb^{GDP}$ within 60 minutes with a kinetic closely resembling an exponential decay (figure 4.1.2).

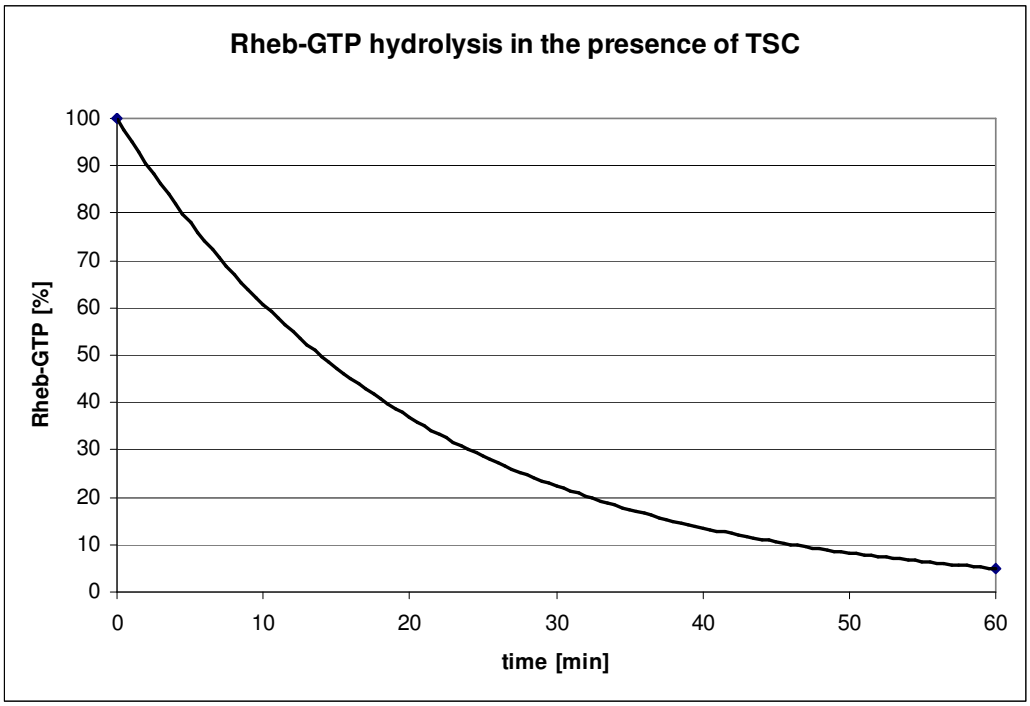

Figure 4.1.2 Representation of the Rheb^{GTP} hydrolysis. *The plot represents the curve of the exponential decay for the Rheb^{GTP} hydrolysis in the presence of TSC, which catalyses this reaction. The time of 95% completion of GTP hydrolysis was derived from experimental data from Inoki et al., 2003 and used to plot the exponential decay curve.*

The curve equation for the exponential decay is:

$$y = y_0 \cdot e^{-k_2 \cdot t} \tag{4.1.1}$$

where y is a quantity at time t, y_0 is an initial amount of Rheb^{GTP}, and k_2 indicates the decay constant. From (4.1.1) and the assumption that at time $t = 60\,\text{min}$ only 5% of Rheb^{GTP} is left, the decay rate is:

$$k_2 = \frac{\ln 0.05}{-t} = 0.04992\ \text{min}^{-1} \tag{4.1.2}$$

The half time of the $Rheb^{GTP}$ hydrolysis thus calculated as

$$t_{1/2} = \frac{\ln 2}{k_2} \cong 14 \text{ min} \tag{4.1.3}$$

During the course of this study another paper was published, which we could use for our model parameterization [*Marshall et al., 2009*]. The authors explored the molecular mechanism of the $Rheb^{GTP}$ hydrolysis alone or in the presence of TSC. Experiments were based on a real-time assay, which took advantage of nuclear magnetic resonance (NMR) spectroscopy. According to their results, "addition of TSC to GTP-bound Rheb at a 1:2 molar ratio increased Rheb's rate of GTP hydrolysis by 50-fold (compared to the experiment of GTP hydrolysis in absence of TSC) to $k = 0.031 \text{min}^{-1}$" [*Marshall et al., 2009*]. The time of 95% $Rheb^{GTP}$ hydrolysis based on this rate constant calculates as 100 minutes, with a corresponding half time of the reaction $t_{1/2} = 21.7 \text{min}$. While this is slightly longer than the half time determined from Inoki et al., it still displays a good match between independent studies. We therefore decided to calculate the average value of k_2 from these two publications, which is:

$$k_2 = 0.04046 \text{ min}^{-1}$$

The average half time of the $Rheb^{GTP}$ hydrolysis is:

$$t_{1/2} \cong 17 \text{ min.}$$

Using the model in absence of all reactions except for R_2 we could show that k_2 corresponded to published data. The plot below shows the hydrolysis of $Rheb^{GTP}$ in the presence of TSC:

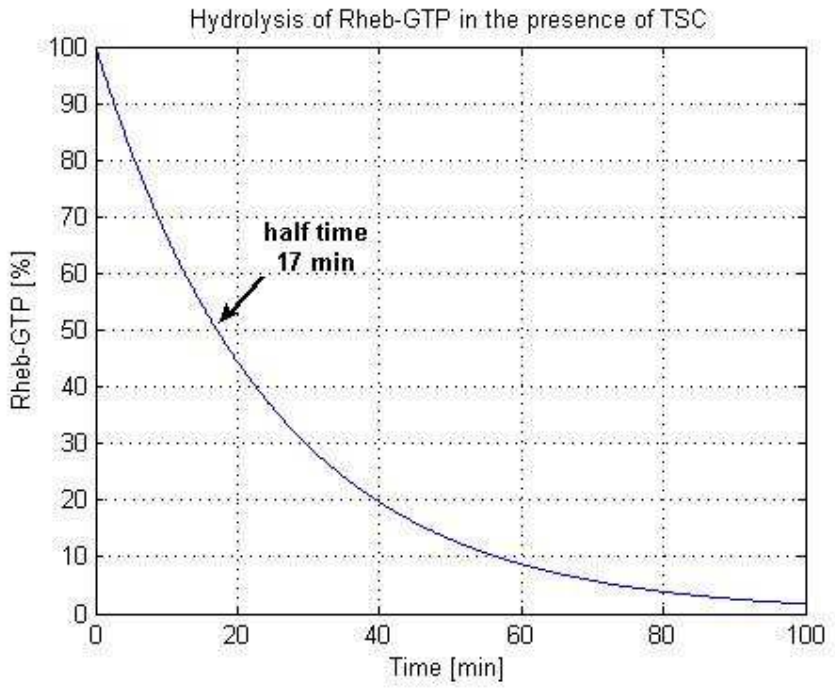

Figure 4.1.3 Result of the simulation for reaction R_2 ***with decay constant*** $k_2 = 0.04046$ ***min^{-1}.*** *The plot was made as a result of a simulation in SBtoolbox for MatLab and shows the exponential decay of* $Rheb^{GTP}$ *by TSC catalysed hydrolysis. The half time for this reaction is* $\cong 17$ *minutes, corresponding well with published data.*

4.1.1.2 Parameter k_1

To calculate the parameter k_1 for our model, we focused again on Inoki et al. Experimental data from this paper indicated that the ratio of GTP/GDP- bound Rheb in

living cells comes to $\frac{Rheb^{GTP}}{Rheb^{GDP}} = 1.66$. The ratio is formulated in the steady state condition, that is:

$$\frac{dRheb^{GTP}}{dt} = \frac{dRheb^{GDP}}{dt} = 0 \tag{4.1.4}$$

From the ordinary differential equations, which describes change in concentrations of the proteins, where $\frac{dRheb^{GDP}}{dt} = -k_1 \cdot Rheb^{GDP} + k_2 \cdot Rheb^{GTP}$ and $\frac{dRheb^{GTP}}{dt} = k_1 \cdot Rheb^{GDP} - k_2 \cdot Rheb^{GTP}$, the ratio is equivalent to:

$$\frac{Rheb^{GTP}}{Rheb^{GDP}} = \frac{k_1}{k_2} \tag{4.1.5}$$

From this we calculated k_1 by

$$k_1 = k_2 \frac{Rheb^{GTP}}{Rheb^{GDP}} \tag{4.1.6}$$

According to the equation above, parameter k_1 for our model comes to

$$k_1 = 0.06716 \text{ min}^{-1}$$

The half time for the TCTP catalysed conversion of $Rheb^{GDP}$ into $Rheb^{GTP}$ calculates as:

$$t_{1/2} \cong 10 \text{ min.}$$

Using the model in absence of all reactions except for R_1 a similar simulation as before was made to check the correct software implementation of the parameter k_1, which drives reverse reaction to $Rheb^{GTP}$ hydrolysis, converting $Rheb^{GDP}$ to $Rheb^{GTP}$:

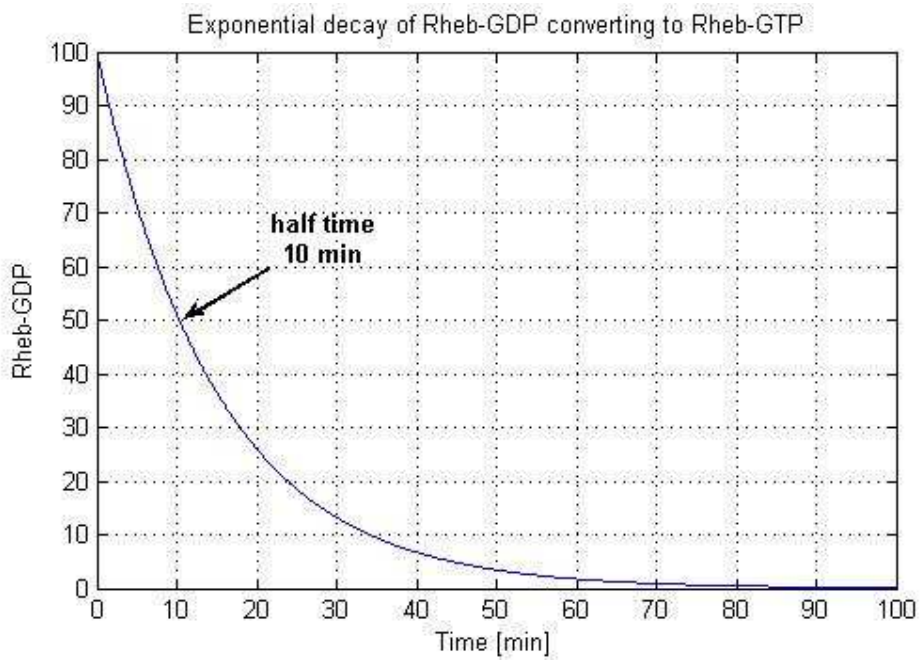

Figure 4.1.4 Result of the simulation for reaction R_1 ***with decay constant for*** $Rheb^{GDP}$ $k_1 = 0.06716$ ***min^{-1}.*** *The plot was made by a simulation in SBtoolbox for MatLab and shows the exponential decay of* $Rheb^{GDP}$ *by conversion into* $Rheb^{GTP}$*. The half time for this reaction is* $\cong 10$ *minutes, which corresponds well with calculated half time above).*

4.1.1.3 Model testing for parameters k_1 and k_2

Using SBtoolbox, the rate expressions based on figure 4.1.1 and parameters k_1 and k_2 obtained as above, we tested the model for the two first reactions, which represents turnover of $Rheb^{GTP}$ into $Rheb^{GDP}$ and *vice versa*. The simulations conducted show two different initial conditions: a) when $Rheb^{GTP}(0) = 100$ and $Rheb^{GDP}(0) = 0$; b) when $Rheb^{GTP}(0) = 0$ and $Rheb^{GDP}(0) = 100$. The first condition represents oversaturated nutrient conditions, when all Rheb is in an active GTP-bound form. The second condition mimics nutrients starvation, when all $Rheb^{GTP}$ is converted to the inactive form. These two scenarios thus show opposite extreme conditions.

In the first scenario we expect that $Rheb^{GTP}$ levels should decrease, because a part of it is converted to $Rheb^{GDP}$. On the other hand, the level of $Rheb^{GDP}$ should increase. Ultimately, a steady state ratio $\frac{Rheb^{GTP}}{Rheb^{GDP}}$ of 1.66 was expected to be achieved.

In the second condition we expected that $Rheb^{GTP}$ levels increase because of conversion of $Rheb^{GDP}$ into $Rheb^{GTP}$. In this scenario also the experimentally determined steady state ratio of 1.66 should be reached.

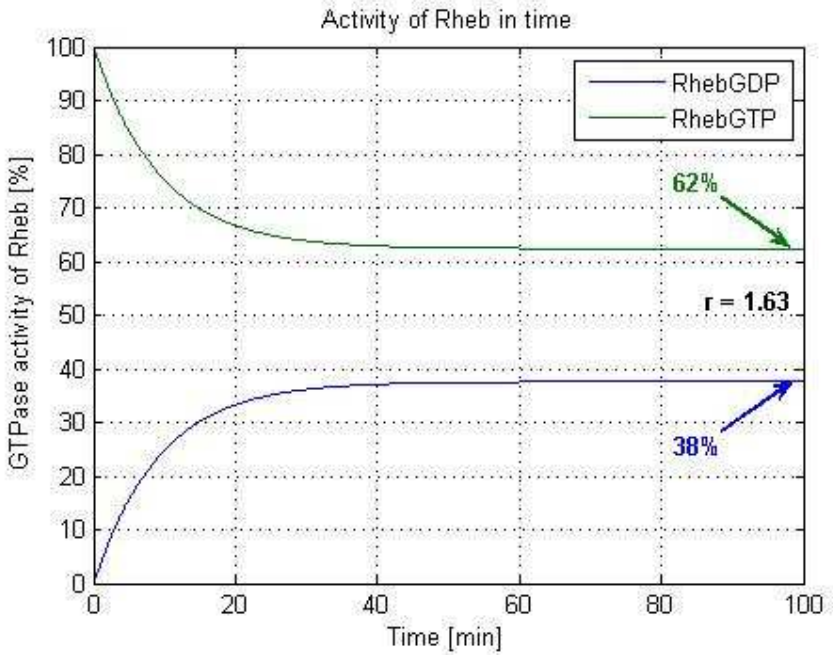

Figure 4.1.5a Result of the simulation for reactions R_1 ***and*** R_2 ***when*** $Rheb^{GTP}(0) = 100$ ***and*** $Rheb^{GDP}(0) = 0$. *A ratio* $r = 1.63$ *of* $\frac{Rheb^{GTP}}{Rheb^{GDP}}$ *is reached after 100 minutes, closely approaching the steady state of 1.66.*

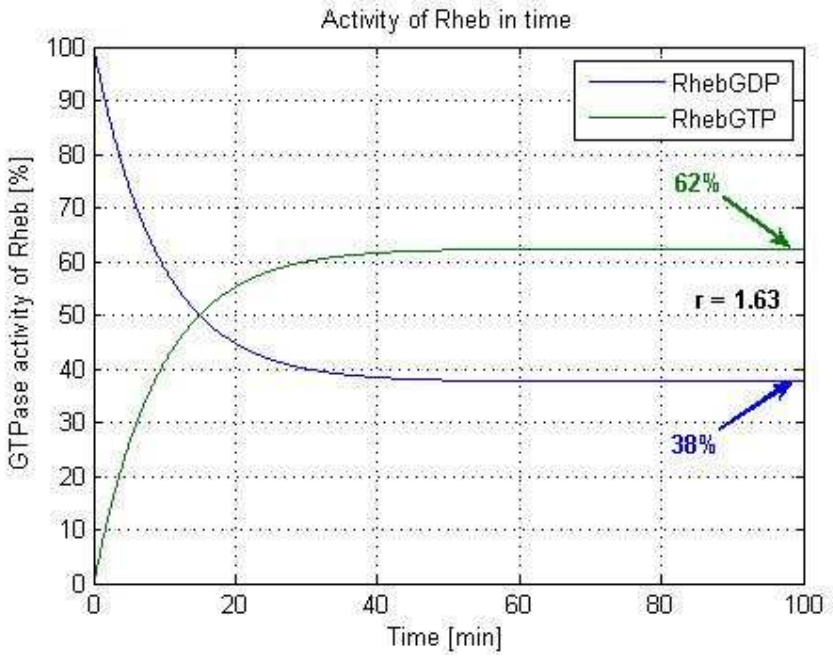

Figure 4.1.5b Result of the simulation for reactions R_1 ***and*** R_2 ***when*** $Rheb^{GTP}(0) = 0$ ***and*** $Rheb^{GDP}(0) = 100$. *A ratio* $r = 1.63$ *of* $\frac{Rheb^{GTP}}{Rheb^{GDP}}$ *is reached after 100 minutes, closely approaching the steady state of 1.66.*

In both plots (4.1.5a and 4.1.5b) we can see that the value of the ratio of GTP/GDP-bound Rheb after 100 minutes is $\frac{Rheb^{GTP}}{Rheb^{GDP}} = 1.63$. We also made simulations for the same conditions for a time 1000 minutes (figure not shown). We could observe that the final levels of $Rheb^{GTP}$ and $Rheb^{GDP}$ were slightly different than this one after 100 minutes. They reached 62.5% and 37.5% respectively, which gives a ratio 1.66.

We therefore conclude that we successfully implemented this pair of reactions and can re-model the published biological behaviour of the reactions R_1 and R_2.

4.1.2 Parameterization of kinetic constants k_3 and k_{-3}

Parameters k_3 and k_{-3} for the second pair of reactions (figure 4.1.6) were derived from the two publications by Bai et al and Sato et al [*Bai et al., 2007 and Sato et al., 2009*].

Figure 4.1.6 represents the following reactions which are implemented in our model. FKBP38, by direct binding to mTOR, inhibits the activity of mTORC1 [*Bai and Jiang, 2009; Bai et al., 2007*]. The interaction of FKBP38 with mTOR is controlled by Rheb in the GTP-dependent manner [*Bai and Jiang, 2009*]. $Rheb^{GTP}$ inhibits this association by competitively binding to FKBP38 [*Bai et al., 2007*], and in turn results in activation of mTOR.

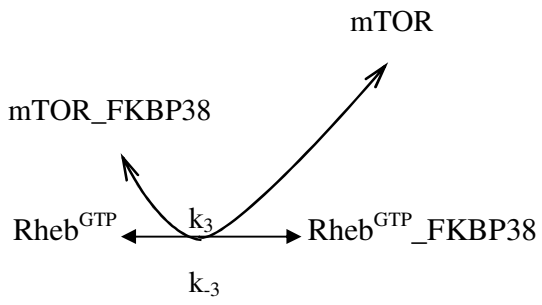

Figure 4.1.6 Reaction of $Rheb^{GTP}$-dependent mTOR activation and FKBP38-dependent mTOR inhibition. *Rheb in the active GTP-bound form binds to FKBP38 and leads to mTOR activation. In the reverse reaction mTOR is inhibited by FKBP38 through direct binding [references for that reactions: Bai & Jiang, 2009; Bai et al., 2007; Kim, 2009; Sato et al., 2009; Wang et al., 2008].*

Rate expressions extracted from the figure 4.1.6:

$$\upsilon_3 = k_3 \cdot Rheb^{GTP} \cdot (mTOR\_FKBP38)$$

$$v_{-3} = k_{-3} \cdot (Rheb^{GTP} \_ FKBP38) \cdot mTOR$$

4.1.2.1 Parameter k_3

Sato and colleagues experimentally showed that $Rheb^{GTP}$ activates mTOR [*Sato et al., 2009*]. Cells were first starved to shut down mTOR activity. In starvation mTOR binds to its endogenous inhibitor FKBP38. The kinase activity was measured by measuring phosphorylation of the mTOR substrate 4E-BP1. The phosphorylation of 4E-BP1 during the starvation period is minimal, but the addition of $Rheb^{GTP}$ enhanced the mTOR kinase activity substantially (figure 4.1.7).

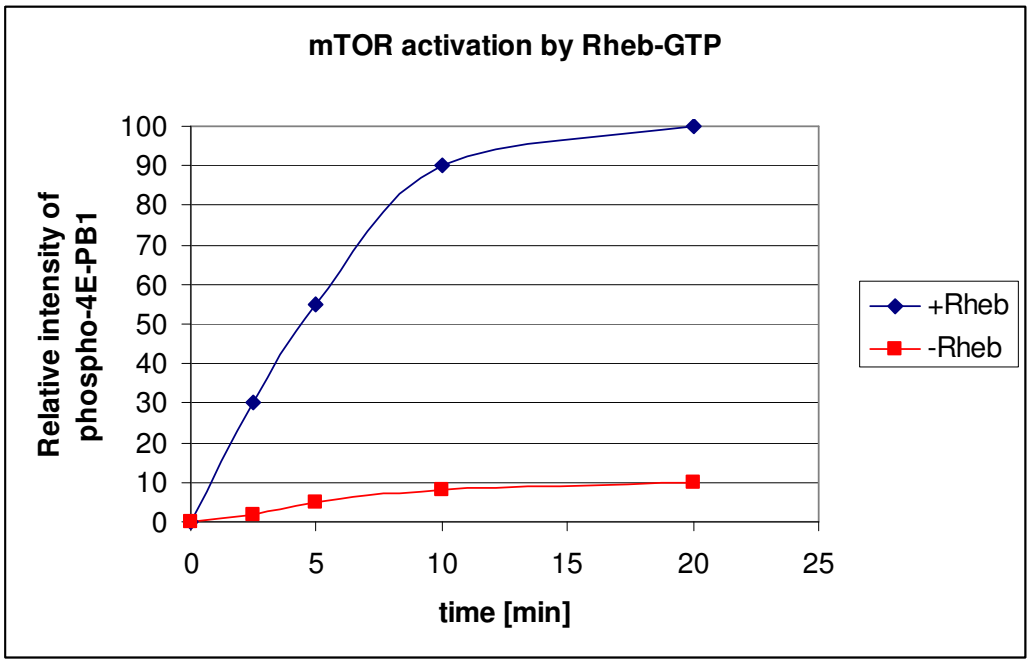

Figure 4.1.7 mTOR activation by $Rheb^{GTP}$. *Activation of mTOR is measured as an intensity of the phosphorylation of 4E-BP1. Figure shows results in starvation (red squares) and after addition of $Rheb^{GTP}$ (dark blue squares). Plot based on figure 1C, page 12785 from Sato et al., 2009, modified and plotted in Microsoft Office Excel 2003.*

As we can see, after addition of active Rheb to the starving cells, full activation of mTOR occurs in 20 minutes (figure 4.1.7). According to the figure above and the figure 4.1.6, we therefore can say that time to achieve completion of reaction R_3 is approximately 20 minutes. Based on all this information we can assume that after addition of Rheb, amount of an inactive mTOR-FKBP38 complex decrease with the same kinetics as mTOR activity increases (figure 4.1.8).

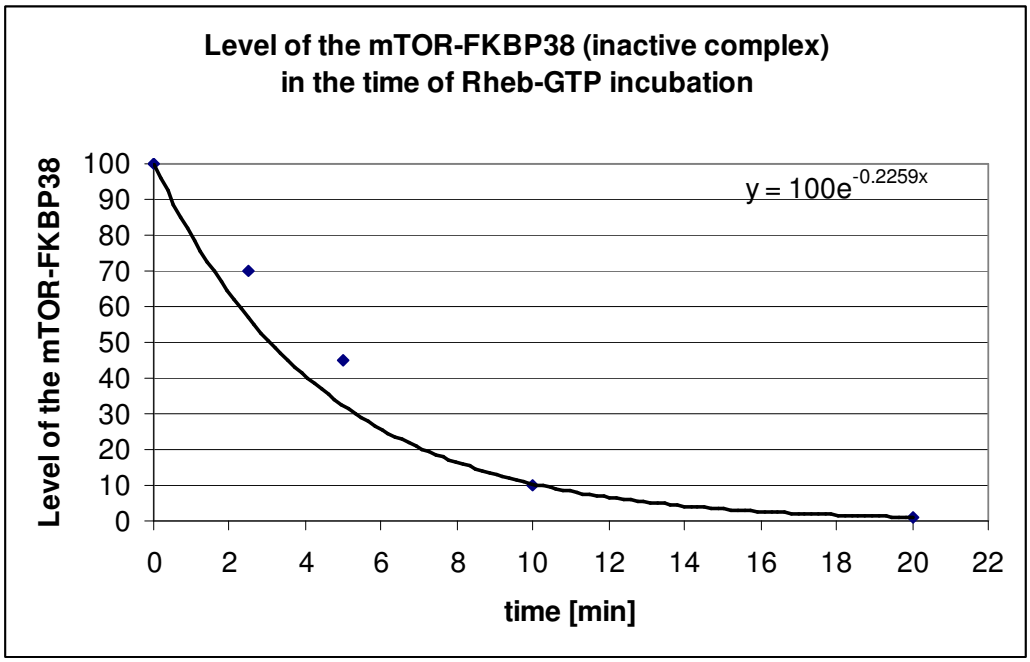

Figure 4.1.8 Decrease of the mTOR_FKBP38 complex after addition of Rheb^{GTP} to the starving cells. *The equation of the exponential decay, with the decay constant* $k_3 = 0.2259\ min^{-1}$*, was given after adding the best suited trend line in Microsoft Office Excel 2003. Plot made based on figure 5.6 and Bai et al., 2007.*

The half time of the mTOR-FKBP38 complex decreasing

$$t_{1/2} = \frac{\ln 2}{k_3} \cong 3 \text{ min} \tag{4.1.7}$$

which also can be observe from the figure 4.1.8.

As we can see from the rate expression, which is based on the figure 4.1.6, $\upsilon_3 = k_3 \cdot Rheb^{GTP} \cdot (mTOR\_FKBP38)$, reaction R_3 is dependent on $Rheb^{GTP}$. Both mTOR_FKBP38 complex and $Rheb^{GTP}$ are reactants consumed in reaction R_3. These reactions are different to the reactions in the previous chapter; here we have two reactants and we can say that they have a nature of second-order process, in which the concentrations of the two reactants behave the same.

For a second-order reactions the half time is depended on the initial value of the reactant A:

$$t_{1/2} = \frac{1}{k \cdot [A_0]} \tag{4.1.8}$$

Base on above equation we could calculate the rate constant for reaction R_3, which is:

$$k_3 = \frac{1}{t_{1/2} \cdot [mTOR\_FKBP38]} \tag{4.1.9}$$

and assuming, that the initial value for the complex is $mTOR\_FKBP38(0) = 100$ rate constant comes then to $k_3 = 0.00333\,\text{min}^{-1} \cdot u^{-1}$, where u represents relative unit, in our model [%].

Using the model in absence of all reactions except for R_3 we could show that k_3 could reproduce the published data. The plot below shows the exponential decay of mTOR_FKBP38 complex after addition of active $Rheb^{GTP}$.

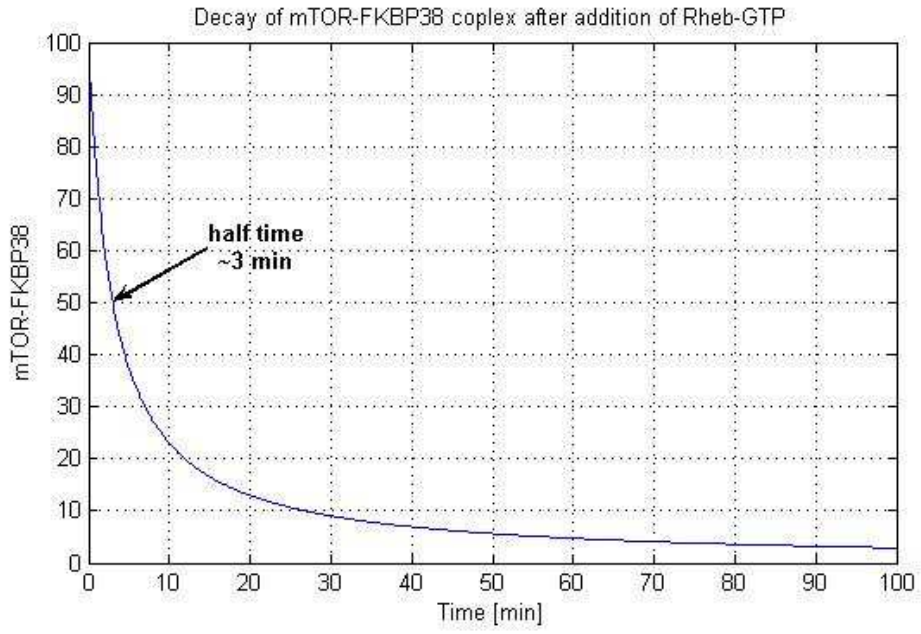

Figure 4.1.9 Result of the simulation for reaction R_3 ***with decay constant for mTOR_FKBP38 decreasing*** $k_3 = 0.00333\,\text{min}^{-1} \cdot u^{-1}$. *The plot was made as a result of simulation in SBtoolbox for MatLab and shows the exponential decay of mTOR_FKBP38 in the reaction of mTOR activation. The half time for this reaction is* $\cong 3$ *minutes, corresponding well with published data. (u represents relative unit, %).*

4.1.2.2 Parameter k_{-3}

To derive parameter k_{-3} for the reverse reaction, inhibition of mTOR activity by FKBP38, we have studied publication by Bai et al., where they describe inhibition of mTOR kinase activity by FKBP38.

In their experiment, the inhibitory effect of FKBP38 on mTOR activity was tested. From the material and methods chapter we know that to determine the effect of FKBP38 on the kinase activity, 2 µg of FKBP38 was used and incubated with the cells for 10 minutes. After the time of incubation mTOR activity was decreased to 40% of the initial value (figure 4.1.10).

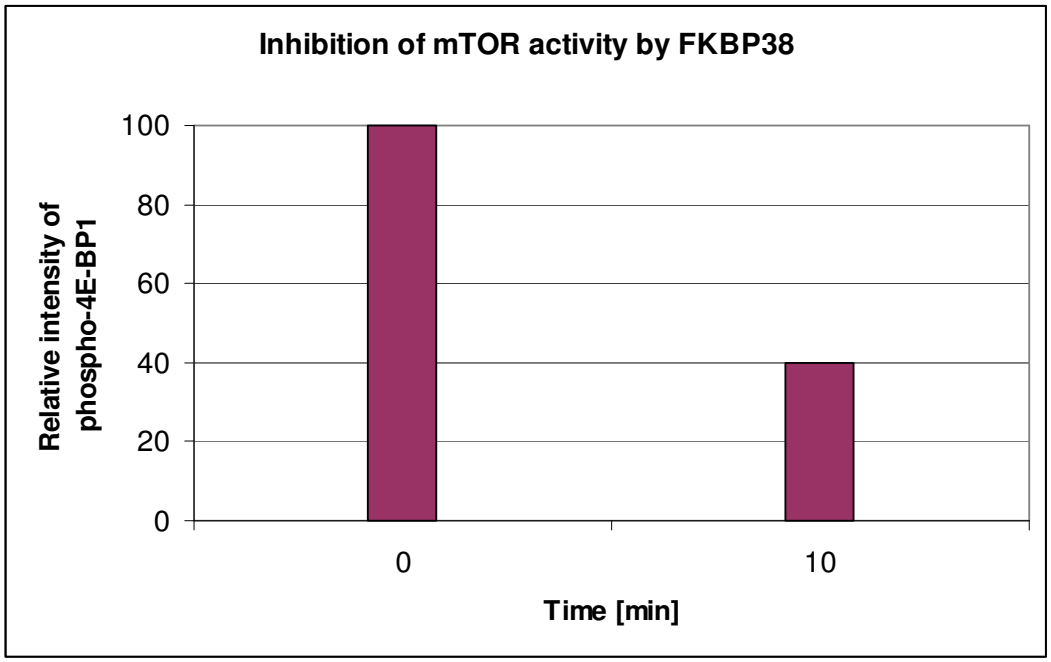

Figure 4.1.10 Effect of FKBP38 on the mTOR kinase activity*. After 10 minutes of incubation with 2 µg of FKBP38, the activity of mTOR dropped to 40% of initial activity. Figure based on data from Bai et al., 2007 and figure 2D from this publication.*

Since the mTOR_FKBP38 complex decreases in exponential decay manner after addition of Rheb (k_3 parameterization), we can assume that mTOR activation, as a reverse reaction, proceeds with similar characteristic. Based on that the curve equation for the exponential decay of mTOR activity is:

$$y = y_0 \cdot e^{-k_{-3} \cdot t} \tag{4.1.10}$$

at time $t = 10$ min the value of $y = 0.4$ is achieved. The kinetic rate therefore is:

$$k_{-3} = \frac{\ln 0.4}{-t} = 0.09163 \text{ min}^{-1} \tag{4.1.11}$$

and a half time for the inhibition:

$$t_{1/2} = \frac{\ln 2}{k_{-3}} \cong 7.5 \text{ min} \tag{4.1.12}$$

According to the method which was used above (k_3 parameterization) we can calculate the rate constant for the reaction R_{-3}. Here again we have two reactants, mTOR and $Rheb^{GTP}$_FKBP38, both of which are consumed in the reaction. We can say that they have a nature of second-order process. With the assumption that the initial value for mTOR is $mTOR(0) = 100$, we can use equation (4.1.9) to derived k_{-3}, which comes then to $k_{-3} = 0.00133 \text{min}^{-1} \cdot u^{-1}$.

Using the model in absence of all reactions except for R_{-3} we could show that the calculated k_{-3} matches published data. The plot below shows exponential decay of mTOR-FKBP38 complex after addition of active $Rheb^{GTP}$.

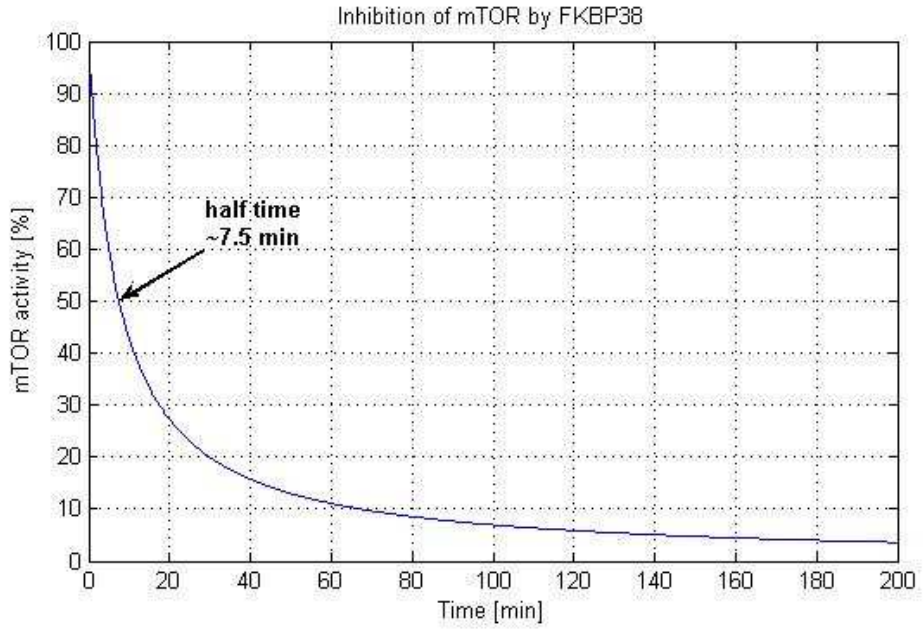

Figure 4.1.11 Result of the simulation for reaction R_{-3} with decay constant for mTOR decreasing $k_{-3} = 0.09163\,\mathrm{min}^{-1} \cdot u^{-1}$. *The plot was made as a result of simulation in SBtoolbox for MatLab and shows the exponential decay of mTOR8 in the reaction of mTOR inhibition by FKBP38. The half time for this reaction is* $\cong 7.5$ *minutes, corresponding well with published data.*

4.1.2.3 Model testing for parameters k_3 and k_{-3}

Using SBtoolbox, the rate expressions based on figure 4.1.6 and parameters k_3 and k_{-3} obtained as above, we tested the model for two reactions, which represent activation of mTOR by $Rheb^{GTP}$ and mTOR inhibition by FKBP38, respectively. The simulations show two different initial conditions: a) when $Rheb^{GTP}(0) = 100$ and $mTOR(0) = 0$ ($mTOR\_FKBP38(0) = 100$ and $Rheb^{GTP}\_FKBP38(0) = 0$); b) when $Rheb^{GTP}(0) = 0$ and $mTOR(0) = 100$ ($mTOR\_FKBP38(0) = 0$ and $Rheb^{GTP}\_FKBP38(0) = 100$).

The first condition represents oversaturated nutrient conditions, when all Rheb is in an active GTP form. In this scenario we expected that the level of $Rheb^{GTP}$ should decrease, because it is converted to the complex with FKBP38. Activity of mTOR should rapidly increase, because $Rheb^{GTP}$, which is necessary for this activation, is already in a full GTP state. In turn, the level of inactive complex mTOR-FKBP38 should rapidly decrease, as a reverse reaction to mTOR activation. Also the $Rheb^{GTP}$_FKBP38 complex was supposed to increase with mTOR activation.

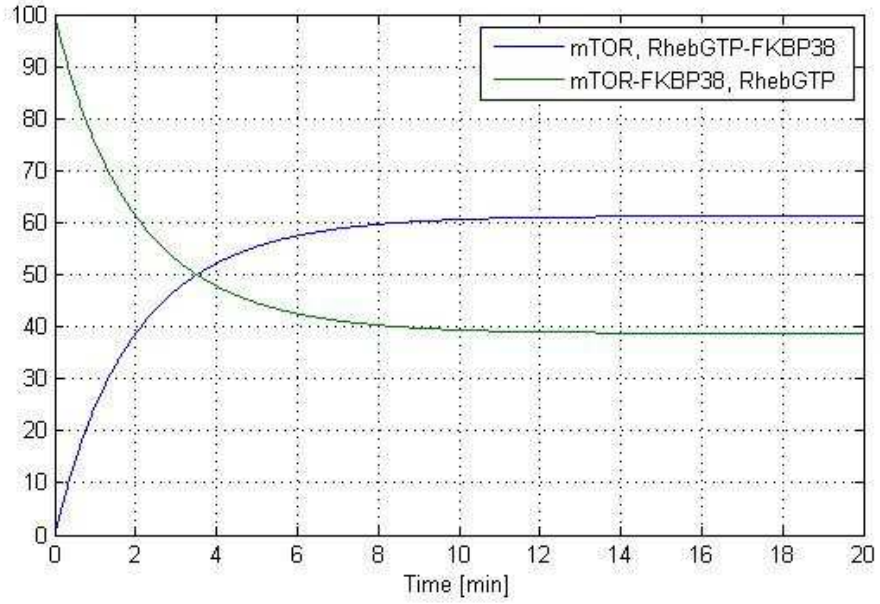

Figure 4.1.12a Result of the simulation for reactions R_3 and R_{-3} when $Rheb^{GTP}(0) = 100$ ***and*** $mTOR(0) = 0$. *With the increasing activation of mTOR, the level of the* $Rheb^{GTP}$ *decreases, since it is used for this activation.*

The second condition mimicked nutrient starvation, when all $Rheb^{GTP}$ is converted to the inactive form, but mTOR remains present in an active form. In this

scenario we expect that the level of $Rheb^{GTP}$ should increase, because it is released from the complex $Rheb^{GTP}$_FKBP38 in the reaction R_{-3}. The activity of mTOR should decrease, because $Rheb^{GTP}$_FKBP38 complex which is necessary for its inhibition is present in the system. In turn, the level of inactive complex mTOR_FKBP38 should increase, as a consequence of the mTOR inhibition. Also the $Rheb^{GTP}$_FKBP38 complex was expected to decrease as long with mTOR activation.

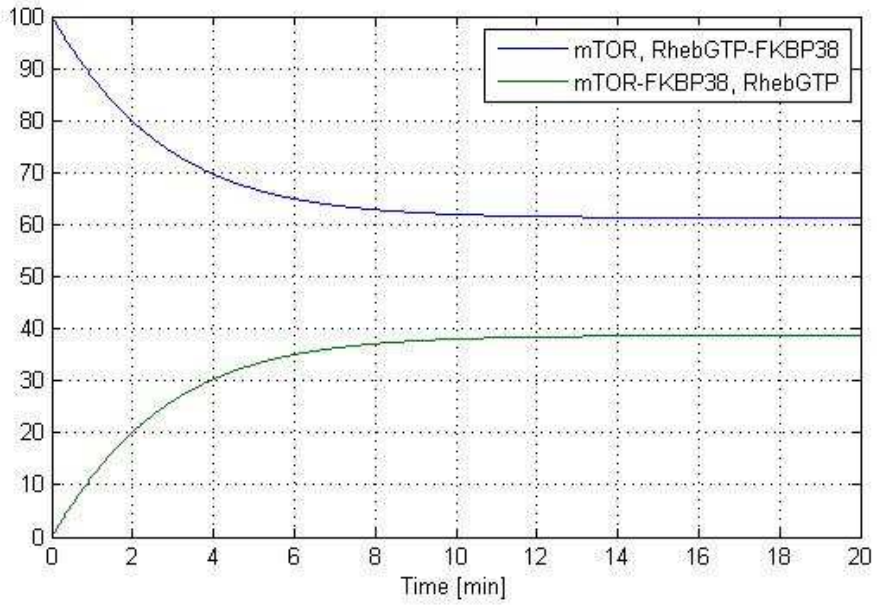

Figure 4.1.12b Result of the simulation for reactions R_3 and R_{-3} when $Rheb^{GTP}(0) = 0$ ***and*** $mTOR(0) = 100$. *Because of inhibition by FKBP38, mTOR decreases. At the same time, RhebGTP increases, since it is a product of this inhibition.*

In both plots (figure 4.1.12a and 4.1.12b) we observe that the final steady state values of the all products are the same respectively in both conditions, and they come to ~62% for mTOR and $Rheb^{GTP}$-FKBP38 and to ~38% for $Rheb^{GTP}$ and mTOR-FKBP38. To compare parameters k_3 / k_{-3} with k_1 / k_2 we can see that reactions R_3 and R_{-3} are

faster and they approached steady state after approximately 15 minutes (compare to reactions R_1 and R_2 approximately 60 minutes).

We showed here results of the simulations with the simplified condition of nutrient saturation. The majority of mTOR is in its active state (62%) which correlates with the biological experimental data.

4.1.3 Parameterization of kinetic constants k_4 and k_5

Parameters k_4 and k_5 for the reactions R_4 and R_5 (figure 4.1.13) were derived from the publication by Kamada et al [*Kamada et al., 2000*].

Figure 4.1.13 represents the reactions R_4 and R_5 which are implemented in our model. Under nutrient rich conditions, and when the cell is in a normal living state, active mTOR keeps Atg13 in a hyperphosphorylated state, that is, almost all Atg13 is phosphorylated to Atg13_P. During cell starvation mTOR is inhibited and this results in dephosphorylation of Atg13_P.

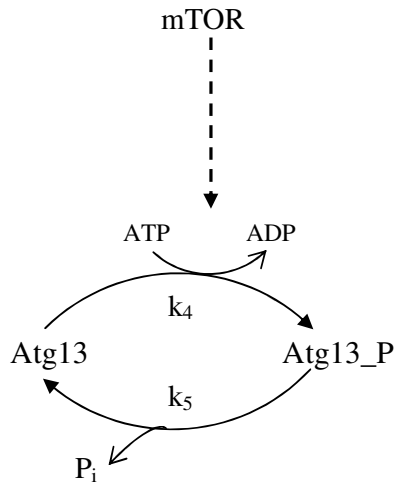

Figure 4.1.13 mTOR controls the level of phosphorylation of Atg13*. Under nutrient rich conditions, almost all Atg13 is phosphorylated to the form Atg13_P. Inhibition of mTOR, which occurs during starvation, results in Atg13 dephosphorylation [references for the reactions: Kamada et al., 2000; Kamada et al., 2010; Hosokawa et al., 2009; Klionsky and Emr, 2000].*

Simplified rate expressions extracted from the figure 4.1.13:

$$\upsilon_4 = k_4 \cdot Atg13 \cdot mTOR$$
$$\upsilon_5 = k_5 \cdot (Atg13\_P)$$

In these rate expressions, for simplicity we have deliberately suppressed the influence of other substrates. We initially assume that energy equivalents such as ATP are not limited; therefore we can leave ATP, ADP and Pi out of the calculations. An unknown phosphatase that takes part in reaction R_5, Atg13 dephosphorylation [*Klionsky and Emr, 2000; Kamada et al., 2000*] is assumed to have a constant influence on the

reaction rate. Therefore, any dependence on this phosphatase is absorbed into the constant k_5.

4.1.3.1 Parameter k_5

Kamada and colleagues experimentally investigated the biochemical character of Atg13 [*Kamada et al., 2000*]. They observed that in growing cells Atg13 occurs in the phosphorylated form, and after starvation or mTOR inhibition by rapamycin this form disappeared (dephosphorylation). In starvation condition Atg13 dephosphorylation takes 30 minutes, whereas after rapamycin treatment only 5 minutes (figure 3A from the *Kamada et al., 2000*). This difference in reaction rates stems from the fact that rapamycin acts direct on mTOR by blocking its activity, whereas the signal from amino acids deprivation first results in the transformation of $Rheb^{GTP}$ to $Rheb^{GDP}$, and then Rheb in this inactive form mediates inhibition of mTOR (figure 4.1).

For our calculations we used the data from the rapamycin treatment, because we were interested in the immediate effects of mTOR inhibition on Atg13 dephosphorylation. Within 5 minutes after rapamycin treatment Atg13 was dephosphorylated. The same publication, based on the experiment suggested, that "Atg13 remains partially phosphorylated under starvation conditions" [*Kamada et al., 2000*]. We therefore assumed that after 5 minutes after rapamycin treatment 95% of Atg13 was transformed into the unphosphorylated form (figure 4.1.14).

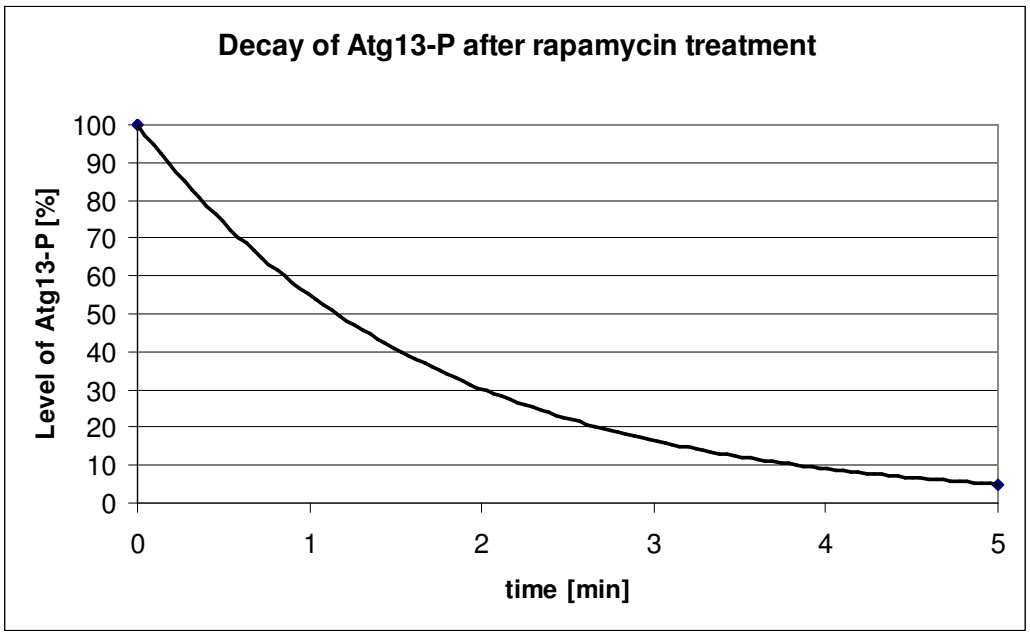

Figure 4.1.14 Representation of the Atg13-P dephosphorylation. *The plot represents the curve of the exponential decay for the Atg13-P dephosphorylation after rapamycin treatment. The time of 95% completion of Atg13-P dephosphorylation was derived from experimental data from Kamada et al., 2000 and used to plot the exponential decay curve.*

The curve equation for the exponential decay is:

$$y = y_0 \cdot e^{-k_5 \cdot t} \tag{4.1.13}$$

where y is a quantity at time t, y_0 is an initial amount of Atg13_P, and k_5 indicates the decay constant. From (4.1.13) and the assumption that at time $t = 5\,\text{min}$ only 5% of Atg13_P is left, the decay rate is:

$$k_5 = \frac{\ln 0.05}{-t} = 0.5991\ \text{min}^{-1} \tag{4.1.14}$$

The half time of the Atg13_P dephosphorylation thus calculated as

$$t_{1/2} = \frac{\ln 2}{k_5} \cong 1.15 \text{ min} \qquad (4.1.15)$$

Using the model in absence of all reactions except for R_5 we could show that k_5 corresponded to published data. The plot below shows the dephosphorylation of Atg13-P after rapamycin treatment (4.1.15):

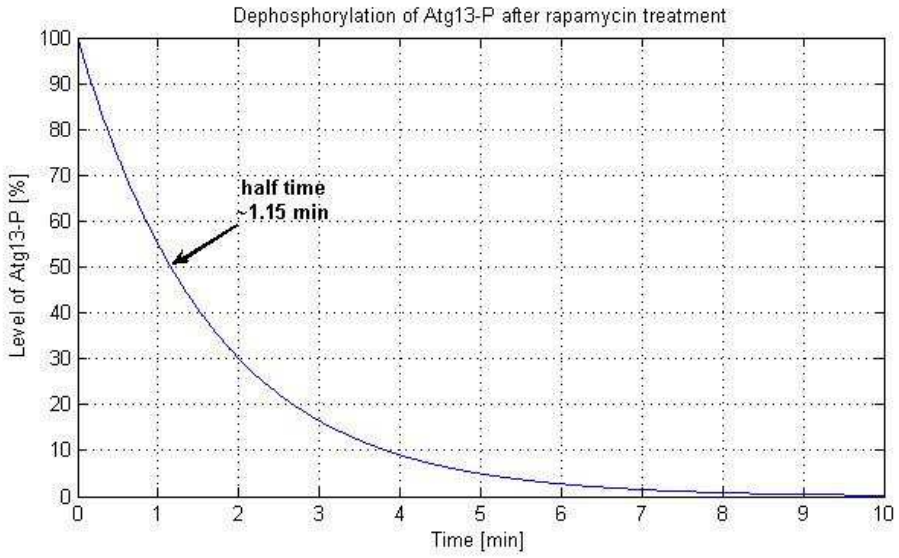

Figure 4.1.15 Result of the simulation for reaction R_5 ***with decay constant*** $k_5 = 0.5991$ ***min^{-1}.*** *The plot was made as a result of a simulation in SBtoolbox for MatLab and shows the exponential decay of Atg13-P after treatment with rapamycin. The half time for this reaction is* $\cong 1.15$ *minutes, which corresponds well with published data.*

4.1.3.2 Parameter k_4

In the next experiment Kamada and colleagues were again testing the sensitivity of the phosphorylation state of Atg13 [*Kamada et al., 2000*]. They found that after re-

addition of growth medium to the starved cells, the dephosporylated form of Atg13 was phosphorylated within 10 minutes (figure 3D from the *Kamada et al., 2000)*. This means, according to the diagram of the biochemical reaction involved in the autophagy pathway (figure 4.1), that reactions R_1, R_3 and R_4 together take 10 minutes. But from the previous calculations, which were based on experimental publications, we already know the half times for the reaction R_1, which is 10 minutes, and for the reaction R_3, which is 3 minutes. We can assume that all three reactions take 15 minutes (which is still in the correct range, compare to 10 minutes from *Kamada, et al, 2000*) and thereby, reaction R_4 is estimated to take 2 minutes.

Based on this information we know that after re-addition of the growth medium, due to phosphorylation, amount of Atg13 decrease (figure 4.1.16).

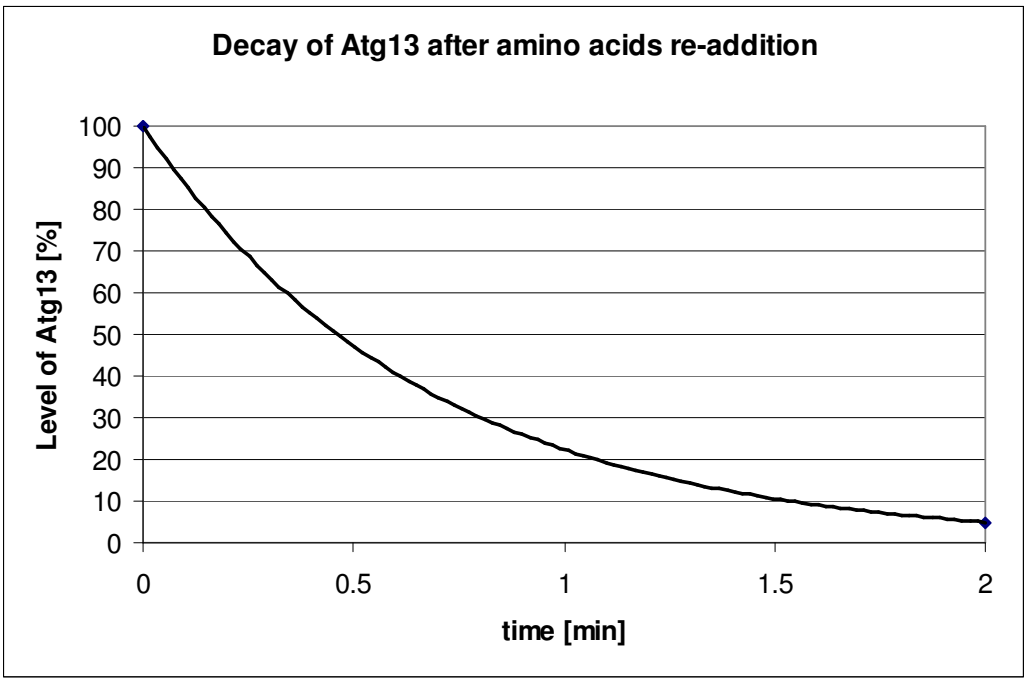

Figure 4.1.16 Representation of Atg13 phosphorylation. *The plot represents the curve of the exponential decay for the Atg13 due to phosphorylation after re-addition the growth medium to the staved cells. The data of Atg13 phosphorylation was derived from experimental data from Kamada et al., 2000 and used to plot the exponential decay curve.*

According to the equations (4.1.13) and (4.1.14) the decay rate for Atg13 during phosphorylation is $k_4 = \frac{\ln 0.05}{-t} = 1.4979 \ \text{min}^{-1}$ and the corresponding half time calculated as in (4.1.15) comes to $t_{1/2} = \frac{\ln 2}{k_4} \cong 0.46 \ \text{min}^{-1}$.

As we can see from the reaction rate $\upsilon_4 = k_4 \cdot Atg13 \cdot mTOR$, which is based on figure 4.1.13, reaction of Atg13 phosphorylation is dependent on mTOR (k_4 includes already influence from mTOR). In reaction R_4 mTOR acts as an enzyme, which catalyses this reaction and increases the reaction rate. To derive the exact rate constant

for reaction R_4, we have to divide it by the concentration of the enzyme (mTOR). This leads to the value of constant $k_4 = 0.01498\,\text{min}^{-1}\cdot u^{-1}$, where u represents relative unit, %.

Using the model in absence of all reactions except for R_4 and implementing mTOR as a constant value ($mTOR(0) = 100$ and $\frac{d(mTOR)}{dt} = 0$) together with the value of k_4 above, we can reproduce the published data. The plot below shows the exponential decay of Atg13 after re-addition of amino acids to the starved cells (figure 4.1.17).

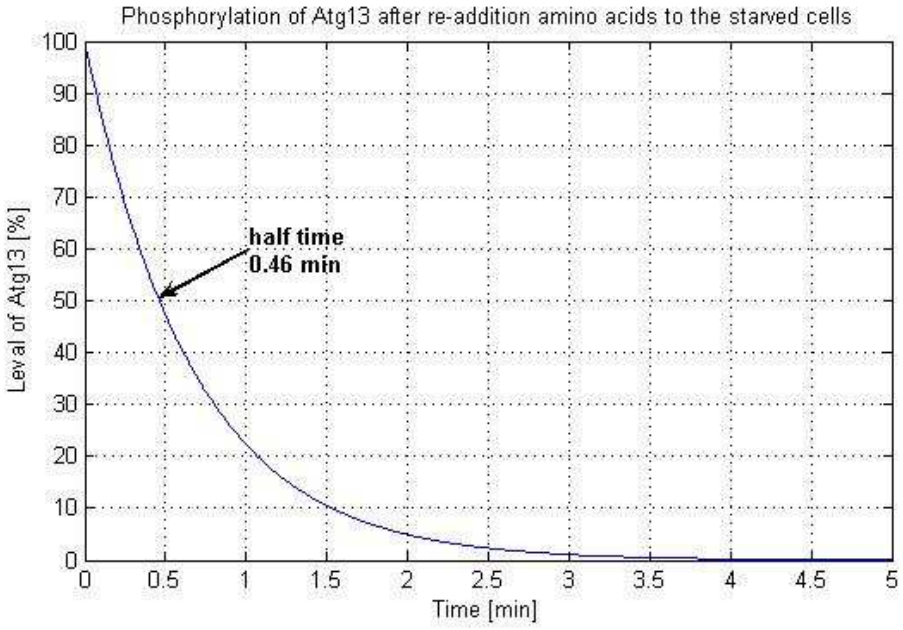

Figure 4.1.17 Result of the simulation for reaction R_4 with decay constant $k_4 = 0.01498\,\text{min}^{-1}\cdot u^{-1}$. *The plot was made as a result of a simulation in SBtoolbox for MatLab and shows the exponential decay of Atg13 after re-addition of the growth medium to the starved cells. The half time for this reaction is $\cong 0.46$ minutes, corresponding well with published data.*

4.1.3.3 Model testing for parameters k_4 and k_5

Using SBtoolbox, rate expressions based on figure 4.1.13 and parameters k_4 and k_5 obtained above, we tested the model for the reactions R_4 and R_5, which represents turnover of Atg13 into the phosphorylated form Atg13-P and *vice versa*. The simulations conducted show two different initial conditions: a) when $Atg13\_P(0) = 100$ and $Atg13(0) = 0$; b) when $Atg13\_P(0) = 0$ and $Atg13(0) = 100$. The first condition represents oversaturated nutrient conditions, when all Atg13 is in a phosphorylated form. The second condition mimics nutrients starvation, when all Atg13 is converted to the unphosphorylated form. These two scenarios thus show opposite extreme conditions.

In the first scenario we expect that Atg13-P levels should decrease, because a part of it is converted to Atg13. On the other hand, the level of Atg13 should increase. In the second condition we expected that Atg13 levels decrease because a part of it is converted to phosphorylated Atg13-P form. In both scenarios Atg13-P should reached higher level in the steady state conditions.

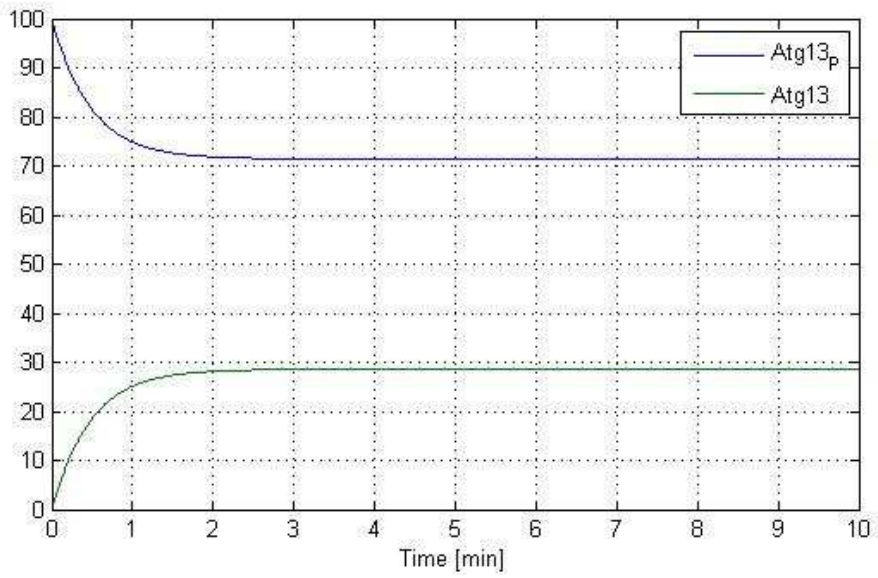

Figure 4.1.18a Result of the simulation for reactions R_4 ***and*** R_5 ***when*** $Atg13\_P(0) = 100$ ***and*** $Atg13(0) = 0$. *With the decreasing in the phosphorylated form of Atg13, the level of the unphosphorylated Atg13 increases.*

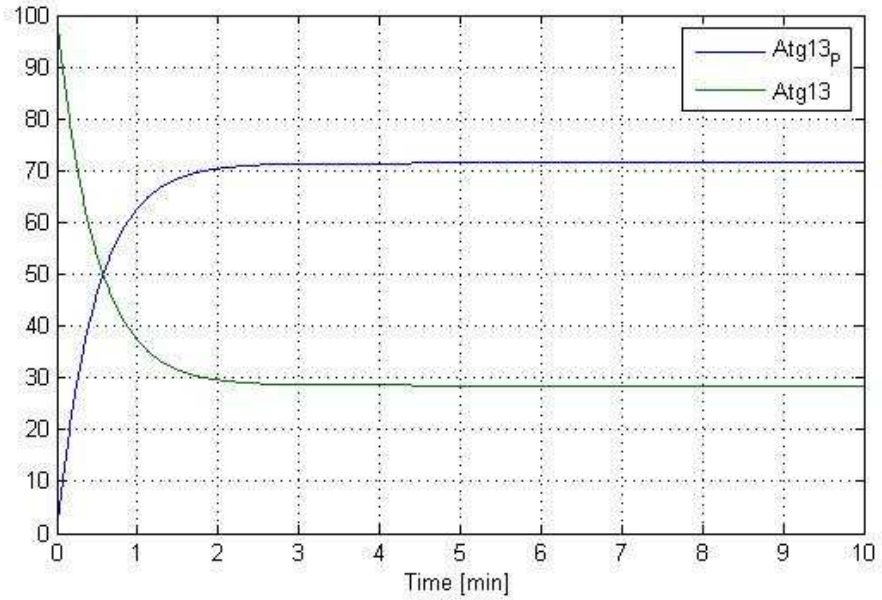

Figure 4.1.18b Result of the simulation for reactions R_4 ***and*** R_5 ***when*** $Atg13\_P(0) = 0$ ***and*** $Atg13(0) = 100$***.*** *With the decrease in the unphosphorylated form of Atg13, the level of the phosphorylated Atg13_P increases.*

On both plots (figure 4.1.18a and 4.1.18b) we can observe that final steady states values of the products are the same respectively in both conditions, and they come to ~72% for Atg13-P and to ~28% for Atg13.

4.1.4 Parameterization of kinetic constants k_6, k_{-6} and k_7

Figure 4.1.19 represents the next reactions which are implemented in our model. Parameters k_6, k_{-6} and k_7 for the next reactions were derived from the publication by Kamada et al [*Kamada et al., 2000*].

Under nutrient rich conditions, during the normal cellular life, active mTOR keeps Atg13 in hyperphosphorylated state (reaction R_4). In starvation mTOR is

inhibited and this results in Atg13 dephosphorylation (reaction R_5). Dephosphorylated Atg13 has a high affinity to Atg1, and together they create a complex (reaction R_6). Atg1_Atg13 complex spontaneously break up in reverse reaction (reaction R_{-6}), and also after re-activation of mTOR (reaction R_7).

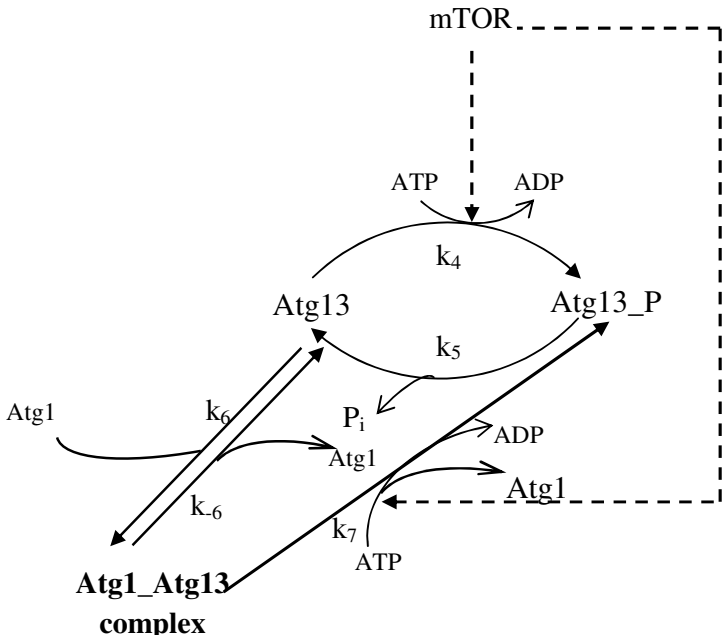

Figure 4.1.19 The level of phosphorylation of Atg13 controlled by mTOR and Atg1_Atg13 complex formation. *Under nutrient rich conditions Atg13 occurs in the highly phosphorylated form (reaction 4). Inhibition of mTOR, for example during cell starvation, results in Atg13 dephosphorylation (reaction 5) and Atg1_Atg13 complex formation (reaction 6). This complex can break up in the reverse reaction (reaction -6) and after mTOR re-activation (reaction 7) [references for the reactions: Kamada et al., 2000; Kamada et al., 2010; Hosokawa et al., 2009; Klionsky and Emr, 2000].*

Simplified rate expressions extracted from the figure 4.1.19:

$$\upsilon_4 = k_4 \cdot Atg13 \cdot mTOR$$
$$\upsilon_5 = k_5 \cdot (Atg13\_P)$$

$$\upsilon_6 = k_6 \cdot Atg13 \cdot Atg1$$
$$\upsilon_{-6} = k_{-6} \cdot (Atg1\_Atg13)$$
$$\upsilon_7 = k_7 \cdot (Atg1\_Atg13) \cdot mTOR$$

In the rate expressions some substrates are again deliberately suppressed. To simplify our model initially we assume that energy equivalents such as ATP are not limited; therefore we can leave ATP, ADP and Pi out of the calculations. An unknown phosphatase participates in reaction R_5, Atg13 dephosphorylation [*Klionsky and Emr, 2000; Kamada et al., 2000*]. With assumption that the amount of phosphatase does not change we do not include it into equations.

Kamada et al., 2000 is the only publication that we are aware of, which describes the reactions in Atg1_Atg13 complex formation and which gives some quantitative information on these reactions.

4.1.4.1 Parameter k_7

Reaction R_7 can be treated as a competitive reaction for reaction R_4, where in both Atg13_P is produced, and both are controlled by mTOR. However, reaction R_7 occurs when Atg1_Atg13 complex is present (so in starvation conditions), while reaction R_4 occurs always. Reaction R_7 is also catalysed by mTOR, therefore we can assume that k_7 is equal to k_4, so $k_7 = 0.01498\,\mathrm{min}^{-1} \cdot u^{-1}$, where u represents relative unit, %.

4.1.4.2 Parameter k_6

From the publication by Kamada et al. we know that after rapamycin treatment the formation of the Atg1_Atg13 complex stabilises within about 10 minutes. This includes reactions R_5 and R_6 according to the diagram 4.1.19. As we can see from the rate expression, $\upsilon_6 = k_6 \cdot Atg13 \cdot Atg1$, reaction R_6 is dependent on both Atg13 and Atg1. Both of them are consumed as reactants in the process of complex formation. We can say that they have a nature of second-order process, in which the concentrations of the two reactants behave the same.

Using the model including reactions R_4, R_5, R_6 and R_7, and with implemented parameters k_4, k_5 and k_7, we tried to find parameter k_6. mTOR was implemented as model variable, which after 30 minutes was shut off, to mimic rapamycin action. We optimized k_6 by manual fitting. The goal of the fitting was to find Atg1-Atg13 complex increased up to approximately 85% in 10 minutes after rapamycin treatment [*Kamada et al., 2000*]. An optimal value for k_6 was found with 0.0066 $min^{-1} \cdot u^{-1}$, where u represents relative unit, %. The result of simulation with the fitted value of k_6 is represented on figure 4.1.20.

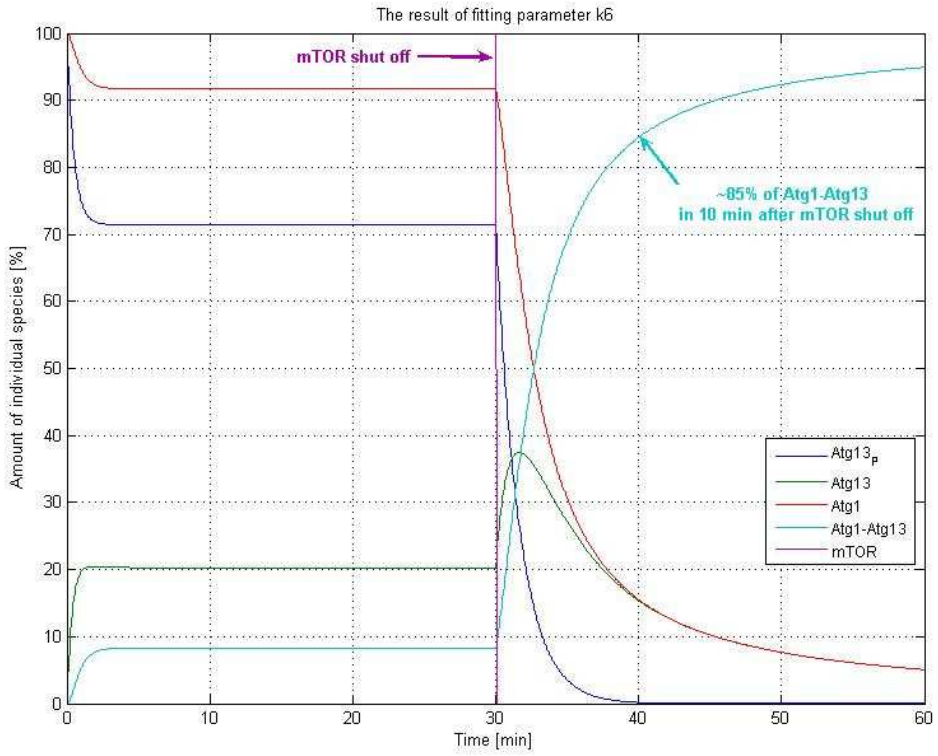

Figure 4.1.20 Result of the simulation with the fitted parameter k_6. *The plot was made as a result of a simulation in SBtoolbox for MatLab and shows the behaviour of Atg1_Atg13 complex after rapamycin treatment. mTOR was shut off after 30 min as a result of rapamycin treatment. In the next 10 min Atg1_Atg13 complex increased to the ~85% level. The time 30 min was chosen randomly to ensure that the system was in steady state before rapamycin treatment.*

In the plot above we can see that in 10 minutes after rapamycin treatment Atg1_Atg13 complex reached ~85% (from the ~8% in steady state condition in presence of mTOR). After mTOR shut off, the level of Atg13 rapidly reached a higher level (due to Atg13_P dephosphorylation) and then decreased due to Atg1_Atg13 complex formation.

4.1.4.3 Parameter k_{-6}

Based on the results from the previous simulations we checked how these plots changed after addition of reaction R_{-6}. We expected a slightly lower level of Atg1_Atg13 complex in the final steady state condition.

Reaction R_{-6}, similar to reaction R_7, eliminates the Atg1_Atg13 complex. However, in reaction R_{-6} parameter k_{-6} does not depend on mTOR and thus represent a spontaneous dissociation reaction.

Using the model in presence of reaction R_4, R_5, R_6, R_{-6} and R_7, and with implemented parameters k_4, k_5, k_6 and k_7, we tried to find the parameter k_{-6} by manual fitting. The goal of the fitting was to find a slightly lower level of Atg1-Atg13 complex after rapamycin treatment, but behaviour of the rest of the species similar to the previous simulation (because there is no a significant influence on the system from reaction R_{-6}). An optimal value for k_{-6} was found with 0.0059 min^{-1}. Together with the rest of the implemented parameters, this combination best represented the changes in the individual species. The result of the simulation with the fitted k_{-6} is represented on figure 4.1.21.

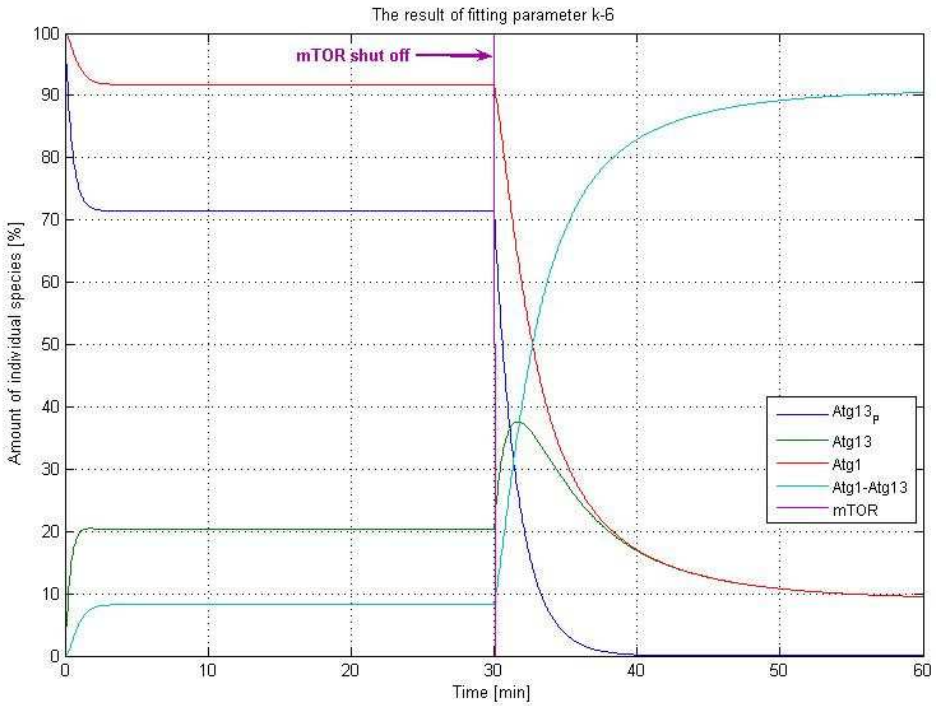

Figure 4.1.21 Result of the simulation with the fitted parameter k_{-6}. *The plot was made as a result of a simulation in SBtoolbox for MatLab and shows the behaviour of Atg1-Atg13 complex after rapamycin treatment. mTOR was shut off after 30 min as a result of rapamycin treatment. The time 30 min was chosen randomly to ensure that the system was in steady state before rapamycin treatment.*

In the plot above we can see that in 10 minutes after rapamycin treatment Atg1-Atg13 complex reached ~83% (from the ~8% in steady state condition in presence of mTOR). Level of Atg13 rapidly after mTOR shut off reached a higher level.

4.1.4.4 Model testing for parameters $k_4 – k_7$

Using SBtoolbox, rate expressions based on figure 5.18 and parameters k_6, k_{-6} and k_7 obtained as above, we tested the model for the reactions R_4, R_5, R_6, R_{-6} and R_7. The simulations conducted show three different initial conditions (table 4.1.1).

Table 4.1.1 Initial conditions for model testing

Species	1st initial conditions	2nd initial conditions	3rd initial conditions
Atg13_P	100	0	0
Atg13	0	100	0
Atg1	100	100	0
Atg1-Atg13	0	0	100

The first condition represents oversaturated nutrient conditions, when all Atg13 is in a phosphorylated form and there is no Atg1-Atg13 complex. The second condition mimics nutrients starvation, when all Atg13 is converted to the unphosphorylated form. The third scenario represents also nutrient starvation condition, when all Atg13 and Atg1 are converted to the Atg1-Atg13 complex.

4.1.4.4.1 Simulations in the normal rich nutrient conditions (in the presence of active mTOR)

We expected that in all three conditions the final steady states for all species will be identical. Figure below presents result of the simulation in the first scenario of initial conditions (table 4.1.1).

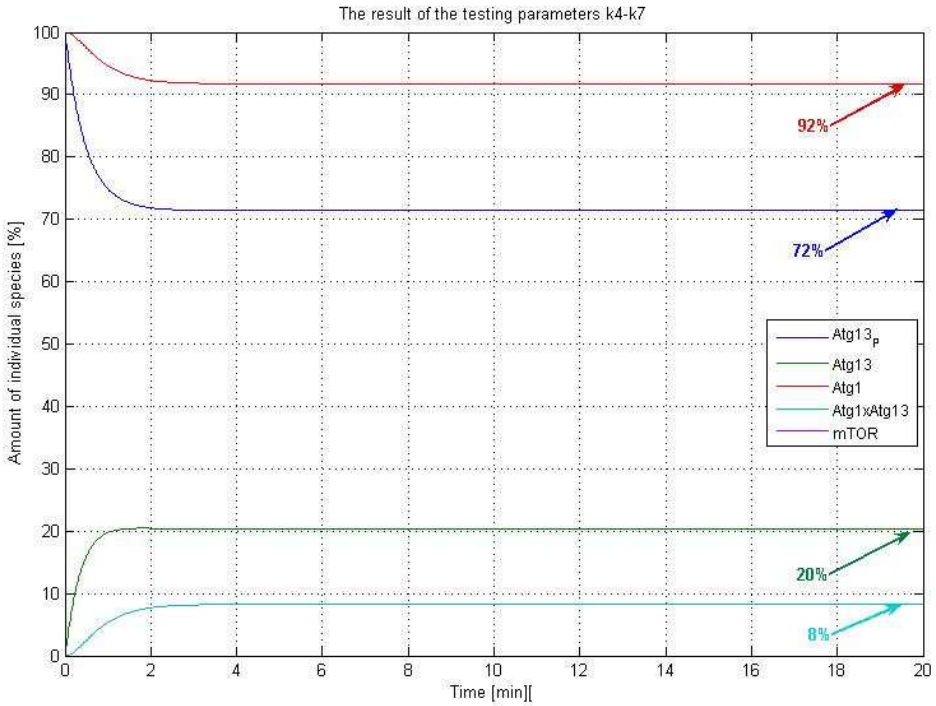

Figure 4.1.22 Result of the model testing for parameters k_4-k_7 in the normal rich nutrient conditions. *The plot was made as a result of a simulation in SBtoolbox for MatLab and shows the behaviour of Atg1_Atg13 complex, Atg13_P, Atg13 and Atg1 in normal nutrient conditions. Initial concentrations for this simulation: Atg13_P(0)=100, Atg13(0)=0, Atg1(0)=100 and Atg1_Atg13(0)=0. Steady state of Atg1_Atg13 complex is lower than 10%, which is reasonable level in rich nutrient conditions.*

Figure below presents result of the simulation in the second scenario of initial conditions (table 4.1.1).

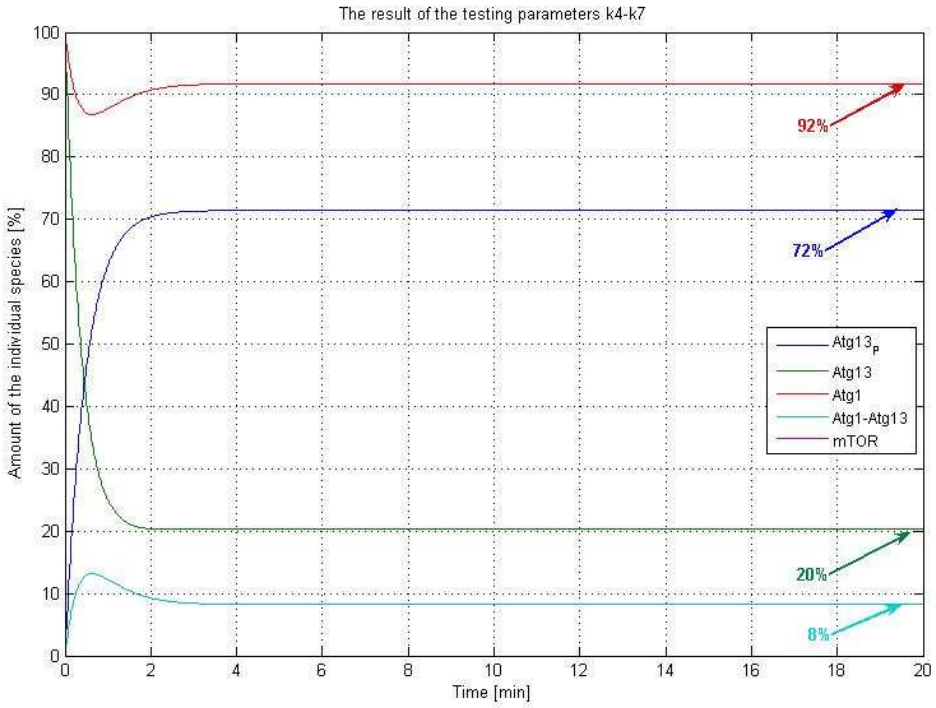

Figure 4.1.23 Result of the model testing for parameters k_4-k_7 in the normal rich nutrient conditions. *The plot was made as a result of a simulation in SBtoolbox for MatLab and shows the behaviour of Atg1_Atg13 complex, Atg13_P, Atg13 and Atg1 in normal nutrient conditions. Initial concentrations for this simulation: Atg13_P(0)=0, Atg13(0)=100, Atg1(0)=100 and Atg1_Atg13(0)=0. Steady state of Atg1_Atg13 complex is lower than 10%, which is reasonable level in nutrient rich conditions.*

Figure below presents result of the simulation in the third scenario of initial conditions (table 4.1.1).

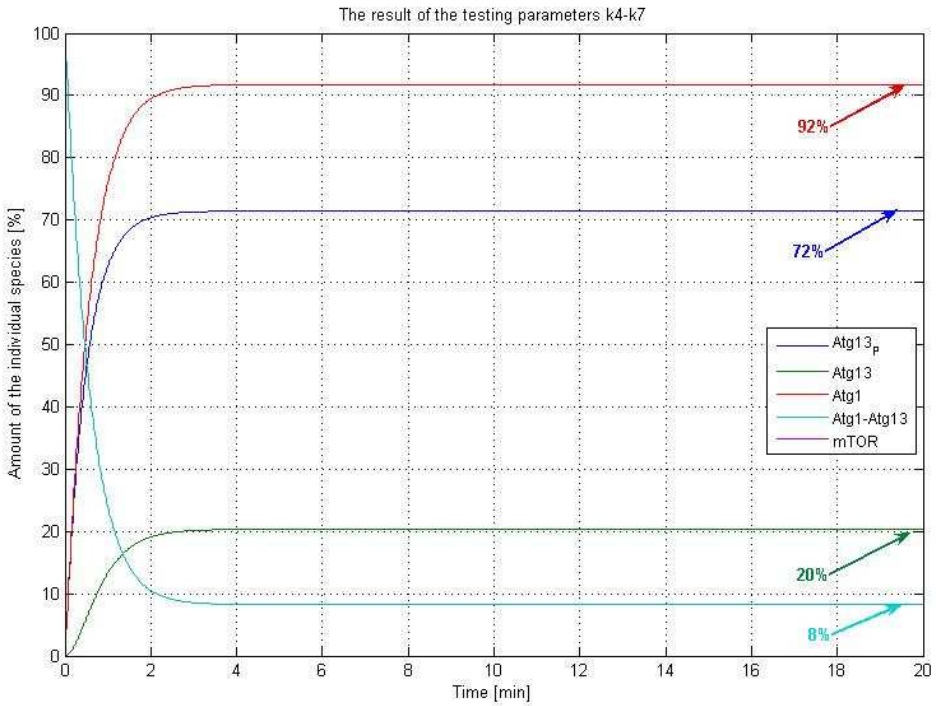

Figure 4.1.24 Result of the model testing for parameters k_4-k_7 in the normal rich nutrient conditions. *The plot was made as a result of a simulation in SBtoolbox for MatLab and shows the behaviour of Atg1_Atg13 complex, Atg13_P, Atg13 and Atg1 in normal nutrient conditions. Initial concentrations for this simulation: Atg13_P(0)=0, Atg13(0)=0, Atg1(0)=0 and Atg1_Atg13(0)=100. The steady state concentration of Atg1_Atg13 complex is less than 10%, which is reasonable level in rich nutrient conditions.*

In all plots (4.1.22, 4.1.23 and 4.1.24) we can see the levels of each individual species reaches the same final level, irrespectively of the initial conditions (table 4.1.1), in the normal nutrient conditions (in the presence of active mTOR). Atg1_Atg13 complex reaches a very low steady states level, on the contrary Atg13_P. Preaches a high level. This result is reasonable in the nutrient rich conditions.

4.1.4.4.2 Simulations in the inhibition of mTOR

In the previous simulations (part 4.1.4.4.1) we tested the model in the presence of active mTOR. Next we wanted to test the model when mTOR is shut off in the first second of simulation, which means that system could not reached the steady state before. We expected that when mTOR is inactive the individual species reach different steady state levels than in mTOR active - scenario. Thus, we expected that Atg1_Atg13 complex, which in our model is a marker of autophagy induction, will be in high level (due to mTOR inhibition).

mTOR was implemented as model variable, which after 0.00005 minutes was shut off, to mimic rapid rapamycin action. We expected that after inhibition of mTOR in all three different conditions (table 4.1.1) final steady states of all species reach the same levels.

Figure below presents result of the simulation in the first scenario of initial conditions (table 4.1.1).

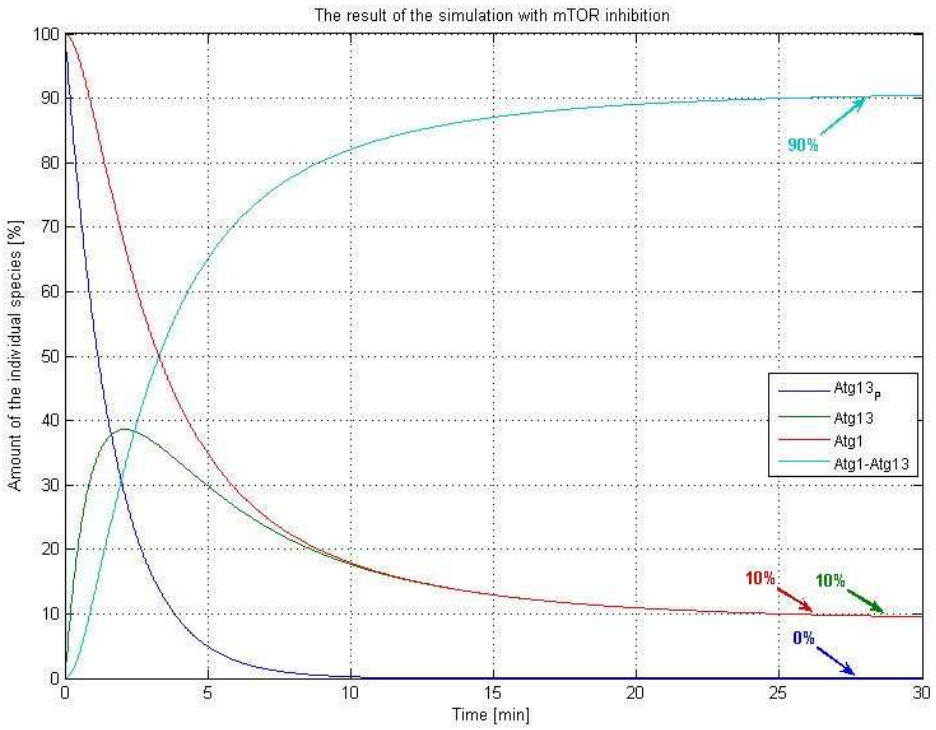

Figure 4.1.25 Result of the model testing for parameters k_4-k_7 in the mTOR inhibition. *The plot was made as a result of a simulation in SBtoolbox for MatLab and shows the behaviour of Atg1_Atg13 complex, Atg13_P, Atg13 and Atg1. Initial concentrations for this simulation: Atg13_P(0)=100, Atg13(0)=0, Atg1(0)=100 and Atg1_Atg13(0)=0. Steady state of Atg1_Atg13 complex is high ~90%, which is reasonable level in the inhibition of mTOR.*

Figure below presents result of the simulation in the second scenario of initial conditions (table 4.1.1).

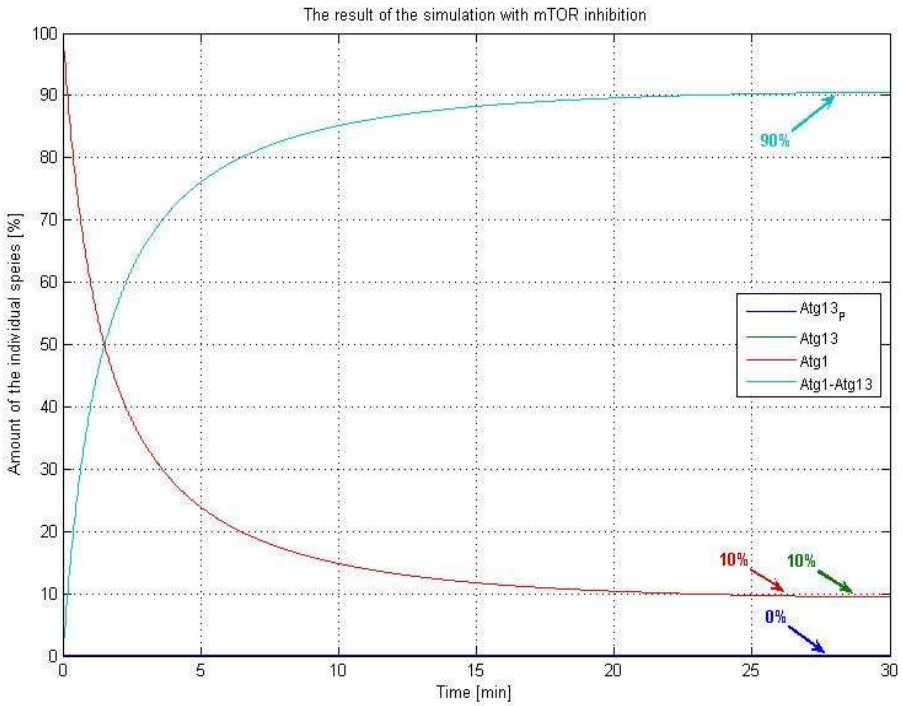

Figure 4.1.26 Result of the model testing for parameters k_4-k_7 in the mTOR inhibition. *The plot was made as a result of a simulation in SBtoolbox for MatLab and shows the behaviour of Atg1_Atg13 complex, Atg13_P, Atg13 and Atg1. Initial concentrations for this simulation: Atg13_P(0)=0, Atg13(0)=100, Atg1(0)=100 and Atg1_Atg13(0)=0. Steady state of Atg1_Atg13 complex is high ~90%, which is reasonable level in the inhibition of mTOR.*

Figure below presents result of the simulation in the third scenario of initial conditions (table 4.1.1).

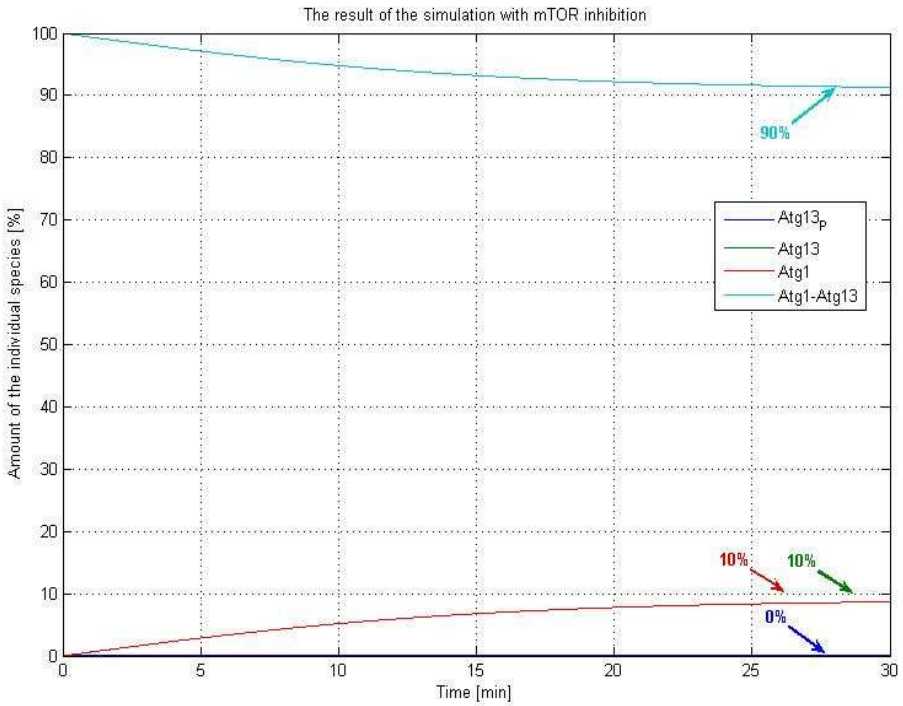

Figure 4.1.27 Result of the model testing for parameters k_4-k_7 in the mTOR inhibition. *The plot was made as a result of a simulation in SBtoolbox for MatLab and shows the behaviour of Atg1-Atg13 complex, Atg13_P, Atg13 and Atg1. Initial concentrations for this simulation: Atg13_P(0)=0, Atg13(0)=0, Atg1(0)=0 and Atg1_Atg13(0)=100. Steady state of Atg1_Atg13 complex is high ~90%, which is reasonable level in the inhibition of mTOR.*

In all plots (4.1.25, 4.1.26 and 4.1.27) we can see the levels of all individual species reached the same level, respectively to all initial conditions (table 4.1.1), in the inhibition of mTOR conditions. Atg1_Atg13 complex reached very high steady states level, on the contrary to Atg13_P, which is on the low level. This result is reasonable in the mTOR inhibition conditions.

4.1.5 Conclusions for model parameterization

We therefore conclude that we successfully implemented all reactions and can re-model the published biological behaviour of the all reactions involved in the induction of the autophagy.

Table 4.1.2 contains all reaction kinetics which are used in the model. References for all the calculations and fittings are also enclose.

Table 4.1.2 Reaction kinetics used in the model.

Rate expression	Parameter	Value of the parameter	Reference
$k_1 \cdot Rheb^{GTP}$	k_1	0.06716 [min^{-1}]	Calculated based on Inoki et al., 2005; Marshall et al., 2009
$k_2 \cdot Rheb^{GTP}$	k_2	0.04046 [min^{-1}]	Calculated based on Inoki et al., 2005; Marshall et al., 2009
$k_3 \cdot Rheb^{GTP} \cdot (mTOR\_FKBP38)$	k_3	0.00333 [$min^{-1} \cdot u^{-1}$]*	Calculated based on Sato et al., 2009
$k_{-3} \cdot (Rheb^{GTP}\_FKBP38) \cdot mTOR$	k_{-3}	0.00133 [$min^{-1} \cdot u^{-1}$] *	Calculated based on Bai et al., 2007

$k_4 \cdot Atg13 \cdot mTOR$	k_4	0.01498 $[min^{-1} \cdot u^{-1}]$ *	Calculated based on Kamada et al., 2000
$k_5 \cdot (Atg13\_P)$	k_5	0.5991 $[min^{-1}]$	Calculated based on Kamada et al., 2000
$k_6 \cdot Atg13 \cdot Atg1$	k_6	0.006649 $[min^{-1} \cdot u^{-1}]$ *	Fitting based on Kamada et al., 2000
$k_{-6} \cdot (Atg1\_Atg13)$	k_{-6}	0.0059 $[min^{-1}]$	Fitting based on Kamada et al., 2000
$k_7 \cdot (Atg1\_Atg13) \cdot mTOR$	k_7	0.01498 $[min^{-1} \cdot u^{-1}]$ *	Assumption based on Kamada et al., 2000

* *u represents relative unit, %.*

In the next part of the thesis we implemented full model with all reactions which are involved in the autophagy induction.

4.2 ODE modelling of the induction of autophagy – initial model

After extraction all parameters for every single reaction (for details see chapter 4.1, Model parameterization) we implemented the initial model which includes reactions 1 to 7. The input to the system is the initial concentrations of species from the first reaction ($Rheb^{GDP}$ and $Rheb^{GTP}$), which are not in the ratio of normal nutrient conditions. This means that the system needs some time to reach the steady state and this time depends on the individual initial concentrations of all species. The output is the amount of Atg1-Atg13 complex, which is essential to induce the autophagy pathway.

4.2.1 Simulations and results for initial model without feedback

The initial conditions of all species for the first 4.2.1A simulation were:

$Rheb^{GDP}(0)=100$, $Rheb^{GTP}(0)=0$, mTOR(0)=0, mTOR-FKBP(0)=100, $Rheb^{GTP}$-FKBP(0)=0, Atg13-P(0)=0, Atg13(0)=100, Atg1(0)=100 and Atg1-Atg13(0)=0. These initial conditions represent an extreme scenario, where there is no mTOR in the active form and all Rheb is in the inactive GDP form. This scenario can mimic starvation conditions. Atg13 is in the unphosphorylated form, which allows fast creation of the Atg1-Atg13 complex. However, after some time, due to normal regular reactions, the system reaches steady states conditions, where the active mTOR concentration is quite high and the concentration of the Atg1-Atg13 complex decreases significantly. Figure 4.2.1 shows the result of simulations with these initial conditions.

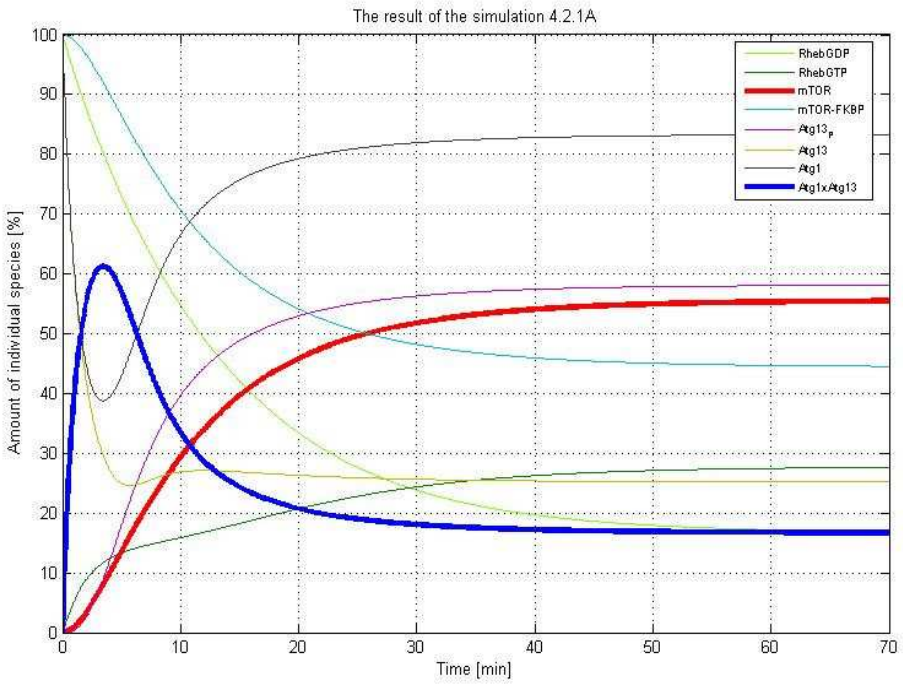

Figure 4.2.1 Result of simulation 4.2.1A for all reactions involved in autophagy induction. *The plot displays the results of a simulation using the SBtoolbox for MatLab and shows the different behaviours of the individual species for the given initial condition. Blue bold line represents Atg1-Atg13 complex, which slowly decreasing with mTOR (red) increase.*

The steady state for all species is given by: $Rheb^{GDP}$=16.7091, $Rheb^{GTP}$=27.7356, mTOR=55.5553, mTOR-FKBP=44.4447, $Rheb^{GTP}$-FKBP=55.5553, Atg13-P=58.1475, Atg13=25.1944, Atg1=83.3419 and Atg1-Atg13=16.6581.

To check the implementation, we run simulation for different initial conditions and tested whether the same steady state was reached. The difference in initial conditions for the second simulation, compared with the first one, is that all Atg13 is in the hyperphosphorylated form, thus Atg13-P(0)=100 and Atg13(0)=0. We expected that the Atg1-Atg13 complex would appear later, compared with the simulation 4.2.1A, and

that its concentration would be lower, because of the inhibitory role of active mTOR. Figure 4.2.2 shows the result of the second simulation.

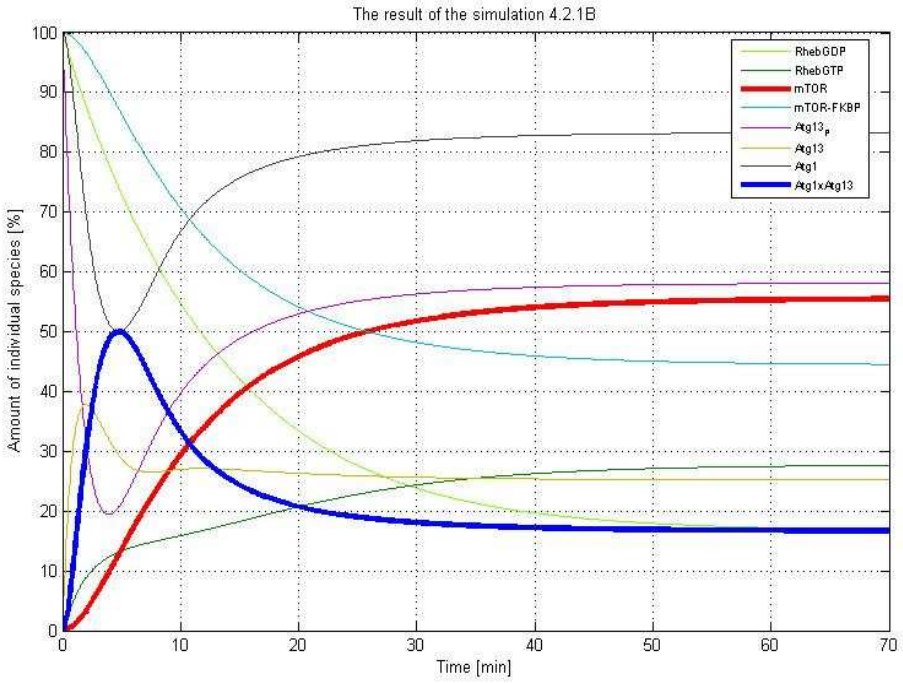

Figure 4.2.2 Result of the simulation 4.2.1B for all reactions involved in autophagy induction*. The plot displays the results of a simulation using the SBtoolbox for MatLab and shows the different behaviour of the individual species for the given initial conditions. Atg1-Atg13 complex (blue) slowly decreases with mTOR (red) increasing. Final steady state values of all the species are the same as in previous simulation.*

Figure 4.2.3 below shows the result of a third simulation. In this case all Rheb is in the active GTP form, thus $Rheb^{GDP}(0)=0$ and $Rheb^{GTP}(0)=100$. This scenario mimics rich nutrient conditions, suggesting that the system will reach steady state faster than in two previous simulations. The plot 4.2.3 shows the result of this simulation.

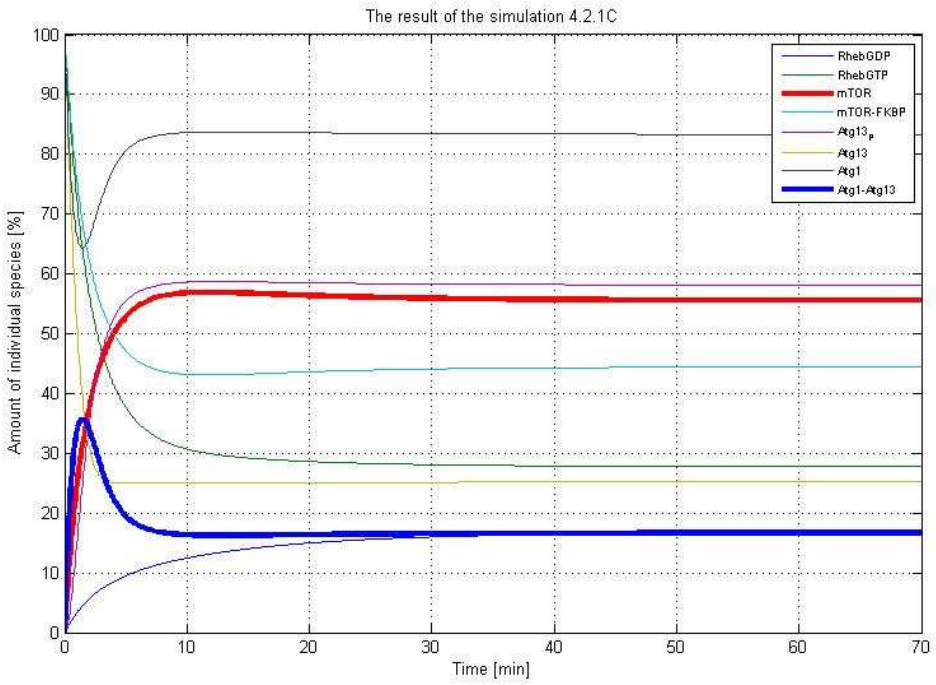

Figure 4.2.3 Result of the simulation 4.2.1C for all reactions involved in autophagy induction. *The plot displays the results of a simulation using the SBtoolbox for MatLab and shows the different behaviour of the individual species for the given initial conditions. mTOR (red) increase very fast, as well as Atg1-Atg13 complex (blue) decreases, due to high level of Rheb in an active GTP form. Final steady state values of all the species are the same as in previous simulation.*

The initial conditions for the simulation 4.2.1D mimic an extreme starvation scenario, when the Atg1-Atg13 complex is in very high concentration, thus Atg13-P(0)=0, Atg13(0)=0, Atg1(0)=0 and Atg1-Atg13(0)=100. While the system is approaching the steady state conditions, the Atg1-Atg13 complex should continuously decrease with the increase of mTOR activity.

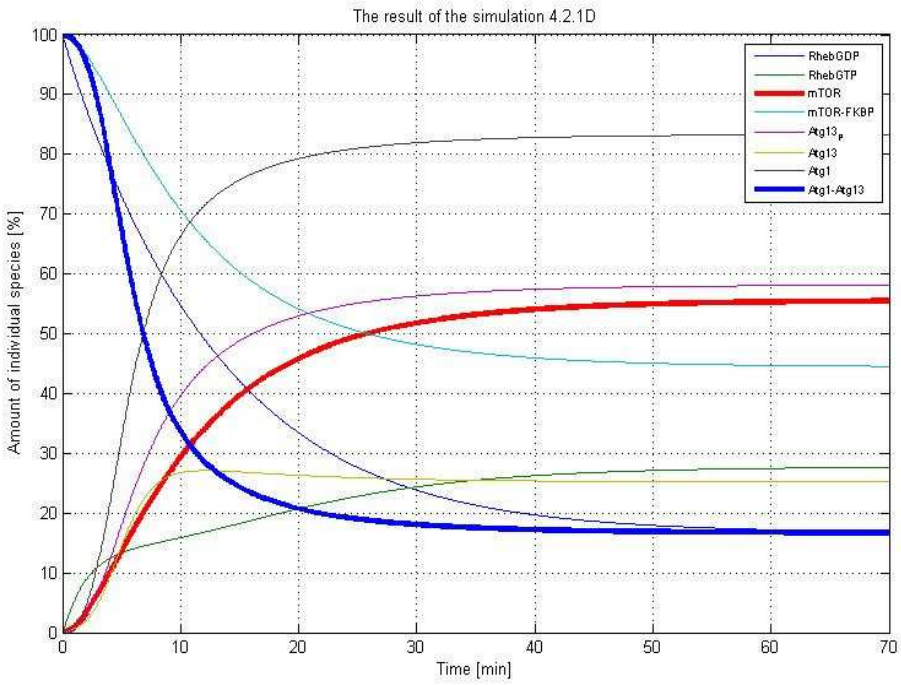

Figure 4.2.4 Result of the simulation 4.2.1D for all reactions involved in autophagy induction. *The plot displays the results of a simulation using the SBtoolbox for MatLab and shows the different behaviour of the individual species for the given initial conditions. Atg1-Atg13 complex (blue) decreases slowly from the very high concentration, with the slowly increasing of mTOR (red). Final steady state values of all the species are the same as in previous simulation.*

In conclusion, our initial model represents the behaviour of all model components in response to changes in initial conditions. In all cases, mTOR was not inhibited but its initial concentration was always 0. The other species were in conditions which might mimic starvation (Rheb in inactive GDP form, Atg13 in unphosphorylated form, high level of atg1-Atg13 complex) or in normal nutrient conditions (Rheb in active GTP form, Atg13 in hyperphosphorylated form). In all scenarios our system reached the same steady state, which is 55.55 % of mTOR and 16.66 % of Atg1-Atg13

complex. Table 4.2.1 shows the list of the initial conditions for all simulations and the final steady states for all the species. The steady state which was approached is the steady state in normal rich nutrient conditions, when all the species function properly. The time taken to reach the steady state depended on initial conditions: the closer to starvation conditions the longer the time taken to reach steady state.

Table 4.2.1 Initial concentrations for all species involved in the model for the first fourth initial simulations 4.2.1A – 4.2.1D

Species	Initial concentrations for simulation				Steady state [%]
	4.2.1A	4.2.1B	4.2.1C	4.2.1D	
$Rheb^{GDP}$	100	100	0	100	16.71
$Rheb^{GTP}$	0	0	100	0	27.74
mTOR	0	0	0	0	**55.55**
mTOR-FKBP38	100	100	100	100	44.44
$Rheb^{GTP}$-FKBP38	0	0	0	0	55.55
Atg13_P	0	100	0	0	58.15
Atg13	100	0	100	0	25.19
Atg1	100	100	100	0	83.34
Atg1-Atg13	0	0	0	100	**16.66**

4.2.2 Implementation of the rapamycin as an mTOR inhibitor

In the previous sub-chapter mTOR was not inhibited for four different sets of initial conditions, the system reached the same steady state. The steady state levels for all the species are characteristic in normal rich nutrient conditions (high mTOR, low Atg1-Atg13 complex).

In the next stage we add mTOR inhibition by rapamycin to the model (simulation 4.2.2). Specifically, we include reaction R_8 which represents inhibition of mTOR by rapamycin (R). The product of the reaction is the inactive mTOR-rapamycin complex (mTOR-R).

$$R_8 : mTOR + R \xrightarrow{k_8} mTOR\_R \tag{4.2.1}$$

The rate expression for this reaction is:

$$\upsilon_8 = k_8 \cdot mTOR \cdot R \tag{4.2.1}$$

Based on the reaction above we can describe the temporal change in concentration of the mTOR, rapamycin and mTOR-R complex by using an ordinary differential equation:

$$\begin{aligned} \frac{d(mTOR)}{dt} &= -\upsilon_8 \\ \frac{dR}{dt} &= -\upsilon_8 \\ \frac{d(mTOR-R)}{dt} &= \upsilon_8 \end{aligned} \tag{4.2.3}$$

The initial concentration of rapamycin for the simulation 4.2.2 is assumed to be 100, the same as the total amount of mTOR (in all different species). This assumption was essential to ensure that rapamycin was able to inhibit all mTOR. Also we updated the model with the initial conditions of all the species obtained from the previous simulation (table 4.2.1). These concentrations represent the amount of the model components in normal cellular conditions. The parameter k_8 for the added reaction was assumed to be 0.02 min^{-1} based on information that after rapamycin treatment the Atg1-Atg13 complex appears in 10 minutes [*Kamada et al., 2000*].

We expected that the level of mTOR would decrease quite fast because rapamycin is its direct inhibitor. Further, the amount of Atg1-Atg13 complex should increase and after 10 minutes we expect a significant rise.

The figure below represents the results of the simulation 4.2.2A.

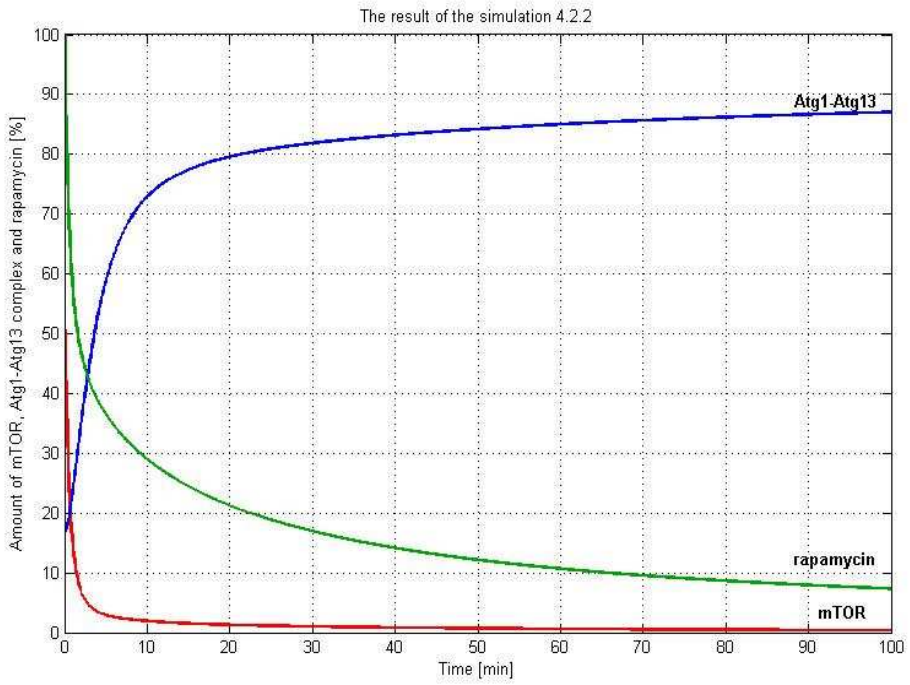

Figure 4.2.5 Result of the simulation 4.2.2 for mTOR and Atg1-Atg13 complex behaviour after mTOR inhibition by rapamycin. *The plot displays the results of a simulation using the SBtoolbox for MatLab and shows the different behaviour of the mTOR and Atg1-Atg13 complex after rapamycin treatment (dose of rapamycin 100%). mTOR (red) decreases very quickly because of direct inhibition by rapamycin. Atg1-Atg13 complex (blue) increases significantly within 10 minutes*

The new steady states after rapamycin treatment (100%) are: mTOR=$4.42389 \cdot 10^{-8}$ and Atg1-Atg13=90.9424. We can say that after rapamycin treatment, mTOR is completely inhibited and the Atg1-Atg13 complex increases up to ~91%, which means that autophagy pathway can be induced.

The figure plots the amount of mTOR and the Atg1-Atg13 complex against the dose of rapamycin.

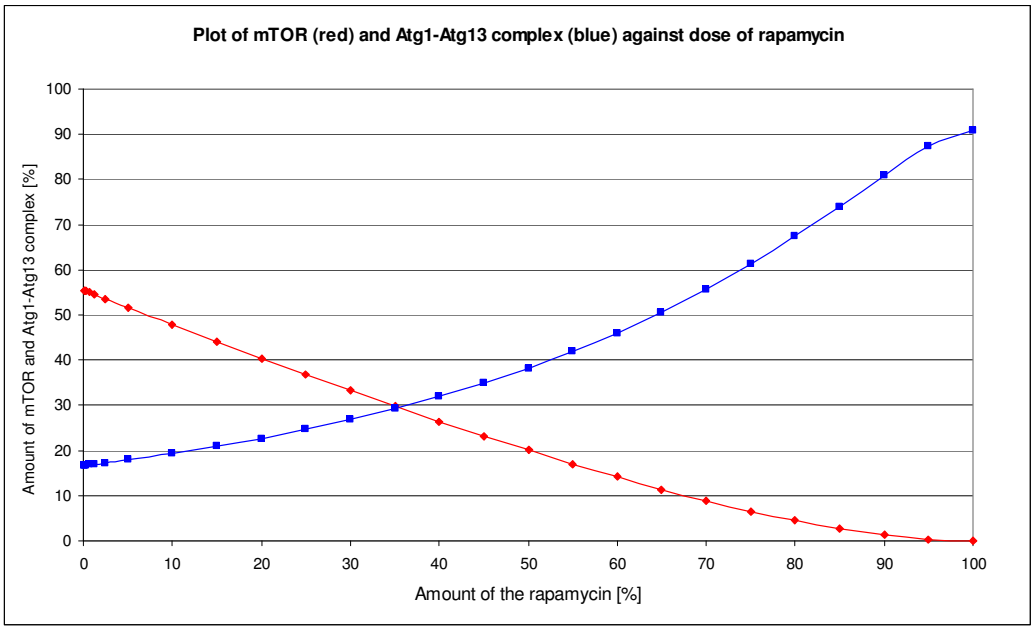

Figure 4.2.6 Dose dependent inhibition of mTOR kinase activity by rapamycin (red) and relationship between dose of rapamycin and Atg1-Atg13 complex (blue) creation. *The plot represents the relation between the mTOR and Atg1-Atg13 complex on different doses of rapamycin. The plot displays the results of a simulation using the SBtoolbox for MatLab.With rising dose of rapamycin mTOR decreases while Atg1-Atg13 complex increases. Dose dependent inhibition of mTOR by rapamycin has linear manner.*

We observed that even small doses of rapamycin (>10%) are able to inhibit mTOR activation. mTOR decreases in a linear manner with higher doses of rapamycin. We can also note that the creation of the Atg1-Atg13 complex is slightly delayed compared to the beginning of mTOR inhibition. Atg1-Atg13 complex has also bigger changes at the end of its curve, and reaches some level of saturation.

Figure 4.2.7 represents the kinetic behaviour of mTOR for different doses of rapamycin. The plot displays the results of a simulation using the SBtoolbox for MatLab.

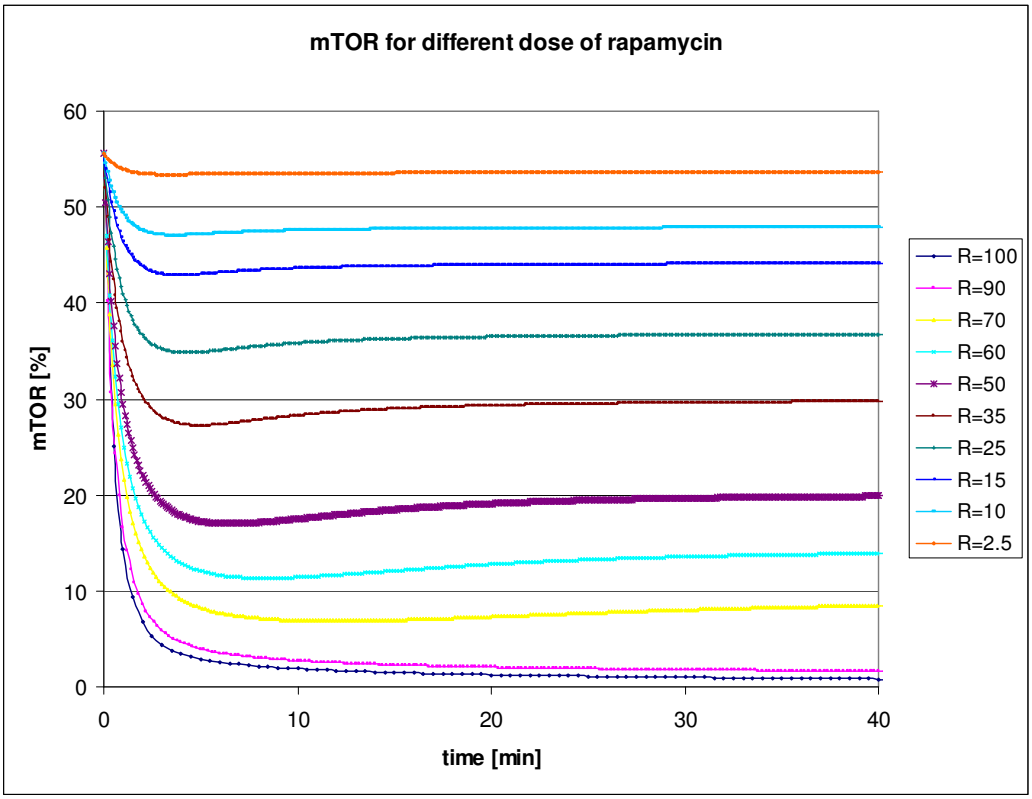

Figure 4.2.7 Representation of the kinetic behaviour of mTOR in response to different doses of rapamycin. *The plot represents the relation between mTOR in different doses of rapamycin and time. The plot displays the results of a simulation using the SBtoolbox for MatLab. We can observe that mTOR inhibition is very fast in all doses of rapamycin.*

The smaller the dose of rapamycin, the faster the steady state is reached and its value is closer to the basic level of the steady state for mTOR (55.55%). The higher dose of

rapamycin, the longer it takes to reach the steady state. mTOR's response to different doses of rapamycin is rather linear, there is no significant threshold.

Figure 4.2.8 represents the kinetic behaviour of the Atg1-Atg13 complex for different doses of rapamycin. The plot displays the results of a simulation using the SBtoolbox for MatLab.

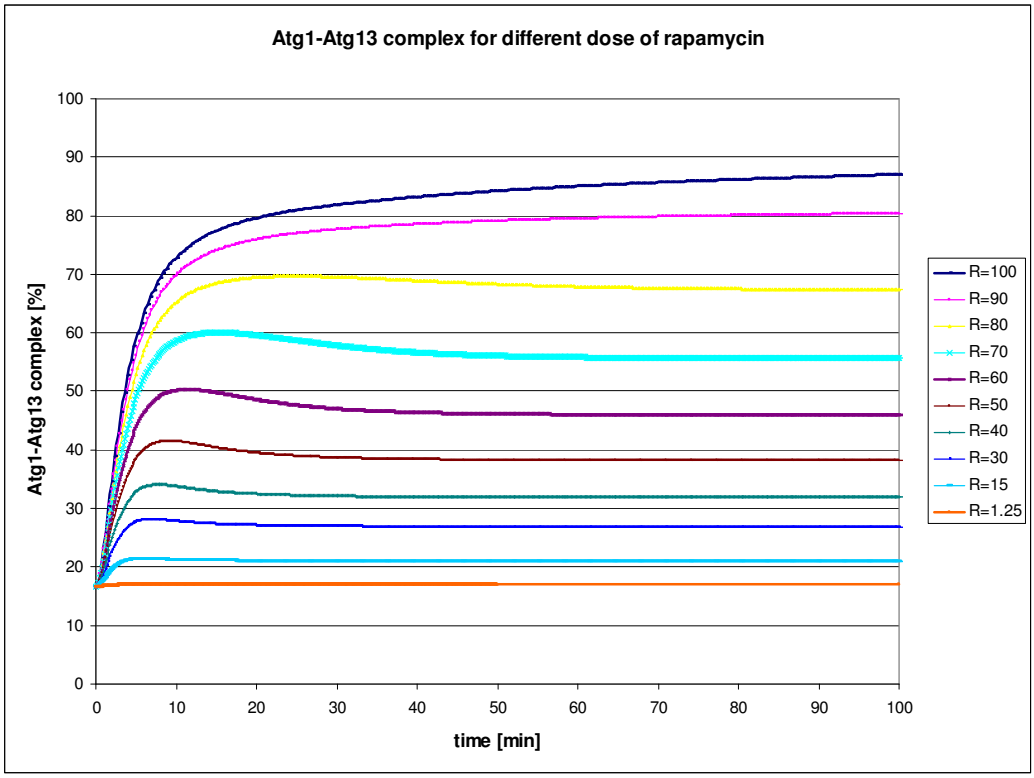

Figure 4.2.8 Representation of the kinetic behaviour of Atg1-Atg13 complex in response to different doses of rapamycin. *The plot represents the relation between the Atg1-Atg13 complex for different doses of rapamycin and time. The plot displays the results of a simulation using the SBtoolbox for MatLab. We can observe that Atg1-Atg13 complex creation is very fast in all doses of rapamycin.*

The smaller the dose of rapamycin, the lower the effect on the Atg1-Atg13 complex and the faster the steady state is reached. The higher the dose of rapamycin, the longer it

takes to reach the steady state. The response of Atg1-Atg13 complex to different doses of rapamycin is rather linear, there is no significant threshold.

4.2.3 Starvation mimic by changing parameter k_1

In the next step we checked our initial model (as implemented in 4.2.1) in starvation conditions by changing the parameter k_1. Parameter k_1 which was calculated in chapter 4.1 is correct in normal rich nutrient conditions. By decreasing its value we can mimic starvation conditions.

For the simulations 4.2.3 the model was implemented exactly the same as in 4.2.1. This time to obtain plots we used MatLab syntax [SBtoolbox code was transferred to the MatLab code by Bartlomiej Tomiczek] and the parameter k_1 was changed automatically. We were interested only in the starvation effect, therefore parameter k_1 has only been changing in the range of (k_1, 0), where k_1=0.06716 min^{-1}. Figure 4.2.9 plots the amount of mTOR and Atg1-Atg13 complex against different values of k_1.

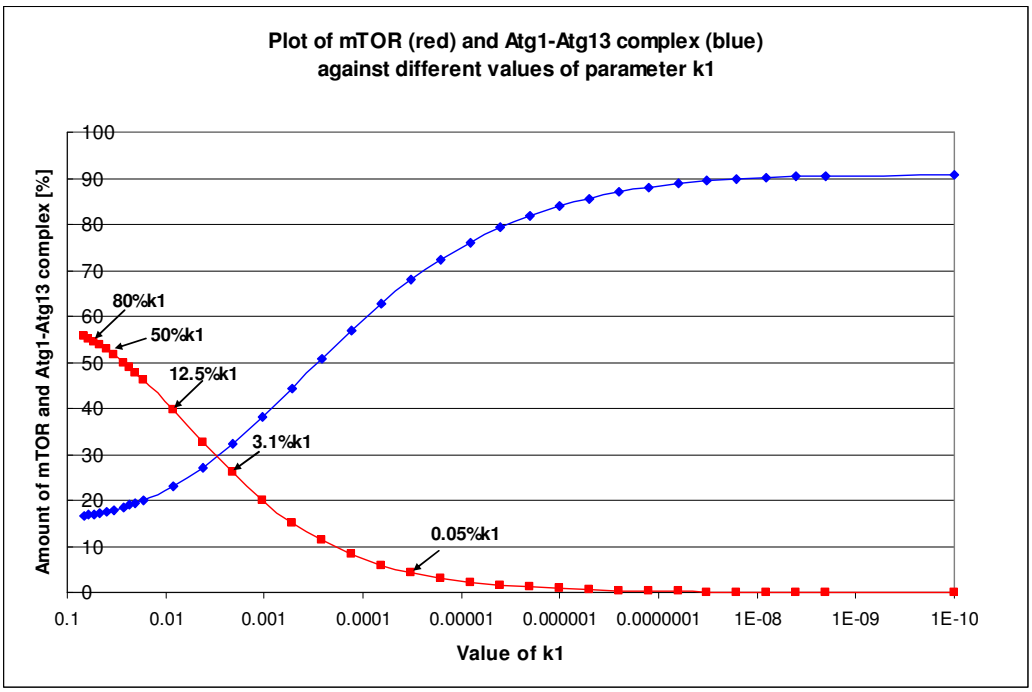

Figure 4.2.9 Inhibition of mTOR kinase activity (red) by decreasing parameter k_1 (starvation mimic). Relation between changes in parameter k_1 and Atg1-Atg13 complex (blue) creation. *Figure plots the mTOR and Atg1-Atg13 complex against different values of k_1. The plot was made using simulations in MatLab. To obtain good autophagy response (high level of Atg1-Atg13 complex) parameter k_1 has to be implemented as very low. With lower values of parameter k_1 mTOR decreases while Atg1-Atg13 complex increases.*

We could observe that to induce autophagy (which is synonymous to an increase in the Atg1-Atg13 complex) we need to decrease parameter k_1 by approximately 90-95%. It means that to get good autophagy response we need almost total starvation. mTOR decreases earlier and more rapidly than the Atg1-Atg13 complex increases. This fact allows us to conclude that mTOR has a buffer character.

Figure 4.2.10 represents the kinetic behaviour of mTOR for different values of parameter k_1. The plot was made using simulation in MatLab.

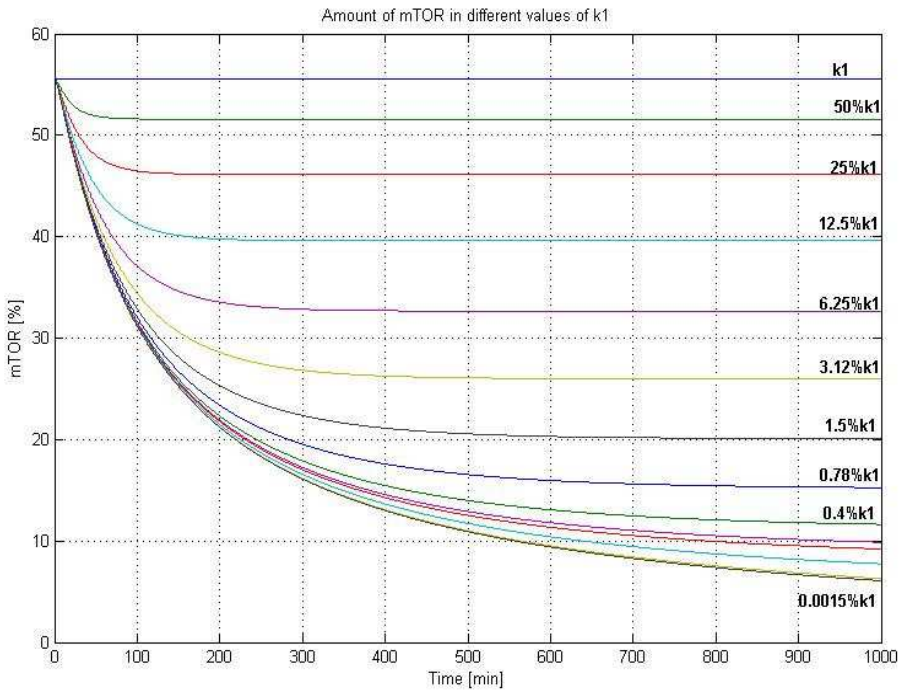

Figure 4.2.10 Representation of the kinetic behaviour of mTOR in response to different value of k_1. *The plot displays the results of a simulation using the SBtoolbox for MatLab. The figure plots mTOR against time for different values of k_1. The level of mTOR decreases with decreasing of the parameter k_1 value. We observe that mTOR inhibition is very slow for all values of k_1, and the smaller k_1 is the longer it takes.*

The higher value of k_1 (closer to value k_1=0.06716) the faster steady state is reached and the closer it is to the basic value of steady state for mTOR (55.55%). The smaller k_1 value, the longer it takes to reach steady state.

Figure 4.2.11 represents the kinetic behaviour of Atg1-Atg13 complex for different values of parameter k_1. The plot was made using simulation in MatLab.

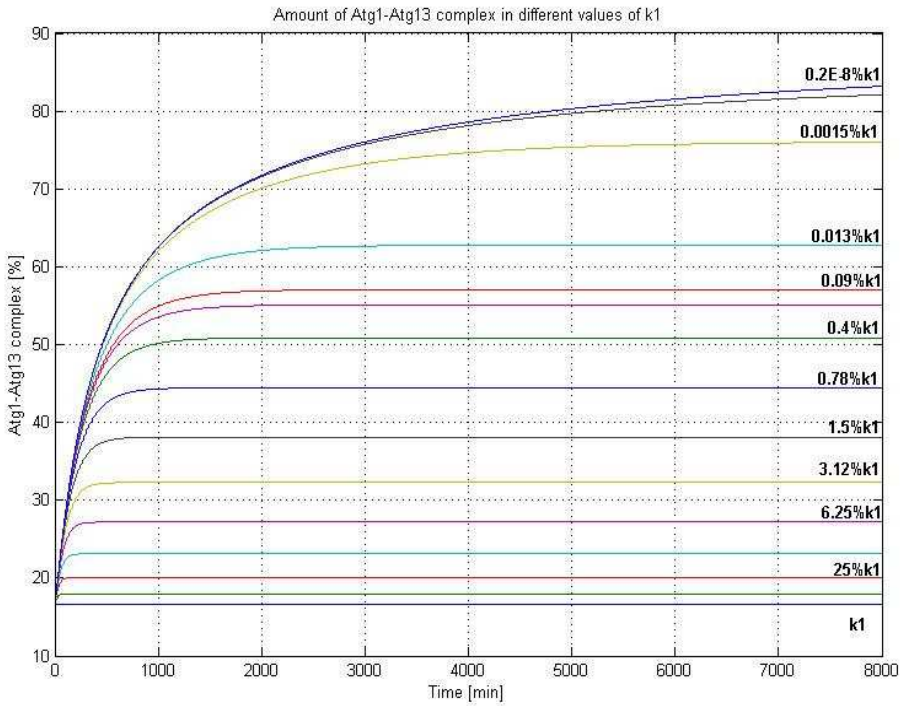

Figure 4.2.11 Representation of the kinetic behaviour of Atg1-Atg13 complex in response to different value of k_1. *The plot was made using simulations in MatLab. The figure plots the Atg1-Atg13 complex against time for different values of k_1. The level of the Atg1-Atg13 complex increases with decreasing of the parameter k_1 value. We could observe that Atg1-Atg13 complex creation is very slow for small values of k_1, which means that to get a high level of complex we have to starve the cell for a long time.*

The higher value of k_1, the lower the effect on Atg1-Atg13 complex and the faster the steady state is reached. The smaller values of k_1 the longer it takes to reach the steady state.

4.2.4 Conclusions for the initial model

We successfully implemented the initial model which includes reactions 1 to 7 (diagram 4.1). We checked the model in three different scenarios (all without feedback): 4.2.1) in normal rich nutrient conditions, 4.2.2) in mTOR inhibition by rapamycin and 4.2.3) in starvation mimic (by decreasing parameter k_1). Simulation 4.2.1 provides the steady state values for all the species involved in the model in normal nutrient conditions. Simulations 4.2.2 and 4.2.3 lead to the induction of the autophagy pathway, due to mTOR inhibition.

Simulation 4.2.1 was performed in the normal rich nutrient conditions, whereby we could get values of the steady states in this scenario. The obtained steady states are reasonable agreement with biological experimental data. In normal nutrient conditions the steady state for mTOR is 55.55%, while for the Atg1-Atg13 complex it is 16.66%. This illustrates that in rich medium conditions mTOR is active and the Atg1-Atg13 complex remains on a low level. This partial amount of complex is required to maintain basal autophagy (Cvt pathway), which is necessary for turnover of long lived proteins.

Based on the last two simulations (with mTOR inhibition by rapamycin and starvation mimic by decreasing k_1) we can observe that induction of autophagy by rapamycin and by starvation has different kinetics, however the final results are similar: simulation 4.2.2 with rapamycin R(0)=100 and simulation 4.2.3 with $k_1 \cong 0$ both gave the results of Atg1-Atg13 complex 90.94 % and mTOR ~10^{-8} % (table 4.2.2). We could also observe significant differences in the amount of rapamycin and the lack of nutrients which are needed for autophagy induction. To increase Atg1-Atg13 complex to ~20%, only 15-20% of rapamycin is needed, while during the starvation scenario almost 90-95% of the k_1 value has to be taken out to obtain the same results.

Table 4.2.2 List of the steady states values for the all species obtained in simulations 4.2.1, 4.2.2 and 4.2.3.

Species	Steady states concentrations [%] in conditions:		
	normal	rapamycin (100%)	mimic starvation k_1=0
	Simulation: 4.2.1	4.2.2	4.2.3
$Rheb^{GDP}$	16.71	0.000632913	100
$Rheb^{GTP}$	27.74	0.00105058	0
mTOR	**55.55**	**$4.42389 \cdot 10^{-8}$**	**$2.54474 \cdot 10^{-8}$**
mTOR-FKBP38	44.44	0.00168349	100
$Rheb^{GTP}$-FKBP38	55.55	99.9983	0
Atg13_P	58.15	$1.10634 \cdot 10^{-7}$	$6.36398 \cdot 10^{-8}$
Atg13	25.19	9.05764	9.05764
Atg1	83.34	9.05764	9.05764
mTOR-R	-	99.9983	-
Atg1-Atg13	**16.66**	**90.9424**	**90.9424**

We also can say that the system has a fast response to rapamycin treatment – mTOR decreases after a maximum of 30 minutes (figure 4.2.7), while in starvation mimic (k_1 manipulation) the response is quite slow and new steady states established in approximately 10^3 minutes (figure 4.2.10 and 4.2.11). This indicates that autophagy induction after rapamycin treatment is 100 times faster than induction due to nutrient starvation.

Possible reasons why there is such a big difference in the time of autophagy induction via rapamycin and starvation include:

- rapamycin is a direct inhibitor of mTOR, which means that to block mTOR activation we can omit reactions 1 and 3 (according to the diagram 4.1)
- to obtain mTOR inhibition by decreasing k_1 (starvation mimic) we have to take into account reactions 1 and 3 (diagram 4.1), which take some time.

In the normal rich nutrient conditions k_1 is bigger than k_2, which allows creation of active $Rheb^{GTP}$. Active $Rheb^{GTP}$ plays the role of mTOR activator. In the starvation scenario k_1 is smaller than k_2, so production of new $Rheb^{GTP}$ is blocked. All fraction of $Rheb^{GTP}$ is in the complex with FKBP38, thus mTOR is activated. To inhibit mTOR in starvation conditions, we need its endogenous inhibitor FKBP38, thus dissociation of $Rheb^{GTP}$-FKBP38 is necessary. The reaction of dissociation, which takes some time, might slow down in general mTOR inhibition in starvation. In different words, to inhibit mTOR in starvation conditions, FKBP38 is needed. And because FKBP38 is in the complex with $Rheb^{GTP}$, it takes some time to dissociate this complex and obtain FKBP38 to block mTOR activity.

From the experimental data [*Kamada et al., 2000*] we know, that inhibition of mTOR after rapamycin is very fast (~5 minutes). Activation of autophagy by starvation is a much slower process and could a take few days [*Chera et al., 2009*]. We can conclude that the results of our initial model agree with experimental data.

4.3 Implementation of the full autophagy model

Next, we could include into the model the total amino acid pool (4.3.1) and feedback from the amino acids created during autophagy pathway (4.3.2).

In this chapter we present results of simulations with the fully implemented model of the autophagy pathway. First we wanted to test again the initial model but this time with the total amino acid pool implementation as a variable. In normal nutrient conditions, when the external amino acid supply is set to 100%, we expected the same results as in the previous simulations (4.2.1) with fixed k_1. Next the feedback from the amino acids produced by autophagy was implemented as a contribution on the total amino acids pool.

4.3.1 The total amino acid pool implementation

Until now reaction 1 was implemented with a fixed k_1 which takes into account normal nutrient conditions. The assumption before was that the external amino acid supply was constant and by manipulating k_1 we could simulate changes in the external amino acids. Amino acids now should become a variable throughout the modelled time frame.

Amino acids are continuously provided (external supply) and consumed by various reactions in the cell. We reduce these processes to the two reactions.

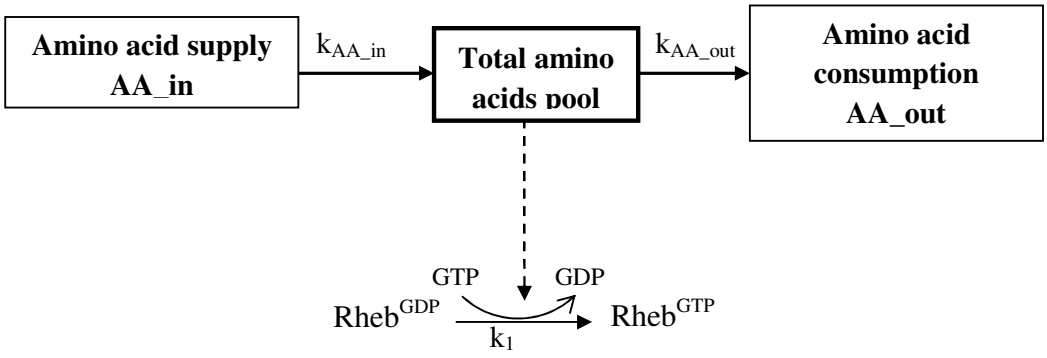

Figure 4.3.1 The total amino acid pool. *Amino acids control the activation Rheb. The total amino acid pool is feed by an external amino acid supply. Amino acids are consumed by various reactions in the cell.*

The mass balance would be:

$$\frac{d(AA)}{dt} = \upsilon_{AA\_in} - \upsilon_{AA\_out} \tag{4.3.1}$$

where:

υ_{AA_in} – inflow of amino acids (for example external supply)

υ_{AA_out} – amino acids consumption by the cell (for example protein production, cell growth and division)

In order to keep things as simple as possible, we consider a constant inflow of the amino acids:

$$\upsilon_{AA\_in} = k_{AA\_in} \tag{4.3.2}$$

and the consumption of the amino acids could be shown as follow:

$$\upsilon_{AA\_out} = k_{AA\_out} \cdot AA \qquad (4.3.3)$$

This is a simply assumption for the amino acids consumption to make sure that the cell reduces its amino acids consumption when the concentration is reduced and that the amino acids concentration will remain positive.

A turnover of the amino acids in mammalian cells is 1% per hour [*Mandelstam, 1960*], which gives the reaction constant k_{AA_out}=0.0001666 min^{-1}. To balance the total amino acid pool, the inflow of amino acids AA_in would have to be $\upsilon_{AA\_in} = \upsilon_{AA\_out}$, which means that $k_{AA\_in} = k_{AA\_out} \cdot AA$ and k_{AA_in}=0.01666 min^{-1}.

Using the model in the case of the amino acid pool implementation, a simulation 4.2.7 was made to check the correct software implementation of parameters k_{AA_in} and k_{AA_out}. We started the simulation with the same initial conditions as all previous simulations to see the behaviour of all of the species. We expected the same steady states values as in 4.2.1 simulation.

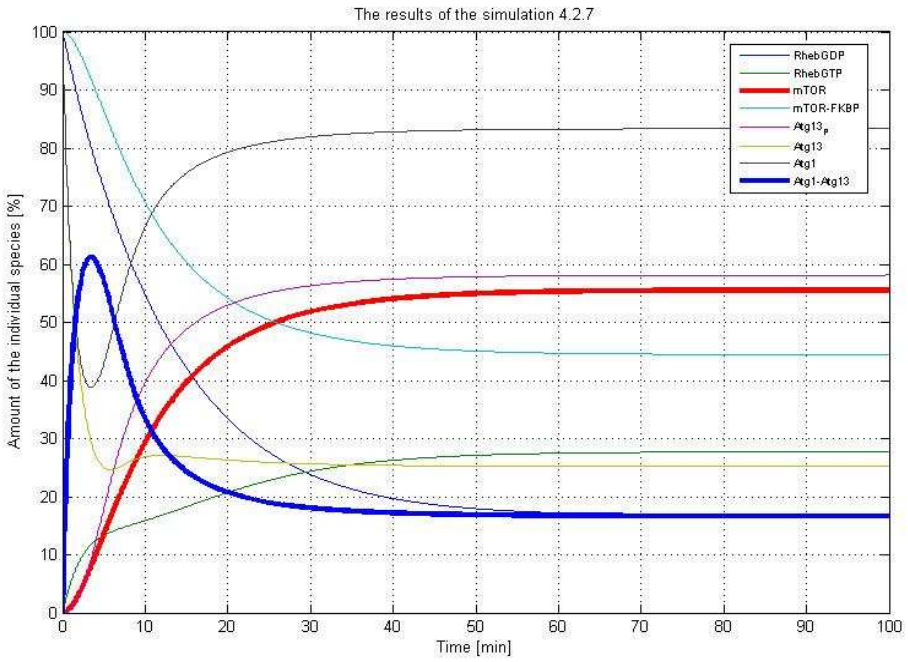

Figure 4.3.2 Result of the simulation 4.2.7 for all reactions involved in autophagy induction*. The plot was made as a result of a simulation in SBtoolbox for MatLab and shows different behaviour of the individual species with set initial conditions. Blue bold line represents Atg1-Atg13 complex, which slowly decreases with mTOR (red bold line) increase. The simulation was similar to 4.2.1A, but in this scenario amino acids were implemented as a catalyser of reaction 1 (see figure 4.3.1).*

The steady states, which are the results of the simulation, are: $Rheb^{GDP}$=16.7091, $Rheb^{GTP}$=27.7356, mTOR=55.5553, mTOR-FKBP=44.4447, $Rheb^{GTP}$-FKBP=55.5553, Atg13-P=58.1475, Atg13=25.1944, Atg1=83.3419 and Atg1-Atg13=16.6581. These steady states values are exactly the same as in simulation 4.2.1. This result proves that the amino acids were implemented correctly.

4.3.2 The contribution of the autophagy feedback on the amino acid pool

In the previous sub-chapters we implemented the initial model without the contribution of autophagy to the amino acid pool. In this part of the thesis the feedback loop has been added (figure 4.3.3), to modify the level of the total amino acid pool. The total amino acid pool is feed now with extra amino acids, which are produced by autophagy. The contribution of these amino acids is added to the model with a time delay and kinetic constant k_F, which represents the strength of the feedback. We use here an idea of time delay for the part of the pathway from autophagosome nucleation to the degradation in lysosome and recycling.

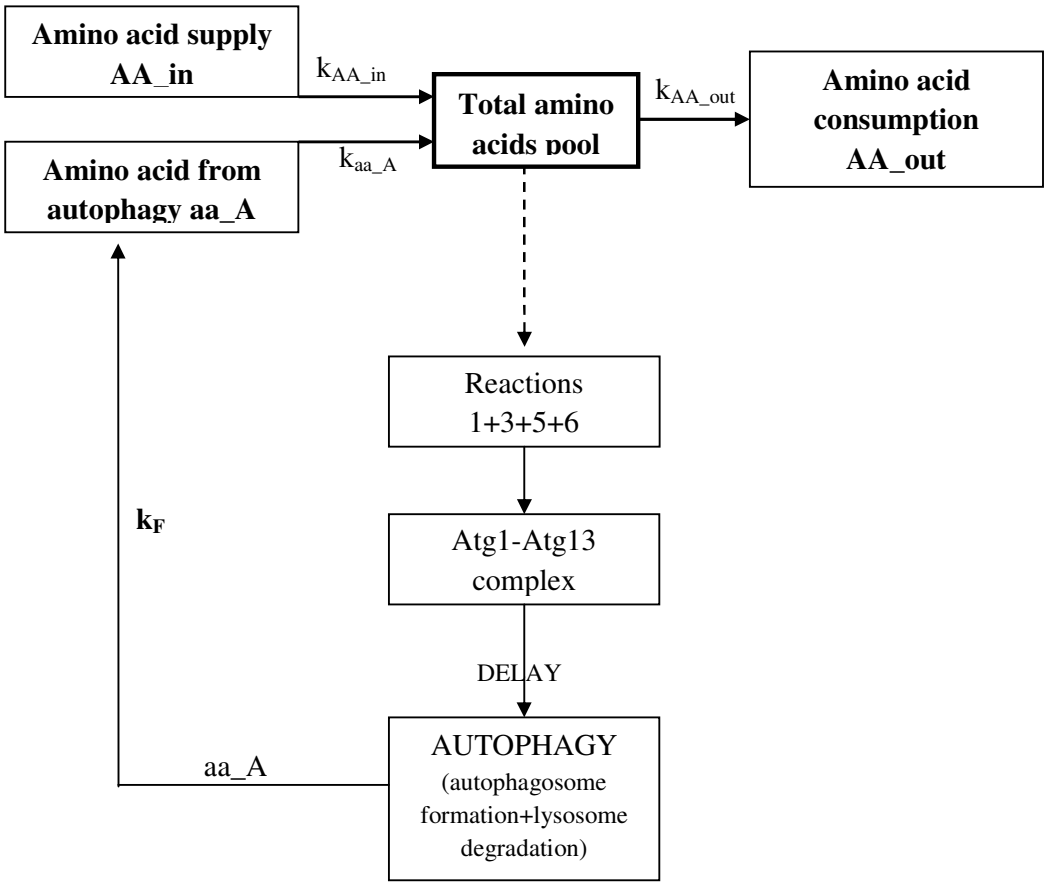

Figure 4.3.3 Diagram of the full model of autophagy pathway. *The total amino acid pool is maintained by two inflows: external amino acids supply and amino acids from the autophagy pathway. Amino acids control induction of the autophagy (reactions 1+3+5+6). The result of the induction is the Atg1-Atg13 complex. The amount of the Atg1-Atg13 complex, with the time delay and strength k_F composes feedback of the system.*

Now the total amino acids mass balance with the autophagy contribution aa_A would be

$$\frac{d(AA)}{dt} = \upsilon_{AA\_in} - \upsilon_{AA\_out} + \upsilon_{aa\_A} \qquad (4.3.4)$$

The process from the autophagosome nucleation and finishing with the lysosomal degradation and recycling is modelled as a time delay (20 minutes). Little is known about the part of the biochemical pathway from the autophagosome nucleation until fusion with the lysosome, but at least we know that it takes approximately 10 minutes [*Yoshimori, 2004*]. The lysosomal pathway for the protein degradation (autophagy) we model as a pure time delay as well (additional 10 minutes time is set for degradation in the lysosome). The total time delay from the Atg1-Atg13 complex formation to the generation of the amino acids from the autophagy therefore was 20 minutes.

We made a simple assumption, that amount of the amino acids which are produced during the autophagy pathway, is proportional to the amount of Atg1-Atg13 complex. Based on this assumption and figure 4.3.3 we could write a rate expression for the feedback reaction

$$\upsilon_F = k_F \cdot (Atg1\_Atg13)_{time\_delay} \qquad (4.3.5)$$

The rate of the amino acids which are produced during autophagy is defined by the strength of the feedback constant k_F.

The part of the model with the time delay and feedback was implemented in the MatLab syntax by Bartlomiej Tomiczek. The reason for switching to the MatLab was that this software is more flexible and it allows more complex work, than SBtoolbox. The time delay was set to 20 minutes. Parameter k_F was assumed to be 1, in order to get the proportional amount of aa_A to the Atg1-Atg13 complex. In other words, we can present this relationship by

$$\frac{d(aa\_A)}{dt} = k_F \cdot \frac{d(Atg1\_Atg13)}{d(t_{delay})} \tag{4.3.6}$$

The parameter k_F is responsible for the velocity of the production of the amino acids during the autophagy pathway. The feedback strength k_F and the time delay are implemented in this way so that none of them influences the level of the amino acids production by the autophagy. The response of the system is not restricted by implementation method. Feedback modifies k_1 and plays a role of the total amino acids pool modulator.

Five simulations were conducted, in scenarios where the total amount of amino acids pool was set to: 100% (normal cellular conditions), 75%, 50%, 25% and 0% (the total starvation conditions). We wanted to check the influence of k_F on the level of the amino acid production by autophagy, in different initial concentrations of the total amino acid pool. The plots below show the result of this simulation. Figure 4.3.4 shows the amount of the amino acids produced by autophagy as a result of the response to the total amino acid pool changes. Figure 4.3.5 shows the amount of the total amino acid pool with the contribution of autophagic amino acids.

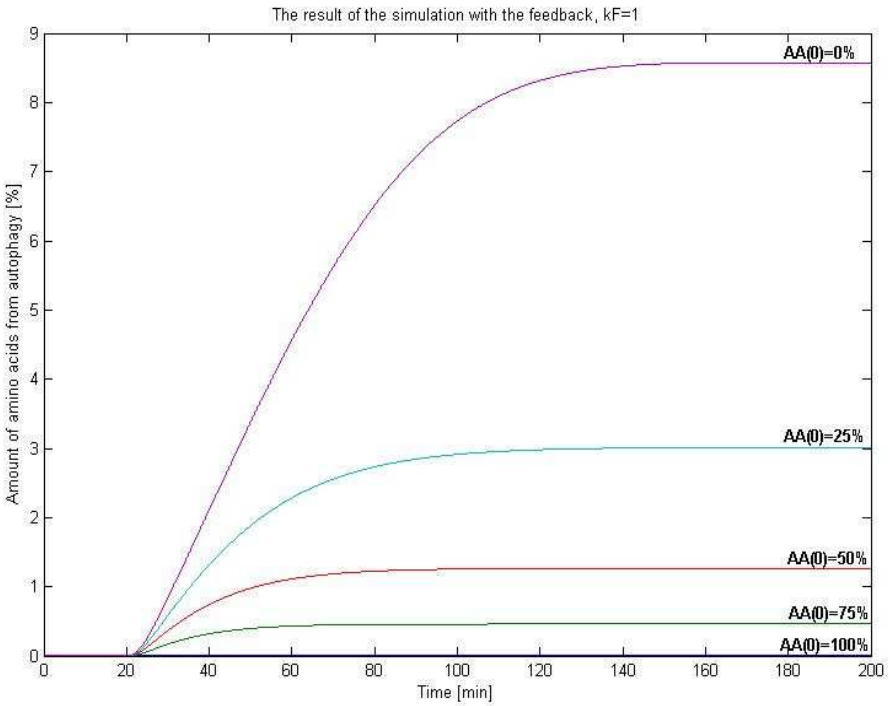

Figure 4.3.4 Result of the simulation with the feedback for k_F=1, for different initial values of the total amino acid pool AA(0). *The plot was made as a result of a simulation in MatLab and shows the amount of amino acids produced in the autophagy pathway. Production of amino acids in this pathway acts as a response to starvation. In the scenario with 100% of the initial amino acid pool there is no autophagy respond (blue). In the case of starvation, when the amount of the initial amino acids is 0%, the production of the internal amino acids, as a response of the system, gives approximately the 8.5% (purple) steady state.*

We can observe that in the scenario when the amount of the initial amino acid pool is a maximum, there is no autophagy response (figure 4.3.4, line blue). In the case of full starvation the system gives approximately the 8.5 % level of the amino acids produced by autophagy.

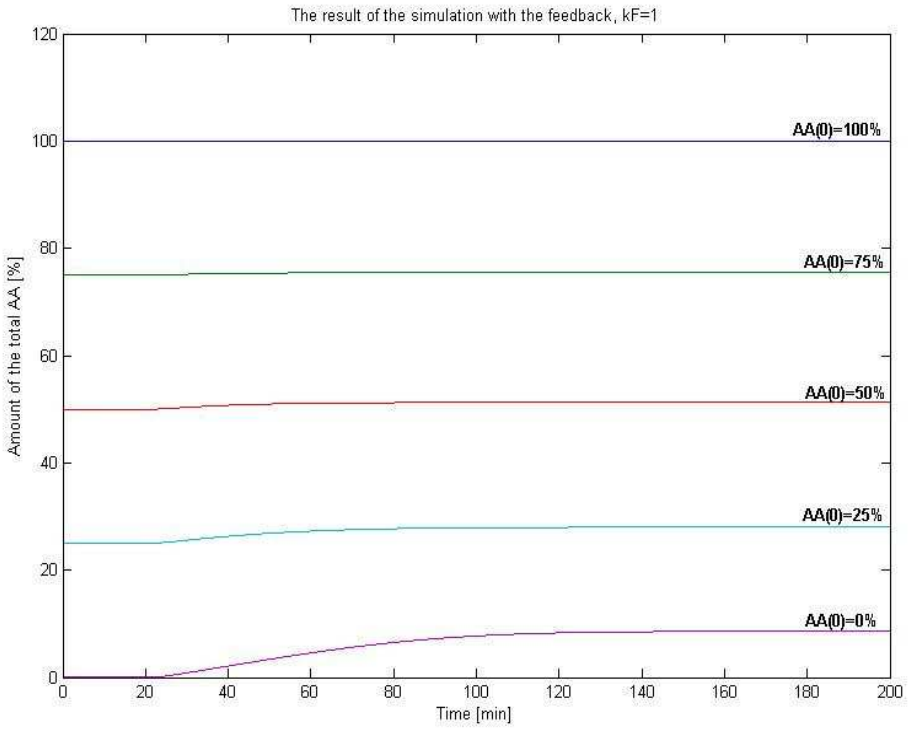

Figure 4.3.5 Result of the simulation with the feedback for k_F=1, for different initial values of the total amino acid pool AA(0). *The plot was made as a result of a simulation in MatLab and shows the amount of the total amino acid pool with the contribution of autophagic amino acids. In the scenario with 100% of the initial amino acid pool, there is no autophagy response and the level of the AA pool stays the same (blue). In the case of starvation, when the amount of the initial amino acid pool is 0%, the production of the autophagic amino acids rises (purple).*

We can observe that in normal nutrient conditions (maximum AA(0)=100%) the level of the total amino acid pool reminds the same. Also for other conditions (AA(0)=75%, 50%, 25%) changes in the total amino acid pool are small. In the starvation scenario, after 20 minutes time delay, due to autophagy, the amount of the amino acid pool increases and after approximately 140 minutes reaches the steady state.

We can conclude that autophagy, which occurs as a response to the starvation conditions, can replace some amount of the amino acids in the total amino acid pool.

In the next step we checked the model for different values of the parameter k_F. This parameter represents the strength of the feedback and is responsible for the speed of the production of the amino acids in the autophagy pathway. In these simulations the influence of the different values of k_F on the production of amino acids was investigated. We tried three values of parameter k_F: 3, which represents a slightly stronger feedback than in the previous simulation; 5, which represents strong feedback; and 0.5 which represents weak feedback. The plots below show the results of these simulations (figure 4.3.6 – 4.3.11). Figures 4.3.6, 4.3.8 and 4.3.10 show the amount of amino acids produced by autophagy as a result of the response to the total amino acid pool changes. Figures 4.3.7, 4.3.9 and 4.3.11 show the amount of the total amino acid pool with the contribution of autophagic amino acids.

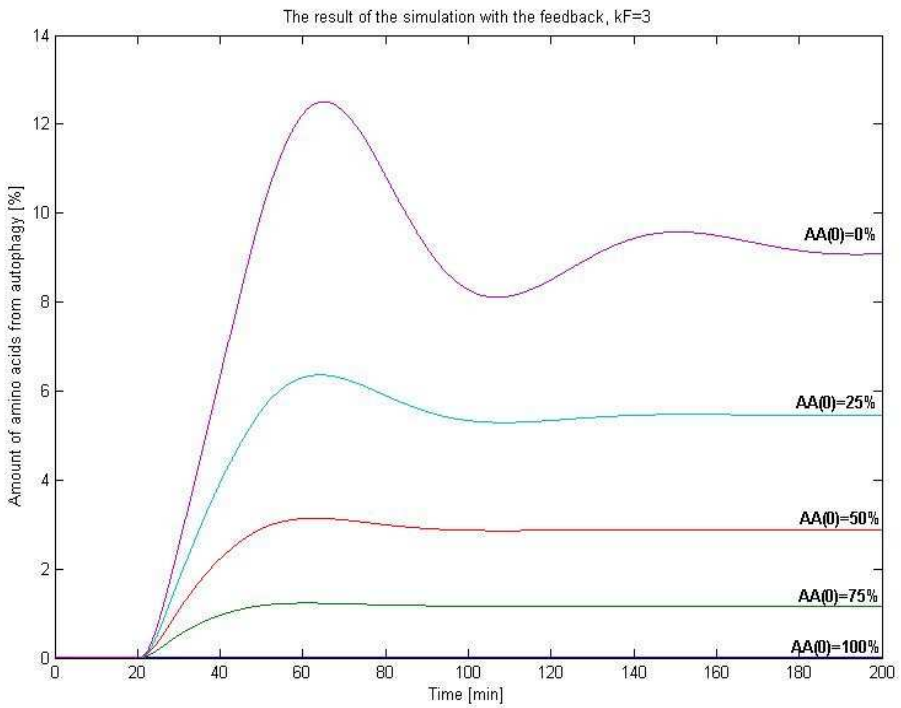

Figure 4.3.6 Result of the simulation with the feedback for k_F=3, for different initial values of the total amino acid pool AA(0). *The plot was made as a result of a simulation in MatLab and shows the amount of amino acids produced in the autophagy pathway. Production of the amino acids in this pathway acts as a response to starvation. In the scenario with 100% of the initial amino acid pool there is no autophagy response (blue). In the case of starvation, when amount of the initial amino acids is 0%, the production of the autophagic amino acids rises up very quickly and after few small oscillations and approximately 200 minutes reaches the 9% steady state (purple).*

We can observe that in the scenario when the amount of the initial amino acid pool is maximum, there is no autophagy response. In the case of full starvation the system

gives approximately the 9% level of amino acids produced by autophagy. In the first 200 minutes, before system reaches the steady state, we can observe small oscillations.

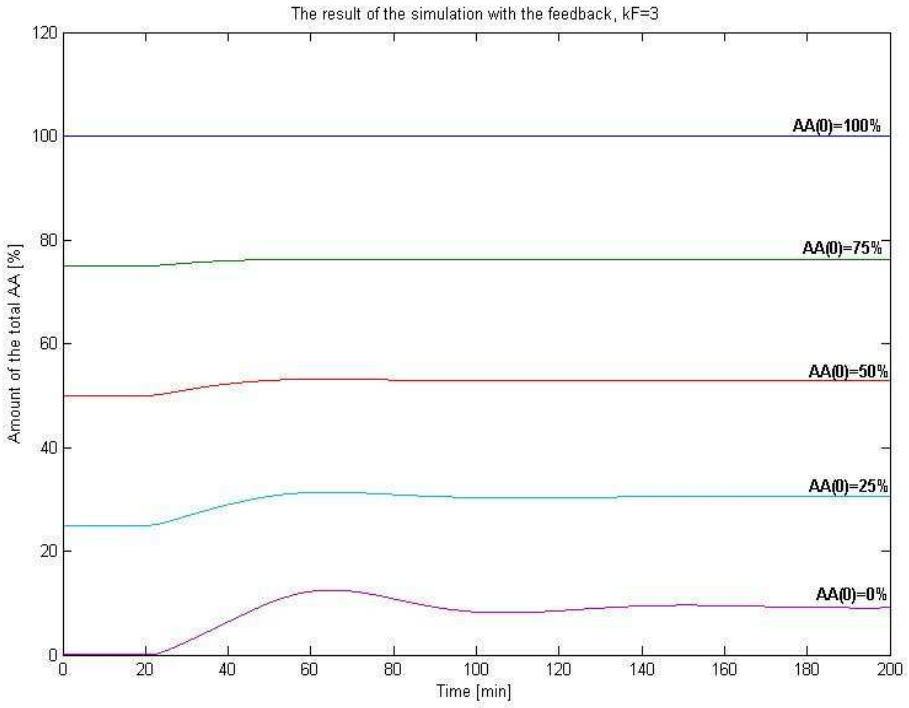

Figure 4.3.7 Result of the simulation with the feedback for k_F=3, for different initial values of the total amino acid pool AA(0). *The plot was made as a result of a simulation in MatLab and shows the amount of total amino acids pool with the contribution of autophagic amino acids. In the scenario with 100% of the initial amino acid pool, there is no autophagy response and the level of AA pool stays the same (blue). In the case of starvation, when the amount of the initial amino acid pool is 0%, the production of the autophagic amino acids rises up (purple) quickly at the beginning and after approximately 160 minutes reaches the steady state.*

We can observe that in normal nutrient conditions (maximum AA(0)=100%) the level of the total amino acid pool remains the same. Also for other conditions (AA(0)=75%, 50%, 25%) changes in the total amino acid pool are small. In the starvation scenario, after a 20 minute time delay, due to autophagy, the amount of the amino acid pool increases and after approximately 160 minutes reaches the steady state. In the first 160 minutes, before it reaches the steady state we can observe small oscillations.

In the next simulation we tested k_F=5. The plots below show the result of these simulations (figure 4.3.8 and 4.3.9). Figure 4.3.8 shows the amount of amino acids produced by autophagy. Figure 4.3.9 shows the amount of the total amino acid pool with the contribution of autophagic amino acids.

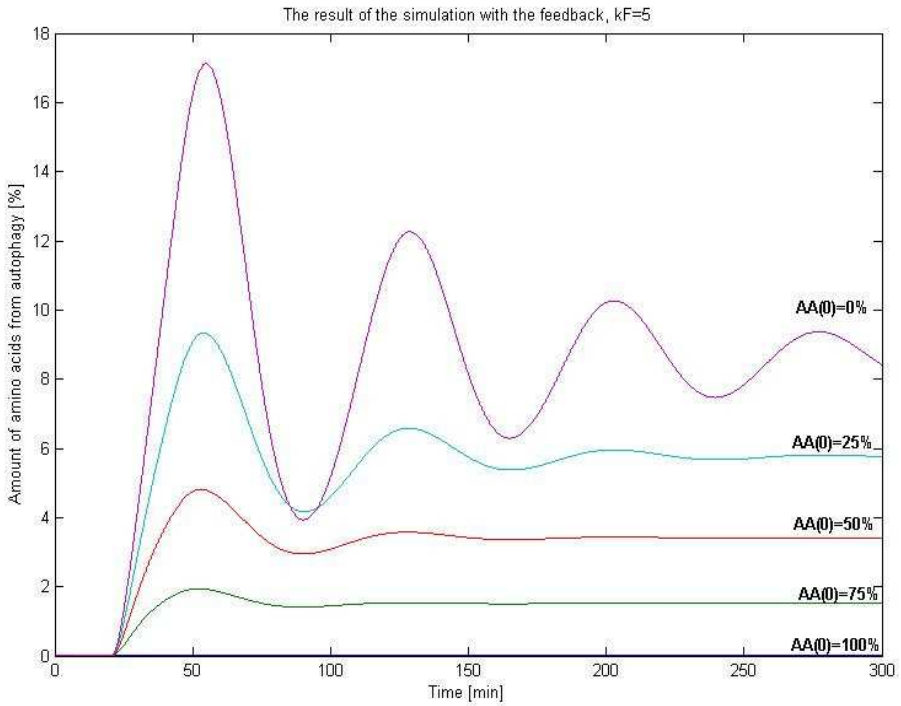

Figure 4.3.8 Result of the simulation with the feedback for k_F=5, for different initial values of the total amino acid pool AA(0). *The results plotted are from MatLab simulations and shows the amount of the amino acids produced in the autophagy pathway. Production of the amino acids in this pathway acts as a response to starvation. In scenario with 100% of the initial amino acid pool there is no autophagy response (blue). In the case of starvation, when amount of the initial amino acids is 0%, the production of the autophagic amino acids rises up very quickly and after many oscillations and approximately 400 minutes reaches the 9% steady state (purple).*

We can observe that in the scenario when the amount of the initial amino acid pool is maximum, there is no autophagy response. In the case of the full starvation the system gives approximately the 9% level of the amino acids produced by autophagy. In the first

400 minutes, before system reaches the steady state, we can observe many oscillations, which at the end reach the same steady state as in the scenario with k_F=1 and k_F=3.

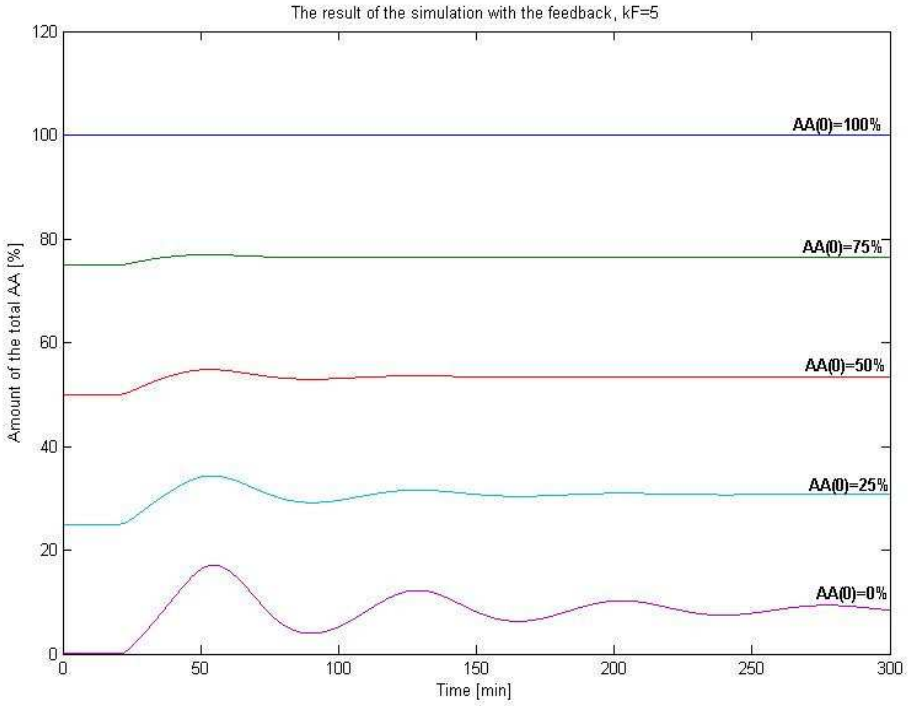

Figure 4.3.9 Result of the simulation with the feedback for k_F=5, for different initial values of the total amino acid pool AA(0). *The results plotted are from MatLab simulations and shows the amount of total amino acids pool with the contribution of autophagic amino acids. In scenario with 100% of the initial amino acid pool, there is no autophagy response and the level of AA pool stays the same (blue). In the case of starvation, when the amount of the initial amino acid pool is 0%, the production of the autophagic amino acids rises (purple) quickly at the beginning and after approximately 350 minutes and many oscillations reaches the steady state.*

We can observe that in normal nutrient conditions (maximum AA(0)=100%) the level of the total amino acid pool remains the same. Also for other conditions (AA(0)=75%, 50%, 25%) changes in the total amino acid pool are small. In starvation scenario, after 20 minutes time delay, due to autophagy, the amount of the amino acid pool increases and after approximately 350 minutes reaches the steady state. In the first 350 minutes, before it reaches the steady state we can observe many oscillations.

We can conclude that in starvation conditions, with higher value of k_F, the autophagic amino acids production is quicker (the first peak grows faster and higher – compare figures 4.3.4, 4.3.6 and 4.3.8). But also the higher k_F the bigger oscillations occur in the system response.

In the next simulation we tested k_F=0.5. The plots below show the results of these simulations (figure 4.3.10 and 4.3.11). Figure 4.3.10 shows the amount of amino acids produced by autophagy. Figure 4.3.11 shows the amount of the total amino acid pool with the contribution of autophagic amino acids.

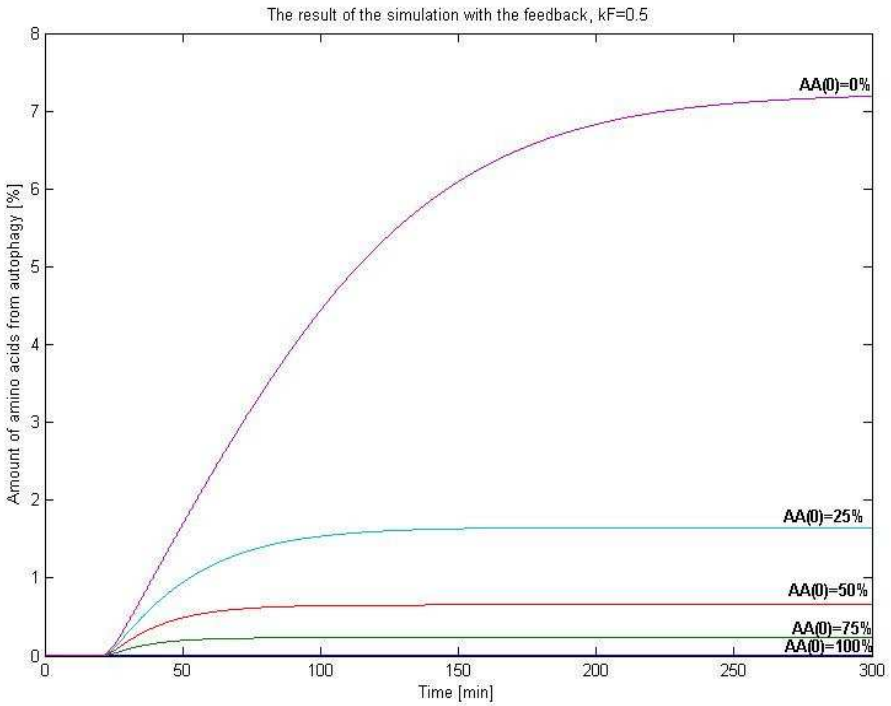

Figure 4.3.10 Result of the simulation with the feedback for k_F=0.5, for different initial values of the total amino acid pool. *The results plotted are from MatLab simulations and shows the amount of amino acids produced in autophagy pathway. Production of the amino acids in this pathway acts as a response to the starvation. In scenario with 100% of the initial amino acid pool there is no autophagy response (blue). In the case of starvation, when amount of the initial amino acids is 0%, the production of the autophagic amino acids rises and after approximately 300 minutes reaches the 7% steady state (purple).*

We can observe that in the scenario when the amount of the initial amino acid pool is maximum, there is no autophagy response. In the case of full starvation the system gives approximately 7% level of the amino acids produced by autophagy. This steady state is lower than in previous simulations, which reached 9%. Compared to figure 4.3.4

with k_F=1, the time which the system takes to reach steady state is longer (300 minutes compare with 160 minutes on figure 4.3.4).

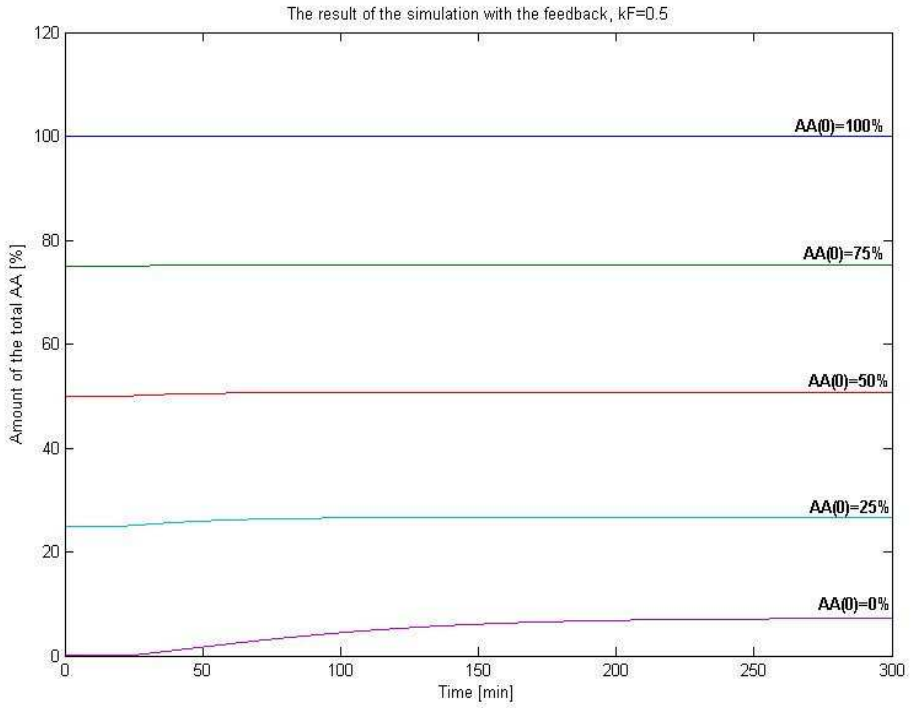

Figure 4.3.11 Result of the simulation with the feedback for k_F=0.5, for different initial values of the total amino acid pool AA(0). *The results plotted are from MatLab simulations and shows the amount of total amino acid pool with the contribution of autophagic amino acids. In scenario with 100% of the initial amino acid pool, there is no autophagy response and the level of AA pool stays the same (blue). In the case of starvation, when the amount of the initial amino acid pool is 0%, the production of the autophagic amino acids rises (purple).*

We can observe that in normal nutrient conditions (maximum AA(0)=100%) the level of the total amino acid pool remains the same. Also for other conditions (AA(0)=75%, 50%, 25%) changes to the total amino acid pool are small. In the starvation scenario,

after a 20 minute time delay, due to autophagy, the amount of the amino acid pool increases and after approximately 250 minutes reaches the steady state. Compare this result to figure 4.3.5 with k_F=1, time which system takes for the achievement steady states is longer (250 minutes compare with 140 minutes on figure 4.3.5).

4.4 Conclusions on the full implemented autophagy model

We successfully obtained results from simulations of a fully implemented model with feedback on the total amino acid pool. In starvation, the total amino acid pool decreases dramatically. Autophagy occurs as a response to the starvation conditions. Based on the simulations, we can conclude that autophagy can replace some of the amino acids in the total amino acid pool. This contribution to the total amino acid pool is approximately 9%.

The parameter k_F is in control of the speed of the production of the amino acids during the autophagy pathway. Base on the simulations, we can conclude that in starvation conditions, with higher value of k_F, the autophagic amino acids production is quicker. But the higher k_F also results in bigger oscillations in the system response. Figure 4.3.12 below shows the influence of the different values of k_F on amount of the amino acids produced by autophagy.

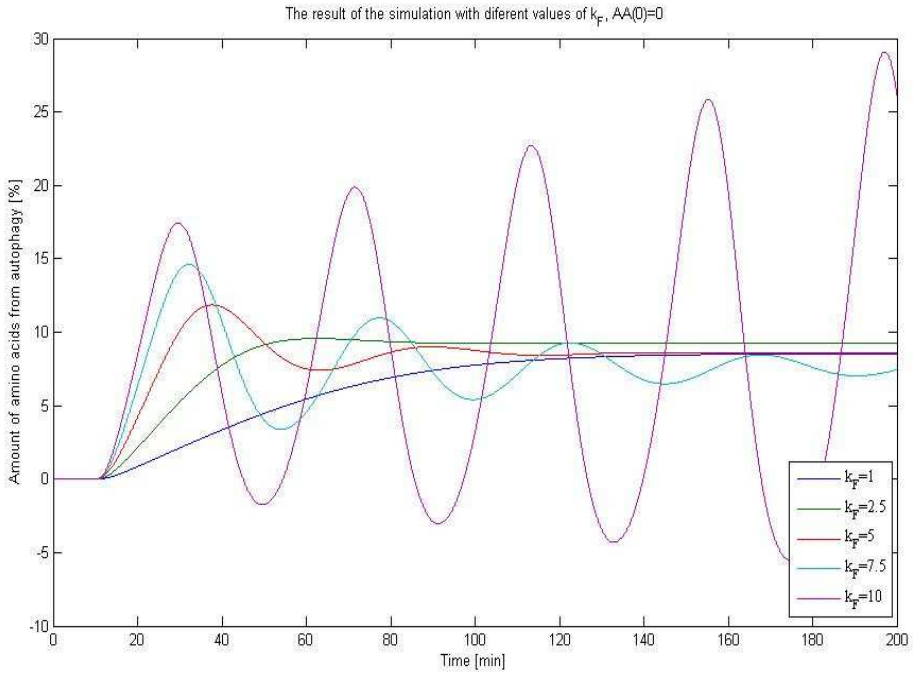

Figure 4.3.12 Result of the simulation with the feedback for k_F=1 (blue), k_F=2.5 (green), k_F=5 (red), k_F=7.5 (light blue) and k_F=10 (purple), in starvation (AA(0)=0). *The plot was made as a result of a simulation in MatLab and shows the amount of the amino acids produced in autophagy pathway. The simulation was conducted in starvation conditions, for different values of k_F. The bigger the value of k_F, the faster and the higher production of the autophagic amino acids. Also bigger and more oscillation occur while we implement bigger value of k_F. The contribution of the autophagy to the total amino acid pool is on the approximately 9% level.*

We can see that the contribution of the autophagy to the total amino acid pool reaches the 9% level. This value does not depend on the value of k_F. We can also conclude that the lower value of k_F has better dampening character.

5. Methods used in model parameterization and implementation

This section describes model parameterization and implementation, and gives an explanation of methods which were used to obtain set of parameters. Our mathematical model is calibrated using published experimental data on the autophagy pathway in mammalian cells.

All simulations were performed with a system of ordinary differential equations (ODE) which describe the biochemical reactions involved in signal transduction between amino acids and components of the mTOR-dependent autophagy induction pathway. The ordinary differential equations were based on mass action kinetics. The diagram, which represents all reactions included in the model, is provided in the chapter 4 (figure 4.2).

5.1 Methods used in the model parameterization

The kinetic constants for the first two reactions were derived from the two publications by Inoki et al and Marshall et al [*Inoki et al., 2003 and Marshall et al., 2009*]. Based on the experimental data [*Inoki et al., 2003*] and by using the equation for exponential decay, we could calculate parameter k_2. Another publication [*Marshall et al., 2009*], which was published during the course of this study, provided the value of k_2. We calculated the average value of k_2 from these two publications for use in our model. To calculate the parameter k_1, we used again experimental data from Inoki et al. They provided the ratio of GTP/GDP- bound Rheb in living cells, which was formulated in the steady state condition. From the ordinary differential equations for the

first and second reaction we could obtain the equation for the ratio $\frac{Rheb^{GTP}}{Rheb^{GDP}} = \frac{k_1}{k_2}$.

From this equation k_1 was calculated by $k_1 = k_2 \frac{Rheb^{GTP}}{Rheb^{GDP}}$. The model was tested using SBtoolbox, rate expressions and calculated parameters. System Biology Toolbox for MatLab (version 1.8) is free software, developed as a suit of MATLAB scripts.

The kinetic constants for the next two reactions were derived from the publications by Bai et al and Sato et al [*Bai et al., 2007 and Sato et al., 2009*]. Based on the experimental data [*Sato et al., 2009*] and using the equation for exponential decay, we could calculate half time for reaction R_3. In this reaction we have two reactants and we can say that they behave like a second order process, in which the concentrations of the two reactants behave the same. For second-order reactions the half time is depended on the initial value of the reactant A.

Based on this we could calculate the rate constant for reaction R_3 as $k_3 = \frac{1}{t_{1/2} \cdot [mTOR - FKBP38]}$.

To derive parameter k_{-3} for the next reaction we have studied publication by Bai et al. Based on their experimental data [*Bai et al., 2007*] and using again the equation for exponential decay, we could calculate the half time for this reaction. As the character of the reaction R_{-3} is the same as the reaction R_3, we could obtain parameter k_{-3} from the equation for the half time in the second-order reaction. This part of model was also tested using SBtoolbox, rate expressions and calculated parameters.

The kinetic constants for the next two reactions were derived from the publication by Kamada et al [*Kamada et al., 2000*]. Based on their experimental data

and using the equation for exponential decay, we could calculate parameter k_5 and also the half time for reaction R_4. Because reaction R_4 has the nature of a second-order process, we could again calculate parameter k_4 from the equation for the half time in the second-order reaction. This part of model was also tested using SBtoolbox, rate expressions and calculated parameters.

The kinetic constants for the next reactions were derived from the publication by Kamada et al [*Kamada et al., 2000*]. Parameters k_6 and k_{-6} were fitted based on their experimental data. Parameter k_6 was optimized by manual fitting. The aim was to get result which correlates with the experimental data, which shows the time of Atg1-Atg13 complex creation after rapamycin treatment. Parameter k_{-6} was also optimized by manual fitting that together with the rest of model components, could represent changes in the system, in the best way according to the experimental data. Parameter k_7 was assumed to be equal to k_4, based on the character of this reaction. Reaction R_7 is a competitive reaction for reaction R_4, where Atg13_P is produce, and both are controlled by mTOR.

5.2 Methods used in the model implementation

All simulations were performed with a system of ordinary differential equations (ODE). The ODEs were solved using SBtoolbox for MatLab and MatLab 7.3.0.267 (R2006b). MatLab used ode15s solver for ordinary differential equations and dde23 solver for delayed differential equations. SB code is available in appendix A and MatLab syntax in appendix B and C.

6. Discussion

A system modelling autophagy is a new area of research. Current understanding of each step in this biochemical pathway is limited. The study of this mechanism is interesting in several aspects: autophagy plays an important role in physiological cellular processes, is a survival mechanism under external stress and is also connected with cancer and neurodegenerative diseases [*Cuervo, 2004; Kondo et al., 2005; Levine, 2007; Pan et al., 2008*].

This work proposes a simple mathematical model of autophagy pathway as a system with feedback, which controls the level of the total amino acid pool. Feedback comes from the amino acids which are produced during the autophagy mechanism which is induced as a result of starvation or rapamycin treatment.

There are limitations in the experimental literature with regards to the possible parameterisation of autophagy models. The research which is currently done on the autophagy pathway is poorly documented with quantitative data. There are no direct useful numbers or data, which can be used in systems biology (like half time of reaction, concentrations, etc.). The work in this field is often described in general terms, like "increasing", "decreasing", "less" or "more", and there is no really interest in specific numbers. Since systems biology has become more popular it is necessary to exchange information about the biological aspects and to provide helpful data. We can suggest at this point that the biochemical experiments might be more focused on quantitative results, which show a more detailed autophagy pathway. Nevertheless, I was able to indirectly extract most of the parameters necessary for the model from the literature and published experimental data. The model, described here, is the first test of an autophagy model. It was implemented using parameters from the published

literature, some of which were estimated and optimized by manual fitting. This thesis details the model in order to serve as a reference for future work on the autophagy pathway.

Still, the model is based on many additional assumptions and simplifications. In order to simplify our work, we did not include into our model other processes, which go on parallel in the cell. Also we did not take into calculations energy equivalents such as GTP, GDP, ATP and ADP. Initially we assumed that they are not limited. Amounts of reaction catalysers, such as TSC, TSTP and unknown phosphatase in reaction R_5, we assumed as constants and we do not consider them in the equations. Autophagy, in contrast to apoptotic cell death signalling, is not a well isolated signalling network. In fact, it is strongly linked with many other cellular signals and processes [*Huett et al., 2010*]. A recent paper in *Nature* reported a proteomic analysis of the autophagy interaction network in human cells in normal nutrient conditions (Cvt pathway), uncovering a network of more than 750 interactions [*Behrends et al., 2010*]. Nevertheless, our initial model still reflects basic features of autophagy signalling.

The initial simulations, which were performed in the normal nutrients scenario, show the behaviour of all model components involved in the autophagy induction. These simulations provided the values of the steady states for all species in normal nutrient conditions.

We tested the initial model in two scenarios: when mTOR was inhibited by rapamycin and in starvation mimic conditions (decreasing parameter k_1). Both of the scenarios lead to the induction of the autophagy pathway. In comparison, induction of autophagy by rapamycin and by starvation has different kinetics. However, the final

steady states are similar; the Atg1-Atg13 complex reaches approximately the 91% level in the full starvation scenario and after 100% rapamycin treatment.

We observe that the system responded faster on rapamycin treatment. The new steady states established in 30 minutes, while in starvation after approximately 10^3 minutes. This indicates that autophagy induction after rapamycin treatment is 100 times faster than induction due to nutrient starvation. Possible reasons why there is such a big difference in the time of autophagy induction via rapamycin and starvation may be due to the character of both reactions. To obtain mTOR inhibition by starvation we have to start from reaction 1 and 3 (diagram 4.1). Because rapamycin is a direct inhibitor of mTOR we can omit these reactions. It means that we "save the time" by taking a shortcut. In the normal rich nutrient conditions k_1 is bigger than k_2. This allows creation of active $Rheb^{GTP}$. Afterwards, $Rheb^{GTP}$ activates mTOR. In starvation conditions production of new $Rheb^{GTP}$ is limited. The entire fraction of $Rheb^{GTP}$ is in the complex with FKBP38, thus mTOR is active. To inhibit mTOR in the starvation scenario, we need its endogenous inhibitor FKBP38. That is why dissociation of $Rheb^{GTP}$-FKBP38 is necessary. Reaction of dissociation, which takes some time, might slow down in general mTOR inhibition in starvation. In other words, to inhibit mTOR in starvation conditions, its endogenous inhibitor FKBP38 is needed. And because FKBP38 is in the complex with $Rheb^{GTP}$, it takes some time to dissociate this complex and obtain FKBP38 to block mTOR activity.

Kamada with his colleagues showed experimentally that inhibition of mTOR after rapamycin is very fast (~5 minutes) [*Kamada et al., 2000*]. In turn, activation of autophagy by starvation is a much slower process and could take even a few days

[*Chera et al., 2009*]. In conclusion, the results of our initial model correspond well to the experimental data.

In the next step the feedback from the amino acids produced by autophagy was implemented as a contribution on the total amino acid pool. The feedback loop modifies k_1 and regulates the level of the total amino acid pool. The contribution of the autophagic amino acids was implemented with a time delay and kinetic constant k_F. Parameter k_F represents the strength of the feedback and is responsible for the velocity of the production of the amino acids during the autophagy pathway. The amount of amino acids which are produced by the autophagy pathway is proportional to the amount of Atg1-Atg13 complex.

During simulations, the influence of the different values of k_F on the production of amino acids was investigated. We could observe that in starvation conditions the autophagic amino acids production was faster with higher value of k_F. But also higher k_F produced bigger oscillations in the system response. The lower values of k_F had better dampening character.

In general, we conclude that during starvation, autophagy is induced and this process can replace some amount of the amino acids in the total amino acid pool. This contribution on the total amino acid pool, amount to the 9% level. This value does not depend on the value of k_F.

From the results in chapter 4.2.3 when we tested model for starvation conditions, we know that 5-10% of the remaining amino acids (during starvation) is sufficient to prevent a significant increase in autophagy. The final simulations with the feedback showed that the autophagy contribution to the total amino acid pool is 9%. In general,

these results allow us to conclude that, the amount of amino acids produced in the autophagy pathway, as a response to starvation, is sufficient to keep basal Cvt pathway, unnecessarily autophagy induction.

The strength of the feedback k_F is not reported in the experimental literature. However, Onodera and Ohsumi presented work on autophagy contribution to the maintenance of the amino acid pool [*Onodera and Ohsumi, 2005*], which might be helpful to obtain this value. They showed that the total amino acid pool decreased dramatically during the first 2 hours of starvation. Next, the pool was partially restored during 3-6 hours of starvation. Finally, the amino acid level reached a slightly lower level than first response. We can compare their result to our one oscillation plot (figure 4.3.6) for the simulation with k_F=3. Our value of the k_F qualitatively correlates to their data. The results are only qualitatively comparable because the investigated species were different – Onodera and Ohsumi used yeasts, while our model is mostly validated based on results on mammalians.

In summary, this thesis presents a mathematical model of amino acids level control via the autophagy pathway as a feedback system. We tested the model in the case of mTOR inhibition by rapamycin and autophagy induction in starvation conditions. In the next step we suggest additional model testing in scenarios of protein overexpression or knock down. That requires experiments to validate model predictions. At the same time the model might assist already in experiments planning.

We mentioned at the beginning of this chapter that our model does not include other reactions which occur in parallel with autophagy in the cell. However autophagy is linked to cell death signalling [*Boya et al., 2005; Levine et al., 2008*]. In mammalian cells there is the Bcl-2 protein family, which is implicated in the control of apoptosis

and autophagy [*Levine et al., 2008*]. As a further step we suggest simulations which might prove the connection of autophagy with apoptosis, which is already well described by system biological studies [*Rehm et al., 2006; Huber et al., 2009*].

Autophagy is also implicated in several human pathologies, such as different kinds of cancer, Parkinson's disease and Alzheimer's disease [*Cuervo, 2004; Kondo et al., 2005; Levine, 2007; Pan et al., 2008*]. In the future, the optimized, improved and fully validated model may help in anticancer research strategies and drag development.

Appendix A

```
********** MODEL NAME
Mathematical model of amino acids level control
via autophagy as a feedback system.

********** MODEL NOTES

********** MODEL STATES
d/dt(RhebGDP) = -v1+v2
d/dt(RhebGTP) = v1-v2-v3+v33
d/dt(mTOR) = v3-v33
d/dt(mTORxFKBP) = -v3+v33
d/dt(RhebGTPxFKBP) = v3-v33
d/dt(Atg13_P) = v4-v5+v7
d/dt(Atg13) = -v4+v5-v6+v66
d/dt(Atg1) = -v6+v66+v7
d/dt(Atg1xAtg13) = v6-v66-v7
d/dt(AA) = vAA_in-vAA_out

RhebGDP(0) = 16.709173735229925
RhebGTP(0) = 27.735575258098557
mTOR(0) = 55.555251006671519
mTORxFKBP(0) = 44.444748993328481
RhebGTPxFKBP(0) = 55.555251006671519
Atg13_P(0) = 58.147525934909623
Atg13(0) = 25.19436723424695
Atg1(0) = 83.341893169156577
Atg1xAtg13(0) = 16.658106830843426
AA(0) = 99.999400001200001

********** MODEL PARAMETERS
k1 = 0.00067159999999999995
k2 = 0.040460000000000003
k3 = 0.0033300000000000001
k33 = 0.00133
k4 = 0.01498
k5 = 0.59899999999999998
k6 = 0.0066499000000000003
k66 = 0.005999
k7 = 0.01498
kAA_in = 0.0166666
kAA_out = 0.00016666660000000001

********** MODEL VARIABLES

********** MODEL REACTIONS
v1 = k1*RhebGDP*AA
v2 = k2*RhebGTP
v3 = k3*(mTORxFKBP)*RhebGTP
v33 = k33*(RhebGTPxFKBP)*mTOR
v4 = k4*Atg13*mTOR
v5 = k5*(Atg13_P)
v6 = k6*Atg13*Atg1
v66 = k66*(Atg1xAtg13)
v7 = k7*(Atg1xAtg13)*mTOR
vAA_in = kAA_in
vAA_out = kAA_out*AA
```

Appendix B

```
%this file is the last version that I was able to write ('Bartomiej
Tomiczek's code')
%please mention in any papers while using this file

function autofagia

clear all;% necesery while using presistent variables
ci=zeros(1,11);%input definition of the concentration
out = [];%input definition of out
d =[];%input definition of matrix d
outt80 = [];%input definition
par = [1]; %input definition of feedback kinetic constant
multiplication
Q = [];%input definition
out1 = [];%input definition
zmien = [1 0.75 0.5 0.25 0];%in this area you put the multiplication
of the chosen parameter(you can use 10^zmien also)
e = [];%input definition
 for z = zmien
%parametr z is being changed acording to zmien matrix elements so the
chosen concentration can be changed
ci(1) = 16.7103;   %RhebGDP
ci(2) = 27.7349;   %RhebGTP
ci(3) = 55.5548;   %mTOR
ci(4) = 44.4452;   %mTORxFKBP
ci(5) = 55.5548;   %RhebGTPxFKBP
ci(6) = 58.1473;   %Atg13_P
ci(7) = 25.1944;   %Atg13
ci(8) = 83.3418;   %Atg1
ci(9) = 16.6582;   %Atg1xAtg13
ci(10) = 99.9999.*z;          %AA
ci(11) = 0;          %AAB

c = ci;

%load('out80.mat'); %for loading variables

 time = 200; %time of the simulation
 tstep =0.1;%time step
 licznik = 0;%counter of the number of solutions dine by dde
 zas = 0;%definition of the variable
 auto = zeros(1,time*tstep); %matrix that has a size of number of
timesteps


 opt = ddeset('RelTol', 1e-1, 'MaxStep', tstep);%options for the
solver relative eror tolerance and time step


 sol = dde23(@oligofago_MSC,[20 10],c,[0:tstep:time],opt,ci,par);
%solve the simulation using oligofago_MSC script

 e = sol.y;%concentration matrix

 d = [d ; (e(11,:)) ];%AAB concentration matrix in different runs
```

```
 Q = [Q ; (e(11,:) + e(10,:)) ];%AA + AAB concentration matrix in
different runs

%  figure;

% out80 = sol.y;
% out80
save('out80.mat');

 end

 %figure,mesh((d)');

 figure,plot(sol.x,d);%plots AAB
 figure,plot(sol.x,Q);%plots AA+AAb
 %legend('100%AA','75%AA','50%AA','25%AA', '0%AA')
 xlabel('time')
 ylabel('AAB')

end
```

Appendix C

```
function out = oligofago_MSC(t,c,Z,ci,par)
% global licznik zas time,ci,auto,licznik,zas
S = [ % 1           2      3       4        5           6         7         8         9
10     11
      %RhebGDP   RhebGTP mTOR  mTORxFKBP RhebGTPxFKBP Atg13_P   Atg13    Atg1
Atg1xAtg13     AA       AAB
       -1           1      0       0        0           0         0         0         0
0      0   %1 RhebGDP  + AA --> RhebGTP
        1          -1      0       0        0           0         0         0         0
0      0   %2 RhebGTP       --> RhebGDP
        0          -1      1      -1        1           0         0         0         0
0      0   %3 mTORxFKBP + RhebGTP --> RhebGTPxFKBP + mTOR
        0           1     -1       1       -1           0         0         0         0
0      0   %4 RhebGTPxFKBP + mTOR --> mTORxFKBP + RhebGTP
        0           0      0       0        0           1        -1         0         0
0      0   %5 Atg13 --> Atg13_P
        0           0      0       0        0          -1         1         0         0
0      0   %6 Atg13_P-->Atg13
        0           0      0       0        0           0        -1        -1         1
0      0   %7 Atg13 + Atg1 ---> Atg1xAtg13
        0           0      0       0        0           0         1         1        -1
0      0   %8 Atg1xAtg13 -->  Atg13 + Atg1
        0           0      0       0        0           1         0         1        -1
0      0   %9 Atg1xAtg13 -->  Atg13_P + Atg1
        0           0      0       0        0           0         0         0         0
1      0   %10 creation
        0           0      0       0        0           0         0         0         0
-1     0    %11 degradation
        0           0      0       0        0           0         0         0         0
0      1   %lag
        0           0      0       0        0           0         0         0         0
0     -1   %lag
        0           0      0       0        0           0         0         0         0
0     -1   %lag
      ];
```

```
k1 = 0.00067159999999999995;
k2 = 0.040460000000000003;
k3 = 0.0033300000000000001;
k33 = 0.00133;
k4 = 0.01498;
k5 = 0.59899999999999998;
k6 = 0.0066499000000000003;
k66 = 0.005999;
k7 = 0.01498;
kAA_out = 0.0001666666;
kAA_in = kAA_out*ci(10);
k11 = 1*par;

cl = Z(:,1);


v = zeros(14,1);
v(1) = k1*c(1)*(c(10)+ par*c(11));  %k1*RhebGDP*AA
v(2) = k2*c(2);   %k2*RhebGTP
v(3) = k3*c(4)*c(2);%k3*(mTORxFKBP)*RhebGTP
v(4) = k33*c(5)*c(3);%k33*(RhebGTPxFKBP)*mTOR
v(5) = k4*c(7)*c(3);%k4*Atg13*mTOR
v(6) = k5*c(6);%k5*(Atg13_P)
v(7) = k6*c(7)*c(8);%k6*Atg13*Atg1
v(8) = k66*c(9);%k66*(Atg1xAtg13)
v(9) = k7*c(9)*c(3);%k7*(Atg1xAtg13)*mTOR
v(10) = kAA_in;%kAA_in
v(11) = kAA_out*c(10);%kAA_out*AA
v(12) = k11*k6*cl(7)*cl(8);%k6*c(7)*c(8);%k6*Atg13*Atg1
v(13) = k11*k66*cl(9);%k66*c(9);%k66*(Atg1xAtg13)
v(14) = k11*k7*cl(9)*cl(3);%k7*c(9)*c(3);%k7*(Atg1xAtg13)*mTOR

out = S'*v;
% out
```

References

1. Avruch, J.; Hara, K.; Lin, Y.; Liu, M.; Long, X.; Ortiz-Vega, S. & Yonezawa, K. (2006), 'Insulin and amino-acid regulation of mTOR signaling and kinase activity through the Rheb GTPase', *Oncogene* **25**(48), 6361—6372.

2. Baba, M.; Osumi, M.; Scott, S. V.; Klionsky, D. J. & Ohsumi, Y. (1997), 'Two Distinct Pathways for Targeting Proteins from the Cytoplasm to the Vacuole/Lysosome', *J. Cell Biol.* **139**(7), 1687-1695.

3. Bai, X. & Jiang, Y. (2009), 'Key factors in mTOR regulation', *Cellular and molecular life sciences : CMLS*.

4. Bai, X.; Ma, D.; Liu, A.; Shen, X.; Wang, Q. J.; Liu, Y. & Jiang, Y. (2007), 'Rheb Activates mTOR by Antagonizing Its Endogenous Inhibitor, FKBP38', *Science* **318**(5852), 977-980.

5. Barkai, N. & Leibler, S. (1997), 'Robustness in simple biochemical networks', *Nature* **387**(6636), 913—917.

6. Beaulaton, J. & Lockshin, R. A. (1977), 'Ultrastructural study of the normal degeneration of the intersegmental muscles of *Antheraea polyphemus* and *Manduca sexta* (Insecta, lepidoptera) with particular reference to cellular autophagy', *Journal of Morphology* **154**, 39-57.

7. Behrends, C.; Sowa, M. E.; Gygi, S. P. & Harper, J. W. (2010), 'Network organization of the human autophagy system', *Nature* **466**(7302), 68--76.

8. Blommaart, E. F. C.; Luiken, J. J. F. P.; Blommaart, P. J. E.; van Woerkom, G. M. & Meijer, A. J. (1995), 'Phosphorylation of Ribosomal Protein S6 Is Inhibitory for Autophagy in Isolated Rat Hepatocytes', *Journal of Biological Chemistry* **270**(5), 2320-2326.

9. Bolender, R. P. & Weibel, E. R. (1973), 'A Morphometric Study of the Removal of Phenobarbital-Induced Membranes from Hepatocytes after Cessation of Treatment', *The Journal of Cell Biology* **56**(3), 746—761.

10. Boya, P.; Gonzalez-Polo, R.-A.; Casares, N.; Perfettini, J.-L.; Dessen, P.; Larochette, N.; Metivier, D.; Meley, D.; Souquere, S.; Yoshimori, T.; Pierron, G.; Codogno, P. & Kroemer, G. (2005), 'Inhibition of Macroautophagy Triggers Apoptosis', *Mol. Cell. Biol.* **25**(3), 1025-1040.

11. Codogno, P. & Meijer, A. J. (2005), 'Autophagy and signaling: their role in cell survival and cell death', *Cell Death Differ* **12**(S2), 1509—1518.

12. Cuervo, A. M. (2004), 'Autophagy: in sickness and in health', *Trends in Cell Biology* **14**(2), 70 - 77.

13. Gozuacik, D. & Kimchi, A. (2004), 'Autophagy as a cell death and tumor suppressor mechanism', *Oncogene* **23**(16), 2891--2906.

14. Hall, M. N. (2008), 'mTOR-what does it do?', *Transplantation proceedings* **40**, S5-S8.

15. Harding, T.; Morano, K.; Scott, S. & Klionsky, D. (1995), 'Isolation and characterization of yeast mutants in the cytoplasm to vacuole protein targeting pathway', *J. Cell Biol.* **131**(3), 591-602.

16. He, C.; Song, H.; Yorimitsu, T.; Monastyrska, I.; Yen, W.-L.; Legakis, J. E. & Klionsky, D. J. (2006), 'Recruitment of Atg9 to the preautophagosomal structure by Atg11 is essential for selective autophagy in budding yeast', *J. Cell Biol.* **175**(6), 925-935.

17. Hosokawa, N.; Hara, T.; Kaizuka, T.; Kishi, C.; Takamura, A.; Miura, Y.; Iemura, S.-i.; Natsume, T.; Takehana, K.; Yamada, N.; Guan, J.-L.; Oshiro, N. & Mizushima, N. (2009), 'Nutrient-dependent mTORC1 Association with the ULK1-Atg13-FIP200 Complex Required for Autophagy', *Mol. Biol. Cell* **20**(7), 1981-1991.

18. Huber, H.; Bullinger, E. & Rehm, M., ed. (2009), *Systems Biology Approaches to the Study of Apoptosis. Essentials of Apoptosis*, Humana Press.

19. Huett, A.; Goel, G. & Xavier, R. J. (2010), 'A systems biology viewpoint on autophagy in health and disease', *Curr Opin Gastroenterol* **26**.

20. Inoki, K.; Li, Y.; Xu, T. & Guan, K.-L. (2003), 'Rheb GTPase is a direct target of TSC2 GAP activity and regulates mTOR signaling', *Genes & Development* **17**(15), 1829-1834.

21. Jaeger, P. A. & Wyss-Coray, T. (2009), 'All-you-can-eat: autophagy in neurodegeneration and neuroprotection', *Molecular Neurodegeneration* **4**.

22. Kabeya, Y.; Mizushima, N.; Ueno, T.; Yamamoto, A.; Kirisako, T.; Noda, T.; Kominami, E.; Ohsumi, Y. & Yoshimori, T. (2000), 'LC3, a mammalian homologue of yeast Apg8p, is localized in autophagosome membranes after processing', *EMBO J* **19**(21), 5720—5728.

23. Kamada, Y.; Funakoshi, T.; Shintani, T.; Nagano, K.; Ohsumi, M. & Ohsumi, Y. (2000), 'Tor-Mediated Induction of Autophagy via an Apg1 Protein Kinase Complex', *J. Cell Biol.* **150**(6), 1507-1513.

24. Kamada, Y.; Yoshino, K.-i.; Kondo, C.; Kawamata, T.; Oshiro, N.; Yonezawa, K. & Ohsumi, Y. (2010), 'Tor Directly Controls the Atg1 Kinase Complex To Regulate Autophagy', *Mol. Cell. Biol.* **30**(4), 1049-1058.

25. Kim, E. (2009), 'Mechanisms of amino acid sensing in mTOR signaling pathway', *Nutr Res Pract. 2009* **3(1):**, 64–71.

26. Klionsky, D. J. (2007), 'Autophagy: from phenomenology to molecular understanding in less than a decade', *Nat Rev Mol Cell Biol* **8**(11), 931—937.

27. Klionsky, D. J. (2005), 'The molecular machinery of autophagy: unanswered questions', *J Cell Sci* **118**(1), 7-18.

28. Klionsky, D. J. & Emr, S. D. (2000), 'Autophagy as a Regulated Pathway of Cellular Degradation', *Science* **290**(5497), 1717-1721.

29. Klionsky, D. J. & Ohsumi, Y. (1999), 'Vacuolar import of proteins and organelles from the cytoplasm', *Annual Review of Cell and Developmental Biology* **15**(1), 1-32.

30. Klipp, E.; Herwig, R.; Kowald, A.; Wierling, C. & Lehrach, H. (2005), *Systems biology in practice: concepts, implementation and application*, Wiley-VCH; 1 edition (May 6, 2005).

31. Kondo, Y.; Kanzawa, T.; Sawaya, R. & Kondo, S. (2005), 'The role of autophagy in cancer development and response to therapy', *Nat Rev Cancer* **5**(9), 726--734.

32. Kopitz, J.; Kisen, G.; Gordon, P.; Bohley, P. & Seglen, P. (1990), 'Nonselective autophagy of cytosolic enzymes by isolated rat hepatocytes', *J. Cell Biol.* **111**(3), 941-953.

33. Korolchuk, V. I.; M., M. F. & C, R. D. (2009), 'A novel link between autophagy and the ubiquitin-proteasome system', *Autophagy* **5**, 862-863.

34. Kunz, J.; Henriquez, R.; Schneider, U.; Deuter-Reinhard, M.; Movva, N. R. & Hall, M. N. (1993), 'Target of rapamycin in yeast, TOR2, is an essential phosphatidylinositol kinase homolog required for G1 progression', *Cell* **73**(3), 585-596.

35. Kwakernaak, H.Sivan, R., ed. (1972), *Linear Optimal Control Systems*, John Wiley & Sons, Inc., New York, NY, USA.

36. Laplante, M. & Sabatini, D. M. (2009), 'mTOR signaling at a glance', *J Cell Sci* **122**(20), 3589-3594.

37. Levine, B. & Yuan, J. (2005), 'Autophagy in cell death: an innocent convict?', *J. Clin. Invest.* **115(10)**, 2679-2688.

38. Levine, B. (2007), 'Cell biology: Autophagy and cancer', *Nature* **446**(7137), 745-747.

39. Levine, B.; Sinha, S. C. & Kroemer, G. (2008), 'Bcl-2 family members: Dual regulators of apoptosis and autophagy', *Autophagy* **4**.

40. Levine, W. S., ed. (1999), *Control System Fundamentals*, CRC Press LLC

41. Liang, X. H.; Jackson, S.; Seaman, M.; Brown, K.; Kempkes, B.; Hibshoosh, H. & Levine, B. (1999), 'Induction of autophagy and inhibition of tumorigenesis by beclin 1', *Nature* **402**(6762), 672-676.

42. Lodish; Berk; Zipursky; Matsudaira; Baltimore & Darnell, 4th edition, ed. (2001), *Molecular cell biology*, W. H. Freeman and company.

43. Lum, J. J.; Bauer, D. E.; Kong, M.; Harris, M. H.; Li, C.; Lindsten, T. & Thompson, C. B. (2005), 'Growth Factor Regulation of Autophagy and Cell Survival in the Absence of Apoptosis'(2), 237--248.

44. Mandelstam, J. (1960), 'The intracellular turnover of protein and nucleic acids and its role in biochemical differentiation', *Microbiol. Mol. Biol. Rev.* **24**(3), 289-308.

45. Marshall, C. B.; Ho, J.; Buerger, C.; Plevin, M. J.; Li, G.-Y.; Li, Z.; Ikura, M. & Stambolic, V. (2009), 'Characterization of the Intrinsic and TSC2-GAP-Regulated GTPase Activity of Rheb by Real-Time NMR', *Science Signaling* **2**(55).

46. Mathew, R.; Kongara, S.; Beaudoin, B.; Karp, C. M.; Bray, K.; Degenhardt, K.; Chen, G.; Jin, S. & White, E. (2007), 'Autophagy suppresses tumor progression by limiting chromosomal instability', *Genes & Development* **21**(11), 1367-1381.

47. Matsuura, A.; Tsukada, M.; Wada, Y. & Ohsumi, Y. (1997), 'Apg1p, a novel protein kinase required for the autophagic process in Saccharomyces cerevisiae', *Gene* **192**(2), 245 — 250.

48. Meijer, A. J. (2008), 'Amino Acid Regulation of Autophagosome Formation', *Autophagosome and Phagosome* , 89--109.

49. Meijer, A. J. & Codogno, P. (2008), 'Autophagy: A Sweet Process in Diabetes'(4), 275—276.

50. Melendez, A. & Levine, B.The C. elegans Research Community, ed. (2009), *Autophagy in C. elegans*, WormBook.

51. Mizushima, N. (2005), 'The pleiotropic role of autophagy: from protein

metabolism to bactericide', *Cell Death Differ* **12**(S2), 1535--1541.

52. Mizushima, N. (2007), 'Autophagy: process and function', *Genes & Development* **21**(22), 2861-2873.

53. Mortimore, G. E. & Schworer, C. M. (1977), 'Induction of autophagy by amino-acid deprivation in perfused rat liver', *Nature* **270**(5633), 174—176.

54. Munafo, D. B. & Colombo, M. I. (2001), 'A novel assay to study autophagy: regulation of autophagosome vacuole size by amino acid deprivation', *J Cell Sci* **114**(20), 3619-3629.

55. Murray R. K., Granner D. K., Mayes P. A., Rodwell V. W., "Harper's biochemistry", 26 edition, 2003

56. Ng, G. & Huang, J. (2005), 'The significance of autophagy in cancer', *Molecular carcinogenesis 43*, 183-187.

57. Onodera, J. & Ohsumi, Y. (2005), 'Autophagy Is Required for Maintenance of Amino Acid Levels and Protein Synthesis under Nitrogen Starvation', *Journal of Biological Chemistry* **280**(36), 31582-31586.

58. Ohsumi, Y. (2001), 'Molecular dissection of autophagy: two ubiquitin-like systems', *Nat Rev Mol Cell Biol* **2**(3), 211—216.

59. Pan, T.; Kondo, S.; Le, W. & Jankovic, J. (2008), 'The role of autophagy-lysosome pathway in neurodegeneration associated with Parkinson's disease', *Brain* **131**(8), 1969-1978.

60. Ravikumar, B.; Duden, R. & Rubinsztein, D. C. (2002), 'Aggregate-prone proteins with polyglutamine and polyalanine expansions are degraded by autophagy', *Hum. Mol. Genet.* **11**(9), 1107-1117.

61. Rehm M., Huber H. J., Dussmann H., Prehn J. H. M., "Systems analysis of effector caspase activation and its control by X-linked inhibitor of apoptosis protein", *The EMBO Journal,* 1-12, 2006.

62. Roccio, M.; Bos, J. L. & Zwartkruis, F. J. T. (2006), 'Regulation of the small GTPase Rheb by amino acids', *Oncogene* **25**(5), 657—664.

63. Rubinsztein, et al. (2005), 'Autophagy and its possible roles in nervous system diseases, damage and repair.', *Autophagy* **1**, 11-22.

64. Sato, T.; Nakashima, A.; Guo, L. & Tamanoi, F. (2009), 'Specific Activation of mTORC1 by Rheb G-protein in Vitro Involves Enhanced Recruitment of Its Substrate Protein', *Journal of Biological Chemistry* **284**(19), 12783-12791.

65. Scott, S. V.; Hefner-Gravink, A.; Morano, K. A.; Noda, T.; Ohsumi, Y. & Klionsky, D. J. (1996), 'Cytoplasm-to-vacuole targeting and autophagy employ the same machinery to deliver proteins to the yeast vacuole', *Proceedings of the National Academy of Sciences of the United States of America* **93**(22), 12304-12308.

66. Scott, S. V.; Nice, D. C.; Nau, J. J.; Weisman, L. S.; Kamada, Y.; Keizer-Gunnink, I.; Funakoshi, T.; Veenhuis, M.; Ohsumi, Y. & Klionsky, D. J. (2000), 'Apg13p and Vac8p Are Part of a Complex of Phosphoproteins That Are Required for Cytoplasm to Vacuole Targeting', *Journal of Biological Chemistry* **275**(33), 25840-25849.

67. Shimizu, S.; Kanaseki, T.; Mizushima, N.; Mizuta, T.; Arakawa-Kobayashi, S.; Thompson, C. B. & Tsujimoto, Y. (2004), 'Role of Bcl-2 family proteins in a non-apoptotic programmed cell death dependent on autophagy genes', *Nat Cell Biol* **6**(12), 1221--1228.

68. Shirane, M. & Nakayama, K. I. (2003), 'Inherent calcineurin inhibitor FKBP38 targets Bcl-2 to mitochondria and inhibits apoptosis', *Nat Cell Biol* **5**(1), 28--37.

69. Takeshige, K.; Baba, M.; Tsuboi, S.; Noda, T. & Ohsumi, Y. (1992), 'Autophagy in yeast demonstrated with proteinase-deficient mutants and conditions for its induction', *J. Cell Biol.* **119**(2), 301-311.

70. Uhlenbrock, K.; Weiwad, M.; Wetzker, R.; Fischer, G.; Wittinghofer, A. & Rubio, I. (2009), 'Reassessment of the role of FKBP38 in the Rheb/mTORC1 pathway', *FEBS letters* volume 583 issue 6 Pages, 965-970.

71. Veenhuis, M.; Douma, A.; Harder, W. & Osumi, M. (1983), 'Degradation and turnover of peroxisomes in the yeast Hansenula polymorpha induced by

selective inactivation of peroxisomal enzymes', *Archives of Microbiology* 134(3), 193—203.

72. Vinod, P. K. & Venkatesh, K. V. (2009), 'Quantification of the effect of amino acids on an integrated mTOR and insulin signaling pathway', *Mol. BioSyst.* **5**(10), 1163--1173.

73. Wang, X.; Fonseca, B. D.; Tang, H.; Liu, R.; Elia, A.; Clemens, M. J.; Bommer, U.-A. & Proud, C. G. (2008), 'Re-evaluating the Roles of Proposed Modulators of Mammalian Target of Rapamycin Complex 1 (mTORC1) Signaling', *Journal of Biological Chemistry* **283**(45), 30482-30492.

74. Wolkenhauer, O.; Sreenath, S. N.; Wellstead, P.; Ullah, M. & Cho, K.-H. (2005), 'A systems- and signal-oriented approach to intracellular dynamics.', *Biochem. Soc. Trans.* **33**, 507-515.

75. Xie, Z. & Klionsky, D. J. (2007), 'Autophagosome formation: core machinery and adaptations', *Nat Cell Biol* **9**(10), 1102—1109.

76. YANG, Ya-ping, L. Z.-q. G. Z.-l. Q. Z.-h. (2005), 'Molecular mechanism and regulation of autophagy', *Acta Pharmacologica Sinica* **26**, 1421-1434.

77. Yi, T.-M.; Huang, Y.; Simon, M. I. & Doyle, J. (2000), 'Robust perfect adaptation in bacterial chemotaxis through integral feedback control', *Proceedings of the National Academy of Sciences of the United States of America* **97**(9), 4649-4653.

78. Yorimitsu, T. & Klionsky, D. J. (2005), 'Autophagy: molecular machinery for self-eating', *Cell Death Differ* 12(S2), 1542—1552.

79. Yoshimori, T. (2004), 'Autophagy: a regulated bulk degradation process inside cells', *Biochemical and Biophysical Research Communications* **313**(2), 453 - 458.

80. Yu, L.; Alva, A.; Su, H.; Dutt, P.; Freundt, E.; Welsh, S.; Baehrecke, E. H. & Lenardo, M. J. (2004), 'Regulation of an ATG7-beclin 1 Program of Autophagic Cell Death by Caspase-8', *Science* 304(5676), 1500-1502.

81. Zempleni J., Dakshinamurti K., "Nutrients and cell signaling", chapter "Amino Acid-Sensing mTOR Signaling" by Erbay E., Kim J. E., and Chen J., *Taylor and Francis Group*, 2005
82. Zhang, Y.; Gao, X.; Saucedo, L. J.; Ru, B.; Edgar, B. A. & Pan, D. (2003), 'Rheb is a direct target of the tuberous sclerosis tumour suppressor proteins', *Nat Cell Biol* **5**(6), 578--581.